SAMRC/NHLS/UCT Molecular Mycobacteriology Research Unit

Targeted depletion of RibF, a putative bifunctional FAD synthetase/ flavokinase in *Mycobacterium smegmatis* using CRISPR interference

Mabule Lucas Raphela

(RPHMAB004)

Molecular Mycobacteriology Research Unit

Division of Medical Microbiology

Department of Pathology

A dissertation submitted to the Faculty of Health Sciences, University of Cape Town, in fulfilment of the requirements for the degree

Masters of Science in Medical Microbiology

Date of Submission: February 2020.

Supervisor: Professor Digby F. Warner

Co-supervisor: Doctor Melissa D. Chengalroyen


"The quality of a person's life is in direct proportion to their commitment to excellence, regardless of their chosen field of endeavour".
Vince Lombardi

Declaration

I declare that this dissertation is my own unaided work; it is being submitted for the degree of Master of Science at the University of Cape Town. It has not been submitted for any degree of examination at any other university.

Signed by candidate

Lucas Raphela

10/02/2020

Date

Abstract

Tuberculosis (TB) is the leading killer globally owing to an infectious disease. There is consequently an urgent need to develop novel TB drugs and shorter regimens to treat the causative agent, *Mycobacterium tuberculosis*, an imperative which demands the identification of new drug targets in essential mycobacterial pathways. To that end, the work presented in this dissertation aimed to functionally characterize *ribF*, an essential gene in the mycobacterial riboflavin (RF; vitamin B_2) biosynthetic pathway. Given the role of RF as a core component of the essential flavin cofactors, flavin mononucleotide (FMN) and flavin adenine dinucleotide (FAD), it was hypothesized that silencing *ribF* would disrupt the biosynthesis of all flavoproteins, crippling numerous (essential) processes within the organism. Moreover, based on previous observations in *Bacillus subtilis*, it was predicted that the mycobacterial *ribF* homolog might play a role in regulating the *rib* operon (comprising a cluster of RF pathway genes) – either directly by binding to the FMN riboswitch, or indirectly through the production of FMN from RF, in turn enabling riboswitch-mediated repression of downstream genes.

CRISPR interference (CRISPRi) technology was used to generate an anhydrotetracycline (ATc)-inducible *ribF* hypomorph of *M. smegmatis*, a widely exploited mycobacterial model. Consistent with other organisms, *ribF* was shown to be essential for *in vitro* growth of *M. smegmatis*: CRISPRi-mediated depletion of *ribF* was bacteriostatic, resulting in a 10-fold growth inhibition in liquid media and corresponding to no reduction (0 log-fold change) in colony forming units (CFU). Moreover, targeted metabolomic analyses revealed that *ribF* depletion was associated with accumulation of 6,7-Dimethylribityllumazine (DMRL), suggesting that the disruption of RibF function blocked conversion of RF to the essential co-factors, FMN and FAD, in turn inhibiting cell growth. Notably, the lethality of *ribF* depletion could not be complemented chemically by exogenous supplementation of growth media with RF, FMN or FAD. Downregulation of *ribF* also caused enhanced susceptibility to the known cell wall-targeting agent, vancomycin, but not to the putative RibF domain inhibitor, thonzonium bromide, suggesting an alternative mechanism of action or impaired bacillary permeation. In summary, these data support the inferred essentiality of *ribF* in mycobacteria, in turn supporting future work which aims to target this enzyme for new TB drug discovery.

Acknowledgements

Foremost, I'd like to thank the **Lord Almighty** for granting me an opportunity not only to have gotten thus far in terms of my academics but also to have lived to the age that I am right now. *Remember life is privilege and not a right*.

To my **Mom, Dad and Grandmother**, I am thankful for their continuous support, prayers and good wishes in everything I've always wanted to pursue. To my younger sister, **Julia**, I hope this dissertation motivates you and shows you that if you put your mind and heart to something, you can achieve it.

To my main supervisor, **Professor Digby Warner**, who has the most humble attitude not to mention his stroke of genius, I would like to express my sincere gratitude for the opportunity you have given me to pursue my postgraduate (MSc) studies with you and for being so transparent, supportive throughout this chapter of my life. Your dedication, heart and passion for science motivates me on a daily and I couldn't have imagined having a better supervisor and mentor.

To my co-supervisor, **Dr Melissa Chengalroyen**, thank you for being so supportive and I personally believe that I wouldn't have come thus far, if it wasn't for you. I have learned a lot from you and your patience and hardworking ethic has made me a better person and scientist professionally. No amount of words can express how grateful I am and I'll forever be indebted to you.

To my friends, **Dr Charles Omollo** and **Rendani Mbau**, I am thankful for receiving me and making this entire experience worthwhile. Despite all our personal challenges, I am proud to see how far we've come and let's keep grinding. The struggle might be real but "*Aluta continua*", comrade. ALL THE BEST WITH YOUR FUTURE ENDEAVOURS.

Last but certainly not least, I would like to thank **Professor Valerie Mizrahi** and the rest of the Molecular Mycobacteriology Research Unit (**MMRU**) lab members for the insightful meetings and all their contributions towards making this dissertation get to the level it is. I certainly couldn't have done any this alone. I appreciate it. In closing, I'd like to thank National Research Foundation (**NRF**), South African Medical Research Council (**SAMRC**) and **MMRU** for their financial support and contributions towards local and international conferences, I am sincerely thankful. It was a privilege to be part of this ecstatic lab, "***MMRU**, my home away from home*".

Presentations

1. **Raphela, M.L.,** Mizrahi, V., Chengalroyen, M.D., and Warner, D.F. Targeted depletion of RibF, a putative bifunctional FAD synthetase/ flavokinase in *Mycobacterium smegmatis*. Poster presented at the WCAIR2019 *Setting our sights on Infectious diseases*, University of Dundee, United Kingdom (UK), 12-15 May 2019.

2. **Raphela, M.L.,** Chengalroyen, M.D., Mizrahi, V., and Warner, D.F. Targeted depletion of RibF, a putative bifunctional FAD synthetase/ flavokinase in *Mycobacterium smegmatis* using CRISPRi. Oral presented at the 13th Annual Early career scientist convention, SAMRC Cape Town, South Africa, 9-11 October 2019.

3. **Raphela, M.L.,** Chengalroyen, M.D., Mizrahi, V., and Warner, D.F. Targeted depletion of RibF, a putative bifunctional FAD synthetase/ flavokinase in *Mycobacterium smegmatis* using CRISPRi. Poster presented at the HUB/IBMS/Pathology Post Graduate Research day, University of Cape Town, South Africa, 26 November 2019.

Table of Contents

List of figures

List of tables

Frequently used abbreviations

µg	Microgram(s)
µl	Microlitre(s)
µM	Micromolar
5-A-RU	5-amino-6-D-ribitylaminouracil
5-OE-RU	5-(2-oxoethylideneamino)-6-d-ribitylaminouracil
5-OP-RU	5-(2-oxopropylideneamino)-6-d-ribitylaminouracil
ab initio	From the beginning
ADP	Adenosine diphosphate(s)
AMP	Adenosine monophosphate(s)
ATc	Anhydrotetracycline
BC	Before Christ
BCG	Bacillus Calmette-Guérin
bp	Base pair(s)
BSA	Bovine serum albumin
CAF	Central analytical facility
cDNA	Complementary DNA
cm	Centimetre(s)
CRISPRi	Clustered regularly interspaced palindromic repeats interference
crRNA	CRISPR RNA
CTAB	cetyl trimethylammonium bromide
$dCas9_{Sth1}$	Deactivated CRISPR-associated protein-9 endonuclease from *Streptococcus thermophilus*
DMB	Dimethylbenzimidazole
DMRL	6,7-Dimethyl-8-ribityllumazine
DMS	Dimethyl sulphide
DNA	Deoxyribonucleic acid
dNTP	Deoxyribonucleotide triphosphate(s)
E. coli	*Escherichia coli*
EDTA	Ethylenediaminetetraacetic acid
EMB	Ethambutol
et al.,	et alia (and others)
EtBr	Ethidium bromide

EtOH	Ethanol
F_0	7,8-didemethyl-8-hydroxy-5-deazaflavin(s)
FAD	Flavin adenine dinucleotide
FADS	FAD synthetase inhibitors
Fe^{3+}	Ferric ion(s)
FMN	Flavin mononucleotide
$FMNH_2$	Reduced FMN
Fwd	Forward
g	Gram(s)
gDNA	Genomic DNA
HIV	Human immunodeficiency virus
hr	Hour(s)
i.e.	*id est* (that is (to say)
IFN	Interferon
IL	Interleukin
INH	Isoniazid
iNKT	Invariant natural killer T cell(s)
JGI IMG/ER	Joint Genome Institute's Integrated Microbial Genomes system-Expert Review
Kan	Kanamycin
KD	Knockdown
KEGG	Kyoto Encyclopedia of Genes and Genomes
KV	Kilovolt(s)
LA	Luria Agar
LB	Luria broth
LCMS	Liquid chromatography mass spectrophotometry
MABA	Microplate alamar blue assay
MAIT	Mucosal associated invariant T cell(s)
mc^2155	*Mycobacterium smegmatis* wild type strain
MDR	Multidrug resistant
MHC	Major histocompatibility complex
MIC	Minimum inhibitory concentration
min	minute(s)
ml	Millilitre(s)

mM	Millimolar
MMRU	Molecular Mycobacteriology Research Unit
mRNA	Messenger RNA
Msm	*Mycobacterium smegmatis*
Mtb	*Mycobacterium tuberculosis*
NaCl	Sodium Chloride
ng	Nanogram(s)
OADC	Oleic Albumin Dextrose Catalase
OD_{600}	Optical density measured at 600 nanometres wavelength
Oligo	Oligonucleotide
PAM	Protospacer adjacent motif
PAS	Para-aminosalicylic acid
PCR	Polymerase chain reaction
pH	Potential of hydrogen
PLZF	Promyelocytic leukemia zinc finger
PZA	Pyrazinamide
qRT-PCR	Real-time polymerase chain reaction
RBP	Riboflavin biosynthetic pathway
RBS	Ribosomal binding site
Rev	Reverse
RF	Riboflavin
RibF	flavokinase or FAD synthetase enzyme
ribF	Gene encoding for flavokinase or FAD synthetase enzyme
RIF	Rifampicin
RNA	Ribonucleic acid
RNAP	RNA polymerase
RoFAD	Roseoflavin adenine dinucleotide
RoFMN	Roseoflavin mononucleotide
RoRγt	Retinoic acid-related orphan receptor γt
rpm	Revolutions per minute
RR	Rifampicin resistant
SD	Standard deviation(s)
SDS	Sodium dodecyl sulphate
s	Second(s)

Seq	Sequencing
sgRNA	Single guide RNA
sigA	Gene coding for RNA polymerase sigma factor A (σ^A)
TAE	Tris-acetate EDTA
TB	Tuberculosis
TCR	T cell receptor
Tfb	Transformation buffer
transcrRNA	Trans-activating crRNA
TY	Trytone yeast
UCT	University of Cape Town
UTR	Untranslated region
UV	Ultra violet
V	Volt(s)
WGS	Whole genome sequencing
WHO	World Health Organization
WT	Wild type
XDR	Extremely drug resistant
Ω	Ohm(s)

Chapter 1: Introduction

1.1 Background

Tuberculosis (TB) is an ancient disease, evidence of which has been identified in Egyptian mummies dating as far back as 2500 BC, yet it continues to plague mankind (Zink et al. 2007). Its causal agent was first described by Robert Koch in 1882 as the "tubercle bacillus" (Sakula 1983) and subsequently named *Mycobacterium tuberculosis* (*Mtb*) in 1886 (Grange 1982). According to the World Health Organization, more than 301 000 new TB cases were reported in South Africa alone in 2018, while the incidence of co-infection with HIV was estimated to be approximately 177 000 cases (WHO 2019). Despite the availability of effective drug regimens, TB remains the number one killer globally owing to an infectious disease: an estimated 21 000 deaths were reported in SA, whereas mortality as a result of co-infection with HIV escalated this to more than 42 000 deaths (WHO 2019). Hence, TB is considered an "opportunistic infection", commonly afflicting those with HIV or immunosuppressive ailments (Holmes et al. 2003; Fenner et al. 2013).

Mycobacterium bovis Bacille Calmette-Guérin (BCG) is the only vaccine against TB, but its protective efficacy is limited to infants and wanes as individuals approach adolescence (Mangtani et al. 2014). Moreover, a negative effect of BCG use has been observed in HIV-positive infants and severely immunodeficient individuals in whom vaccination can lead to disseminated BCG infection and adverse complications, thus posing an enormous threat to patients residing in high HIV-TB disease prevalent countries (Hesseling et al. 2007). While administration of the BCG vaccine has been shown to provide effective partial immunity against TB in animal models, it does not afford a complete clearance of infection (Hinchey 2007). Notably, very recent work suggests that shifting from intradermal to intravenous delivery can dramatically improve efficacy, though this result is still to be validated in humans (Darrah et al. 2020). As administered currently, the effect of the vaccine remains inconsistent and ranges from 0-80% depending on the geographical region and local TB burden (Andersen and Doherty 2005; Fine 1995).

Modern anti-TB drug therapy, which has proven to be very effective in treating patients with drug-susceptible *Mtb* infection, began with the introduction of streptomycin and *para*-aminosalicylic acid dual therapy in the 1940s (**Figure 1.1**) (Feldman et al. 1945; Lehmann 1946; Mitchison and Davies 2012). The currently recommended TB regimen comprises a phased multidrug combination, beginning with an intensive phase of rifampicin (RIF), isoniazid (INH), pyrazinamide (PZA) and ethambutol (EMB) (**Figure 1.1**) for a period of two months (Luciani et al. 2009). Subsequently, an extended "continuation phase" comprising treatment with RIF and INH is utilized to eradicate any remaining bacilli. These drugs are given to patients who have never been on anti-TB treatment before or have been on treatment for less than a month and are considered "new patients", presumably carrying drug-susceptible *Mtb* (WHO 2010).

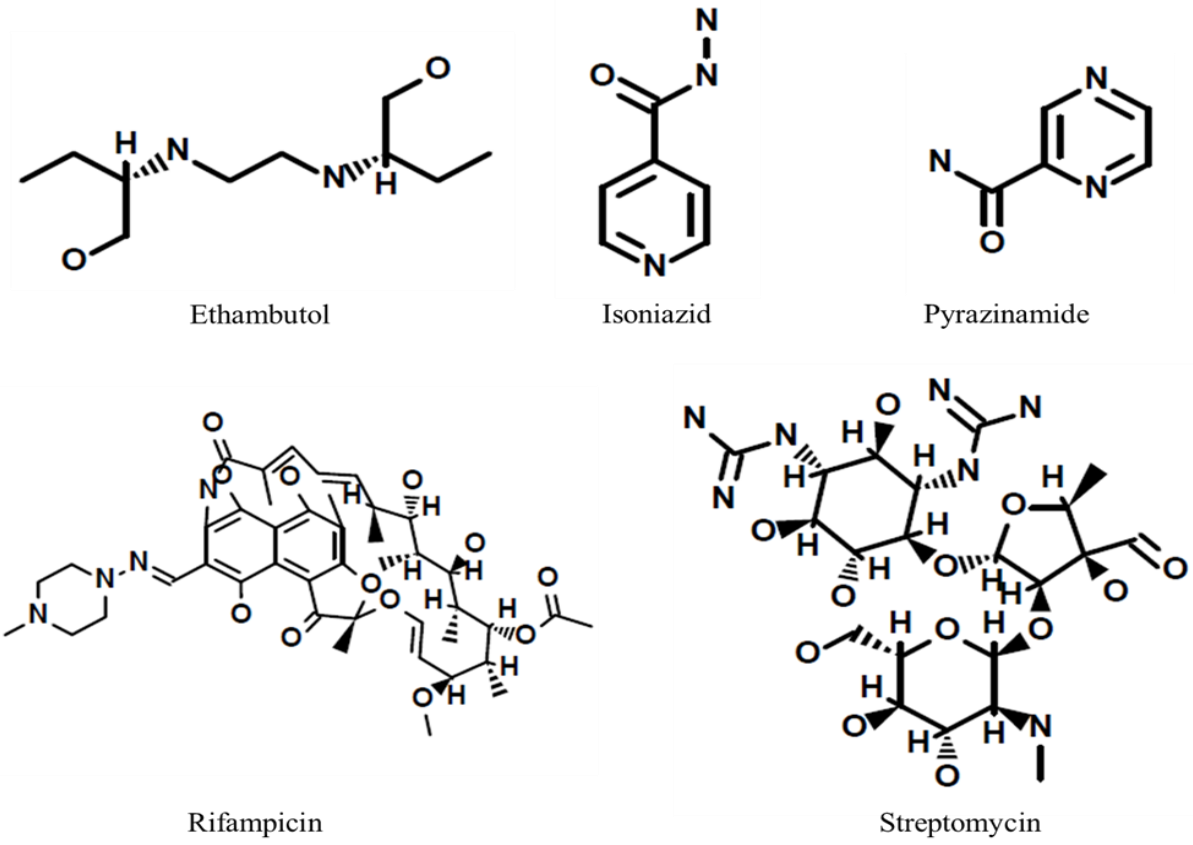

Figure 1.1: Diverse molecular structures of efficacious first line anti-TB drugs used to treat *Mtb (adapted from PubChem Sketcher V2.4).*

However, the major challenge with modern drug therapies is the emergence of drug resistance, and TB disease is no exception with 11 000 new MDR/ rifampicin resistance (RR) TB cases reported in South Africa in 2018 (WHO 2019). Drug resistance is divided into four

categories: mono-resistance, which describes resistance to any single first-line drug; multidrug resistance (MDR-TB) is classified as *Mtb* infection that does not show susceptibility to INH and RIF; and extensively drug resistant (XDR) *Mtb*, defined as MDR plus resistance to any fluoroquinolone in conjunction with one of the three second line injectables: amikacin, capreomycin or kanamycin (WHO 2014b, 2006). In addition, a newly described TB drug resistance has been identified as RR which describes resistance to RIF either as mono- or poly-resistance *i.e.*, MDR or XDR (WHO 2016b). Notably, the newly approved anti-TB drugs, bedaqualine and delamanid, have been licensed for the treatment of both MDR- and XDR-TB (Gler et al. 2012; Cohen 2013). However, both drugs must be used for a standardized period of 24 weeks and are restricted to patients with no other therapeutic options (WHO 2014a).

Bedaquiline is a diarylquinoline (R207910), the first drug in a novel class approved for TB treatment since the approval of rifampicin in 1971 (Avorn 2013). Diarylquinolines are considered similar to quinolones but do not inhibit DNA gyrase, instead targeting the essential, membrane-bound mycobacterial adenosine triphosphate (ATP) synthase, thus interfering with energy production and intracellular metabolism (Andries, Verhasselt, Guillemont, Gohlmann, et al. 2005). Delamanid, previously known as OPC-67683, was derived from the class of nitro-dihydro-imidazooxale compounds which potently inhibit mycolic acid synthesis, an essential component of the mycobacterial cell wall (Matsumoto et al. 2006). Despite compelling evidence that both drugs are potent in targeting specific enzymes from different metabolic pathways, there still exists a need to identify novel drug target candidates within other essential pathways since separate resistances to these drugs have already been detected in patients (Somoskovi et al. 2015; Hartkoorn, Uplekar, and Cole 2014). To that end, the project detailed here was motivated by the need to identify new metabolic targets in essential mycobacterial pathways; specifically, with the aim of elucidating the function and putative essentiality of RibF, a predicted enzyme in the biosynthesis of riboflavin, precursor of the flavin cofactors, flavin mononucleotide (FMN) and flavin adenine dinucleotide (FAD).

1.2 The riboflavin biosynthetic pathway (RBP)

Riboflavin (RF; also known as vitamin B_2) is an essential biochemical component in the cellular metabolic functioning of all life forms and was the third vitamin to be discovered after thiamine (Northrop-Clewes and Thurnham 2012). RF, which comprises an isoalloxazine ring structure linked to a ribityl ring chain at the N10 position (Edwards 2014) (Beztsinna et al. 2016), is a precursor of FMN and FAD, both of which serve as cofactors for multiple metabolic enzymes (**Figure 1.2**). Notably, vertebrates do not have the ability to synthesize RF and must obtain the vitamin from their diets whilst many plants, fungi and microorganisms can generate the vitamin *de novo* (Vogl et al. 2007).

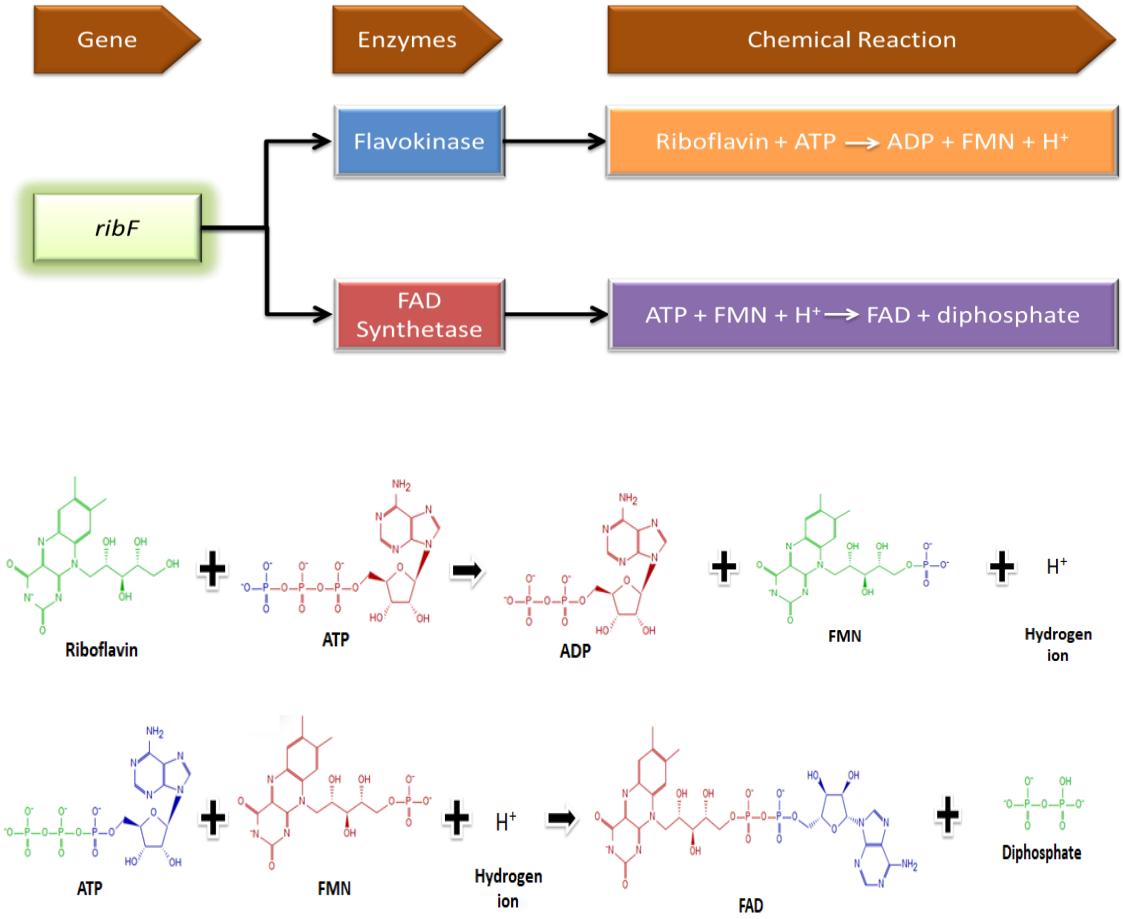

Figure 1.2: Schematic of the RibF-catalyzed conversion of RF to FAD via an FMN intermediate *(adapted from Biocyc).*

In *Mycobacterium smegmatis* (*Msm*), it is postulated that RF is generated by two pathways: through purine metabolism, and via the pentose phosphate route. The enzymes pyrimidine deaminase/reductase (encoded by *ribD*; MSMEG_3067), α-subunit RF synthase (encoded by *ribE*; MSMEG_3071), GTP cyclohydrolase (encoded by *ribAB*; MSMEG_3072), 3,4-dihydroxy 2- butanone 4- phosphate (3,4-DHBP) synthase (also encoded by *ribAB*; MSMEG_3072) and β-riboflavin synthase subunit (*ribH*; MSMEG_3073) produce one RF molecule from a single molecule of guanosine-5-triphosphate (GTP) and two ribulose-5-phosphate molecules (**Figure 1.3**). The genomic context of all RF related genes is provided in **Supplementary figure S2**. The *Mtb* homologs of all RF genes and their functional annotations are listed in **Supplementary table 1**. RF on its own has limited functions and needs to be transformed into its derivatives, the biologically active flavins to fulfil its major role as a source of flavin cofactors. In the cell, RF undergoes a biochemical reaction with flavokinase, an enzyme that utilizes adenine triphosphate (ATP) to generate FMN. Most flavoenzymes require FAD as a cofactor; therefore FAD synthetase must further transform FMN to FAD by attachment of AMP to the pre-phosphorylated FMN molecule, releasing two phosphates (**Figure 1.2**).

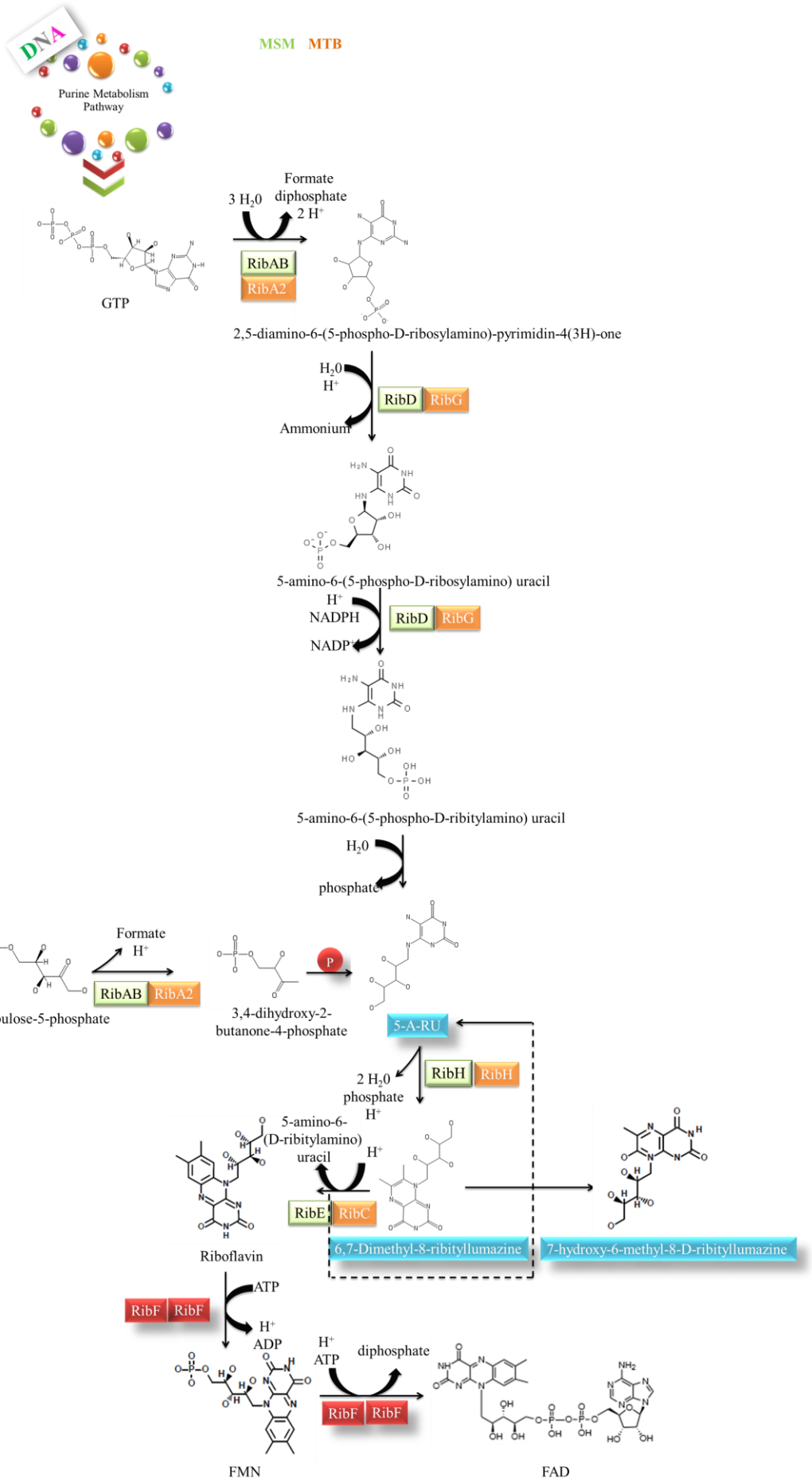
MSM MTB
DNA
Purine Metabolism Pathway
GTP
3 H20
Formate
diphosphate
2 H+
RibAB
RibA2
2,5-diamino-6-(5-phospho-D-ribosylamino)-pyrimidin-4(3H)-one
H20
H+
Ammonium
RibD
RibG
5-amino-6-(5-phospho-D-ribosylamino) uracil
H+
NADPH
NADP+
5-amino-6-(5-phospho-D-ribitylamino) uracil
H20
phosphate
Pentose Phosphate Pathway
Ribulose-5-phosphate
Formate
H+
3,4-dihydroxy-2-butanone-4-phosphate
P
5-A-RU
2 H20
phosphate
H+
RibH
5-amino-6-(D-ribitylamino) uracil
Riboflavin
RibE
RibC
6,7-Dimethyl-8-ribityllumazine
7-hydroxy-6-methyl-8-D-ribityllumazine
ATP
RibF
ADP
FMN
diphosphate
FAD

Figure 1.3A: Predicted RF biosynthetic pathway in *Msm*. The schematic is inferred from the known *B. subtilis* pathway. Pathways are indicated by coloured circles and enzymes responsible for the indicated biotransformations are indicated in rectangles. The enzymes in orange represent *Mtb* homologs of the proposed *Msm* genes (green) in the pathway and immune activating ligands (discussed later) are represented by blue rectangles. RibF, the enzyme which serves as the focus of this project, is highlighted in red rectangles. Note that genetic nomenclature differs across the model bacteria: the bifunctional pyrimidine deaminase/ reductase enzyme (*ribG*) and α-subunit of riboflavin synthase (*ribB*) in *B. subtilis* are named *ribD* and *ribE*, respectively, in *E. coli*. Furthermore, separate genes, *ribB* and *ribA*, code for 3, 4-DHBP synthase and GTP cyclohydrolase, respectively in *E. coli* whereas the same functions are performed by a single *ribA*-encoded enzyme in *B. subtilis (adapted from NCBI Pubmed Biosystems pathway)*.

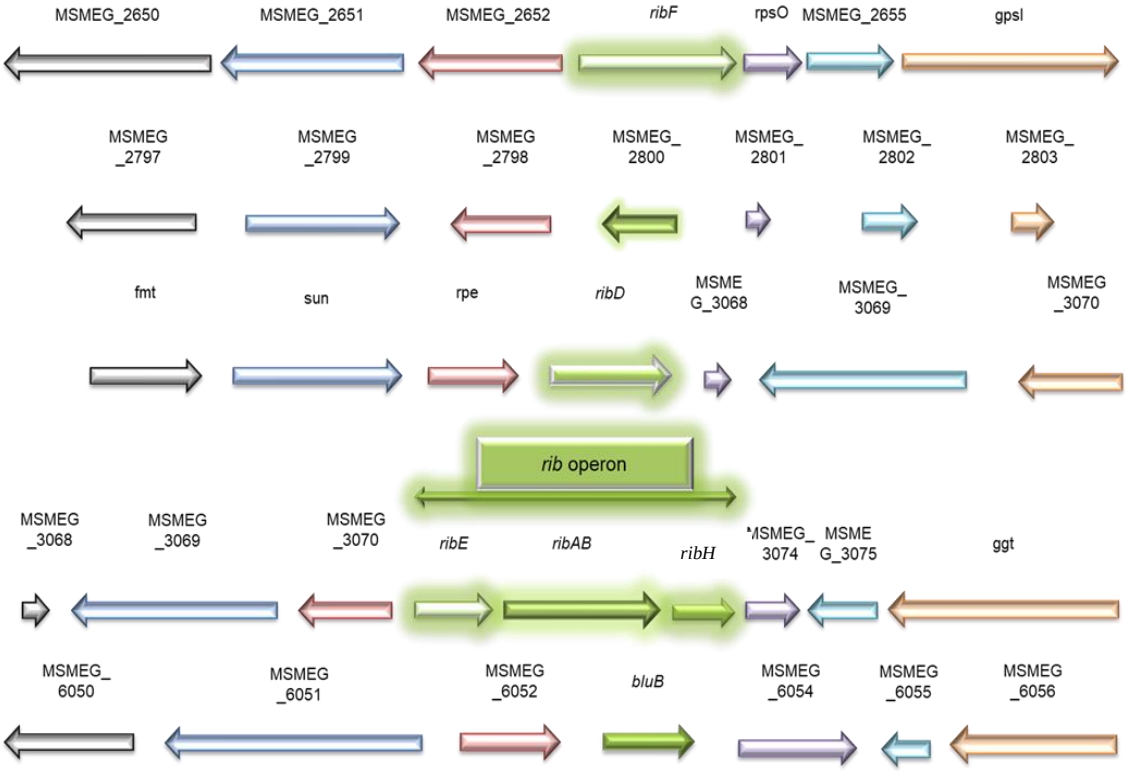

Figure 1.3B: Genomic context of the proposed *rib* genes in *Msm.* Green highlighted genes represent those that participate directly in the RF biosynthetic pathway while non-green highlighted genes located on the left are upstream while those downstream are located on the right of the proposed RBP genes. The putative *rib* operon which comprises genes involved in RF production are also shown *(adapted from the Mycobrowser database, https://mycobrowser.epfl.ch/)*

1.3 The regulation of RF biosynthesis

The RF biosynthetic pathway has not been studied in detail in mycobacteria; therefore, the pathways presented here are based on those elucidated in the model organisms, *E. coli* and *B. subtilis*.

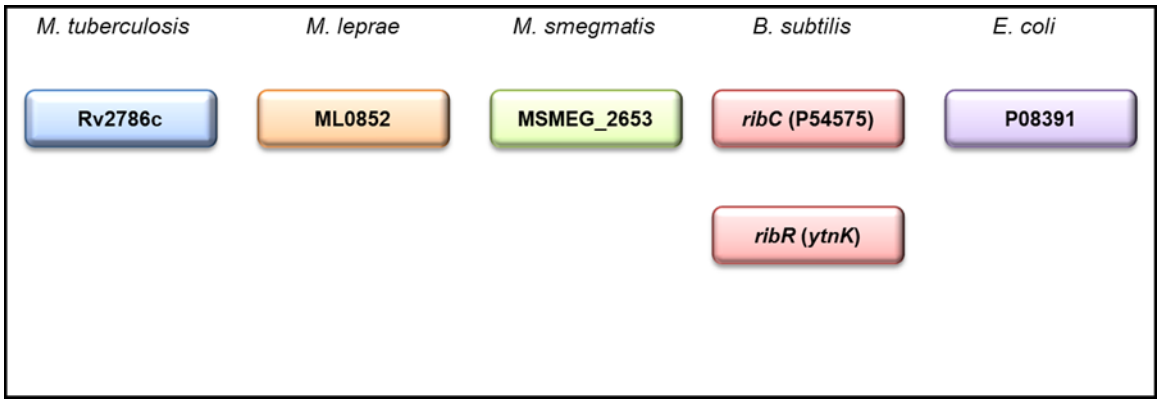

Figure 1.4: Annotation of *ribF* homologs in various microorganisms including model bacteria in which the RF biosynthetic pathway is most studied. *(Mycobacterium species and model bacteria homologs adapted from Mycobrowser [https://mycobrowser.epfl.ch/] and Genolist [[http://genolist.pasteur.fr/] databases respectively).*

In *B. subtilis*, the production of RF is controlled by two regulators, RibC and RibR (**Supplementary figure S4**). RibC is a bifunctional flavokinase/ FAD synthase, similar to mycobacterial RibF (**Supplementary figure S3**) (Mack, van Loon, and Hohmann 1998a), while RibR encodes a monofunctional flavokinase involved in regulating the *rib* operon (RF biosynthetic gene operon) (Solovieva et al. 1999). The inactivation of either gene leads to RF accumulation (Azevedo et al. 1993). In *B. subtilis*, the genes *ribDG-E-AB-H* constitute a solitary transcriptional unit, the expression of which is controlled by a FMN riboswitch (Mironov et al. 2002a; Winkler, Cohen-Chalamish, and Breaker 2002a) (**Figure 1.5**).

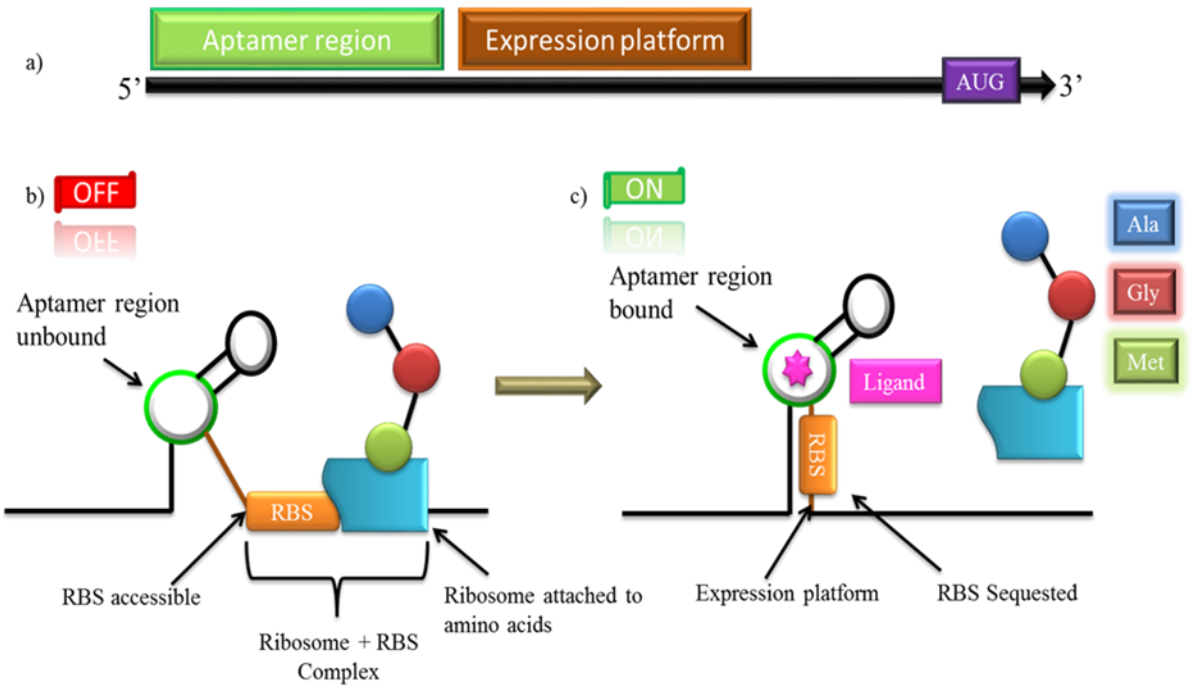

Figure 1.5: Structure of a typical riboswitch. The aptamer domain (green) carries the ligand binding site and the expression platform (brown) adopts a structural conformational change dependent on binding of the effector molecule (pink) which will lead to transcriptional termination or either translational impotence (Garst, Edwards, and Batey 2011).

Bacterial riboswitches are localised in the untranslated region (UTR) of mRNAs that have the capability to bind to natural ligands to regulate the expression of downstream genes (Winkler, Cohen-Chalamish, and Breaker 2002a; Mironov et al. 2002b; Mellin and Cossart 2015; Winkler and Breaker 2005). Structurally, riboswitches possess two functionally distinct segments; an aptamer region containing the ligand binding domain and a regulatory expression platform to regulate downstream genes (Mellin and Cossart 2015; Winkler and Breaker 2005). Mechanistically, upon cognate ligand-aptamer region binding, a conformational alteration is induced in the expression platform to regulate gene expression either through transcriptional attenuation or sequestration of the ribosomal binding site, thereby inhibiting translation (Winkler, Cohen-Chalamish, and Breaker 2002a; Mironov et al. 2002a).

This "*ribDG* FMN riboswitch" is embedded in the 5' untranslated region of the bacterial mRNA and can efficiently control gene expression through alterations in its secondary structure upon binding of the small metabolite, FMN, to the aptamer region

(Mironov et al. 2002a; Winkler, Cohen-Chalamish, and Breaker 2002a; Winkler and Breaker 2005). A second FMN riboswitch is located in the 5' UTR of *ribU* (*ypaA*) (Vogl et al. 2007) which codes for a putative RF transporter (Kreneva et al. 2000).

Thus, upon binding of FMN to the riboswitch, *ribU* translation initiation is impeded through a mechanism involving ribosomal binding site sequestration (Winkler, Cohen-Chalamish, and Breaker 2002a). RibR in *B. subtilis* can act as a positive regulator to overcome repression mediated by the FMN riboswitch, thereby allowing *rib* gene expression under excessive intracellular concentrations of the cofactor FMN by directly interacting with the aptamer region of the riboswitch (Higashitsuji et al. 2007). It is believed that bacteria have evolved this regulatory mechanism to cope with increased levels of FMN when sulphur metabolism is taking place due to co-expression of *ribR* and sulphur compound uptake and degradation factors (Pedrolli, Kuhm, et al. 2015).

Iron levels can also affect the expression of the RF pathway in certain bacteria, likely due to the importance of the flavin cofactors in iron metabolism. In the methanotrophic *Methylocytis* species, flavin secretion levels are increased under iron depletion (Balasubramanian, Levinson, and Rosenzweig 2010). Similarly, the *rib* operon of *Caulobacter crescentus*, an aquatic bacterium, shows upregulated expression when subjected to iron limiting conditions. Furthermore, mutations in the ferric uptake repressor, *fur*, have been shown to induce *rib* transcript overexpression and a putative *fur* binding site was identified in the upstream region of the *rib* operon in this species (da Silva Neto, Lourenco, and Marques 2013).

1.4 Inhibiting FMN riboswitch function

Streptomyces davawensis JCM 4913 (Otani et al. 1974) and *S. cinnabarinus* (Jankowitsch et al. 2012) both synthesize roseoflavin (RoF), an antibiotic structurally similar to RF. This natural chemical analogue is converted to the non-functional cofactor analogues, roseoflavin mononucleotide (RoFMN) and roseoflavin adenine dinucleotide (RoFAD), respectively, via the RibF enzyme domains, flavokinase and FAD synthetase. The mode of action of RoFMN involves binding and downregulating the genes controlled by the FMN riboswitch and has been observed in *Listeria monocytogenes*, *S. coelicolor* and *B. subtilis* (Lee, Blount, and Breaker 2009; Mansjo and Johansson 2011; Ott et al. 2009). When *E.coli* is exposed to RoF, the modified flavins get incorporated into flavoproteins, either adversely affecting their functioning or completely inactivating the enzymes (Grill et al. 2008; Langer et al. 2013;

Walsh et al. 1978). However, in humans (Pedrolli et al. 2011), *B. subtilis* (Grill et al. 2008), *Streptomyces coelicolor* and *S. davawensis* (Pedrolli et al. 2012), the same biochemical reaction is carried out by RibC, a RibF homolog. The biosynthesis of RoF in *S. davawensis* is achieved by three enzymes: first, 8-demethyl-8-aminoriboflavin-5'-phosphate synthase (RosB) converts FMN to 8-demethyl-8-aminoriboflavin mononucleotide (AFMN), an essential RoF intermediate (Schwarz et al. 2016). Next, an unidentified phosphatase catalyses the reaction that converts AFMN to 8-demethyl-8-aminoriboflavin (AF) and, finally, RoF is produced as a result of catalysing AF and *S*-adenosylmethionine by *N*,*N*-8-demethyl-8-aminoriboflavin dimethyltransferase (RosA) (Jankowitsch et al. 2011; Tongsook et al. 2016).

Also, *ribB-M-A-H* and *ribG* have been shown to be responsible for the synthesis of RF in *S. davawensis* and *S. coelicolor* and encode enzymes similar to the *B. subtilis* genes *ribG-B-A-H* that catalyse this synthesis (Grill et al. 2007). Moreover, *ribM* encodes a riboflavin permease which plays a role in importing RoF into the cell (Hemberger et al. 2011). There is also evidence suggesting that *ribB-M-A-H* might be regulated by an FMN riboswitch, based on sequence analysis of the upstream region (Grill et al. 2007). Binding of FMN to the aptamer region of the *ribB* FMN riboswitch is thought to inhibit translation initiation of the *ribB-M-A-H* mRNA (Vitreschak et al. 2002a) in contrast to transcription termination as observed for the *ribG* FMN riboswitch in *B. subtilis* (Winkler and Breaker 2005; Mironov et al. 2002a).

1.5 The role of flavoproteins in cellular processes

Flavin cofactors are necessary for flavoprotein cellular redox reactions and it has been suggested that approximately 1-3% of genes code for flavoproteins in bacteria and eukaryotes (De Colibus and Mattevi 2006). These proteins are involved in abundant energetic reactions such as fat and carbohydrate metabolism, protein metabolism, oxidative stress, photosensitization, and vitamin activation of folate and pyridoxine (Ashoori and Saedisomeolia 2014; Beztsinna et al. 2016; Haase et al. 2014). Their crucial role in metabolic reactions owes to their unique ability to mediate reactions that involve transferring either one or two electrons (Edwards 2014). In addition, they have the capacity to facilitate redox processes such as DNA repair, circadian cycling, light sensing and fruit body development, reinforcing their essentiality in cellular functionality (Tagua et al. 2015; Takahashi 2015; Xu et al. 2015; Christie et al. 2015; Yang et al. 2016). Furthermore, flavins play a role in extracellular mechanisms as illustrated by the marine bacterium, *Marino* sp., which utilizes

dimethyl sulphide (DMS) as a source of sulphur under light emitting conditions. These bacteria secrete photosensitizers, FAD and RF, which undergo catalytic reactions that photooxidize DMS to dimethyl sulphoxide. The presence of FAD induces methanesulphonate, formate, formaldehyde and sulphate production which this organism uses as a sulphur source (Hirano et al. 2003).

It has been theorized that the intestinal pathogen *Campylobacter jejuni* can increase bioavailable iron by extracellular insoluble ferric iron reduction (Fe^{3+}) into soluble ferrous iron (Fe^{2+}); the synthesis of RF intensifies this reductive activity (Crossley et al. 2007). It has also been recognized that RF secreted by *Acidobacteria geothrix fermentans* can act as a secondary electron shuttle which plays a role in approximately 20-30% of electron transfer activities under reduced iron conditions (Mehta-Kolte and Bond 2012). RF secreted by *Shewanella* sp. reduces Fe^{3+} oxides (von Canstein et al. 2008) by directly mediating electron transfer to an electron acceptor electrode (Marsili et al. 2008). Furthermore, the flavin electron shuttle serves as the main extracellular electron transfer system either through direct contact or via nanowires with FAD secretion mediated by the FAD exporter enzyme, Bfe (Kotloski and Gralnick 2013). In addition, recent work illustrated the ability of alkaphilic bacterial consortia to utilize extracellular Fe^{3+} as a distinct electron acceptor under anaerobic respiration where the rate at which Fe^{2+} produced is dependent on the quantity of extracellular RF (Fuller et al. 2014). Surprisingly, the Gram-positive bacterium, *Desulphotomaculum reducens*, has the ability to secrete RF, utilizing this as an electron shuttle in the presence of pyruvate; this occurs through the solid-phase as hydrous ferric oxide gets reduced. However, in these conditions, bacterial growth is modulated by pyruvate fermentation rather than Fe^{3+} respiration, with iron reduction used to dispose of reducing equivalents (Dalla Vecchia et al. 2014).

Apart from RF derivatives, other molecules such as deazaflavins are responsible for mediating a broad range of redox reactions with the aid of flavin-dependent enzymes in an array of biological systems (Hemmerich, Nagelschneider, and Veeger 1970; Walsh 1980). FMN and FAD are therefore widely used cofactors that play an integral part in metabolic reactions across three domains of life; bacteria, archaea and eukarya. However, relatively few organisms have the ability to synthesize and utilize 5-deazaflavins (O'Brien, Weinstock, and Cheng 1967; O'Brien, Weinslock, and Cheng 1970). These compounds are structurally similar to flavins whereby the carbon atom acts as a substitute for the N5 atom of the isoalloxazine ring. Of an array of such compounds, two are found to be biologically relevant:

specifically, 7,8-didemethyl-8-hydroxy-5-deazaflavin (F_0) and its lactyl oligoglutamate phosphodiester derivative (F_{420}) (Cheeseman, Toms-Wood, and Wolfe 1972; Eirich, Vogels, and Wolfe 1978). Generally, the role of F_{420} in bacteria is not fully understood but has been experimentally shown to be synthesized in a single bacterial phylum: the *Actinobacteria* (Saviola and Bishai 2006) which includes the genus, *Mycobacterium*. Phenotypic and biochemical studies have shown evidence of F_{420} synthesis as well as metabolic function and reduction by all members of the Mycobacterial genus including saprophytes, *i.e.*, *Msm*, *M. fortuitum*, the opportunistic pathogens, *M. avium* and *M. kansasii*, and the human pathogens, *Mtb* Complex and *M. leprae* (Lin and White 1986; Bair, Isabelle, and Daniels 2001; Purwantini, Gillis, and Daniels 1997).

Despite massive genome decay (Cole et al. 2001), the observation that *M. leprae* is capable of synthesizing F_{420} supports an evolutionarily conserved role in mycobacterial metabolism. As opposed to methanogens, F_{420} is not considered essential for optimal growth of mycobacteria under standard conditions *in vitro*: the F_{420} biosynthetic gene, *fbiC*, and the F_{420}-dependent glucose-6-phoshphate dehydrogenase, *fgd* – implicated in the mechanism of action of (and resistance to) nitroimidazoles including pretomanid (Baptista et al. 2018) – have successfully been disabled in *Msm* (Taylor et al. 2010; Purwantini and Mukhopadhyay 2009), *Mtb* (*fgd1*) (Gurumurthy et al. 2013; Manjunatha et al. 2006), and *M. bovis* (Choi, Kendrick, and Daniels 2002). However, a range of studies have shown that F_{420} is required under unfavourable conditions (Boshoff and Barry 3rd 2005). Mycobacterial strains unable to synthesize F_{420} are unfit to survive oxygen deprivation, oxidative stress, nitrosative stress or antibiotic treatment (Purwantini and Mukhopadhyay 2009; Gurumurthy et al. 2013; Hasan et al. 2010).

Numerous enzymes have been annotated in mycobacteria which are functionally dependent on F_{420}. The pathogenic *Mtb* codes for the F_{420}-reducing hydroxymycolic acid dehydrogenase (fHMAD) which oxidizes hydroxymycolic acids to ketomycolic acids in the cell wall (Bashiri et al. 2012; Purwantini and Mukhopadhyay 2013). The mycolic acid derivatives participate in the integrity and permeability of the cell envelope causing them to be less susceptible to cytotoxic agents such as antibiotics (Yuan et al. 1998; Dubnau et al. 2000; Sambandan et al. 2013). Furthermore, preliminary data indicate that the flavin/ deazaflavin oxidoreductase superfamily (FDOR-AAs) might also be involved in fatty acid modification, in contrast to other members of the FDOR-Bs superfamily which reduce the degradation of products formed as a result of heme oxygenation (Ahmed et al. 2015),

including biliverdin produced by host heme oxygenase-1 and mycobacterial HugZ in the carbon monoxide (CO) generating pathway and mycobilin produced mycobacterial MhuD in the CO bypass pathway (Kumar et al. 2008; Nambu et al. 2013; Contreras et al. 2014).

1.6 Activation of mucosal-associated invariant T (MAIT) cells by microbial RF derivatives

The host immune system functions to distinguish self from non-self, thus defending against any potential opportunistic invaders (Pancer and Cooper 2006). Very simply, it is divided into innate and adaptive immunity, which differ primarily in the defence mechanisms employed, their time dependence, and their capacity for memory (Janeway 2001), although recent studies elucidating "trained immunity" suggest a more complex interplay (Netea et al. 2016). The innate response serves as the first line of defence since it utilizes the germline-encoded receptors for pathogen recognition and is mostly non-specific. Interaction with these innate receptors induces classical responses such as apoptosis, cytokine release, degranulation and phagocytosis (Medzhitov and Janeway 2002). In contrast, the adaptive response is highly diversified and specific, and utilizes lymphocytes such as B- and T-cells, particularly $CD4^+$ and $CD8^+$ T cells, which form part of the "delayed" adaptive immune response. Adaptive immunity is primarily based on recognition of foreign bodies by antigen-specific receptors expressed on B- or T-cell surfaces (Boehm and Bleul 2007). The adaptive response has classic features, as it relies on clonal expansion and is delayed by 4 to 7 days prior to adaptive response initiation (Janeway 2001). MAIT and invariant Natural killer T (iNKT) cells, referred to as "innate-like" T cells, are semi-invariant cells that recognize non-classical Major Histocompatibility Complex 1 (MHC 1) presenting antigens; that is, the CD1d molecule is recognized by iNKT cells (Kinjo et al. 2011) whereas non-classical MHC class 1, MR1, is recognized by MAIT cells (Keller, Corbett, et al. 2017), in contrast to $CD8^+$ and $CD4^+$ T cells that recognize MHC I and MHC II presenting antigens, respectively (Boehm and Bleul 2007).

MAIT cells are part of a healthy mucosal immune system and are essential in the control of bacteria in these tissue sites. They also have a high population density in the liver, colon lamina propria, lung and female genital tract; constituting approximately 20-40%, 1-8%, and 10-20% of resident T cells in these locations, respectively (Tang et al. 2013; Sundstrom et al. 2015; Treiner et al. 2003; Le Bourhis et al. 2010; Gibbs et al. 2017). MR1-restricted T (MR1T) cells are a subset of T cells that express diverse T Cell Receptor (TCRs)

and react to cells that express MR1 without possession of microbial ligands (Lepore et al. 2017). MAIT cells are regarded as MR1T subsets that express a semi-invariant T-cell receptor composed of unique Vα 7.2-Jα33, Jα12 or Jα20 segment rearrangement and Vβ limited repertoire (Reantragoon et al. 2013; Lepore et al. 2014). Human MAIT cells are classified by their co-expression of the semi-invariant TCRwith an abundant expression of C-type lectin CD161 and the α-subunit of the interleukin 18 receptor (IL-18R) and are highly dependent on the expression of promyelocytic leukemia zinc finger (PLZF) and retinoic acid-related orphan receptor γt (RoRγt), an innate-like transcription factor that highlights their peculiar functions (Dusseaux et al. 2011; Martin et al. 2009; Le Bourhis et al. 2010). These cells are able to induce an innate-like immune response despite being T cells (Treiner et al. 2003; Martin et al. 2009), allowing them to respond at high specificity without the time-lag experienced by the traditional adaptive response, preventing any further pathogen manifestations.

MAIT cells recognize a specific group of microorganisms which includes *Mtb*, *E. coli*, *Lactobacillus* sp. and fungi such as *Candida albicans*, but viruses instead stimulate their activation in an MR1-independent manner. Upon induction, MAIT cells produce pro-inflammatory cytokines – interferon-γ (IFNγ), tumour necrosis factor (TNF), IL-22 and IL-17A and cytotoxic mediators such as granzyme B and perforin, as a response mechanism to potential infection (Gold et al. 2010). MAIT cells recognize a novel class of antigens; in particular, microbial RF-derived metabolites and degraded folic acid derivatives (Kjer-Nielsen et al. 2012). Kjer-Nielsen and colleagues were the first to report 6-formylpterin (6-FP) and 6-(rRL-6-CH_2OH) as MR1 binding ligands (Kjer-Nielsen et al. 2012) which are products of folic acid degradation. Although crystallography data revealed that these products covalently bind to the Lys 43 of the MR1 groove, they do not induce MAIT cell activation (Kjer-Nielsen et al. 2012; Lopez-Sagaseta, Dulberger, Crooks, et al. 2013; Lopez-Sagaseta, Dulberger, McFedries, et al. 2013) but rather antagonize MR1T as a result of competing with other activating ligands (Harriff et al. 2016). More recently, novel bacterial MR1T ligands that have been identified include 7,8-didemethyl-8-hydroxy-5-deazariboflavin (F_0), photolumazine I (PLI) and photolumazine III (PLIII), all secondary products of the RF pathway (Harriff et al. 2018). Also, mass spectrometry used to analyse cell supernatants from *Salmonella typhimurium*, identified rRL-6-CH_2OH as a MR1 ligand. Importantly, rRL-6-CH_2OH is structurally similar to RF precursors and, as such, is considered a secondary metabolite that can robustly activate TRAV1-2^+ MAIT cells, contrary to 6-FP (Kjer-Nielsen

et al. 2012; Lopez-Sagaseta, Dulberger, Crooks, et al. 2013; Lopez-Sagaseta, Dulberger, McFedries, et al. 2013).

Following the identification of 6-FP and rRl-6-CH_2OH, a considerable number of MR1 ligands began to emerge. These include two pyrimidine single-ringed compounds, 5-(2-oxopropylideneaminouracil)-6-D-ribitylaminouracil (5-OP-RU) and 5-(2-oxoethylideneamino)-6-D-ribitylaminouracil (5-OE-RU) (**Figure 1.6**), which are regarded as by-products of both bacteria and host cell glycolysis and have the capability to potently activate MAIT cells (Greene et al. 2017; Corbett et al. 2014). These molecules are products derived from the chemical reaction between the RF biosynthetic intermediate, lumazine precursor (5-amino-6-D-ribitylaminouracil; 5-A-RU) and methylglyoxal and glyoxal (**Figure 1.6**), and bind in the MR1 groove (Corbett et al. 2014).

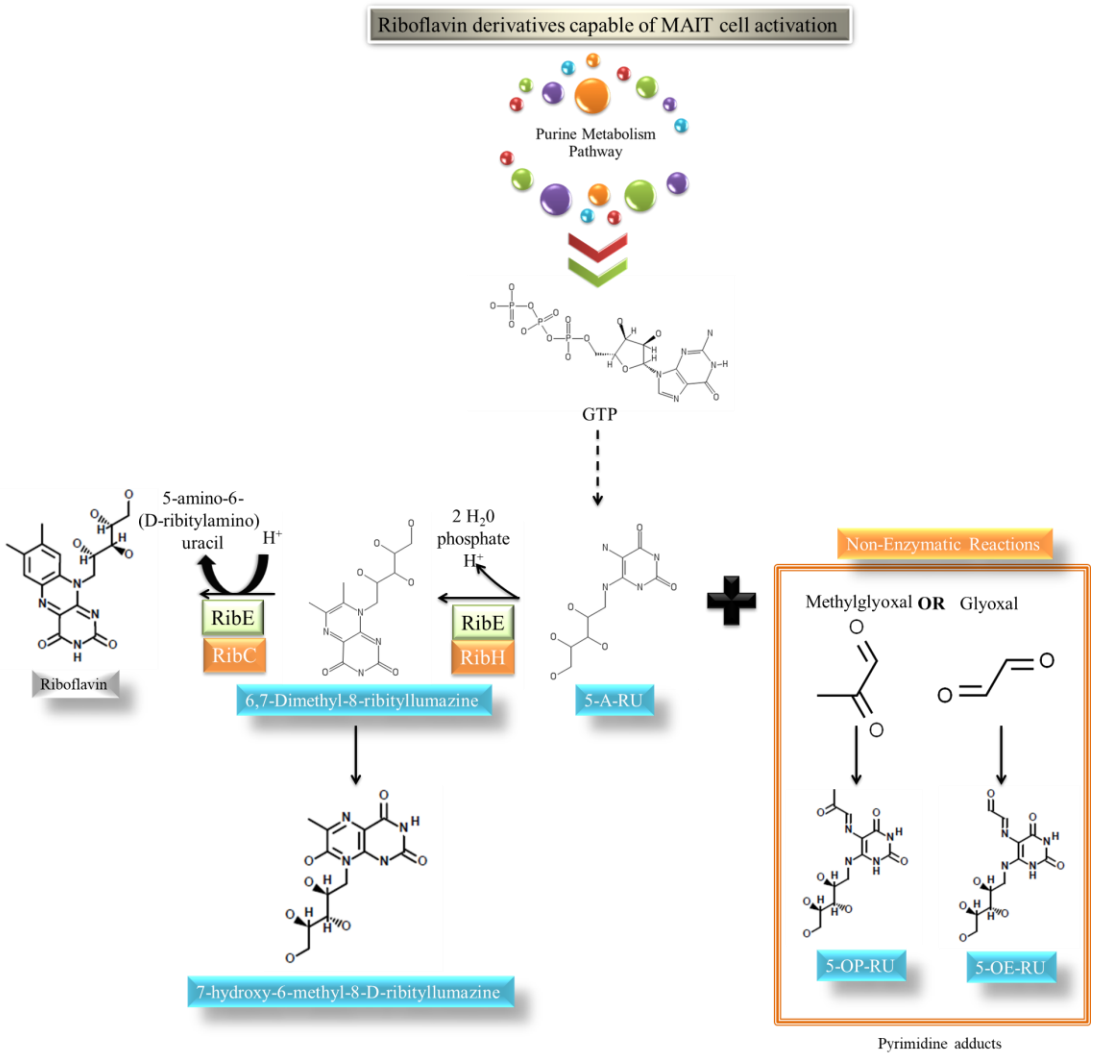

Figure 1.6: Schematic diagram of MAIT cell antigens generated from the RF pathway. Potent RF ligands capable of inducing MAIT cell activation are highlighted in blue rectangles: 7-Hydroxy-6-methyl-8-ribityllumazine, 6,7-Dimethyl -8-ribityllumazine, 5-OE-RU and 5-OP-RU. 5-A-RU acts as a precursor that generates 5-OE-RU and 5-OP-RU as the result of a biochemical reaction with glyoxal and methylglyoxal, respectively.

Accordingly, unstable lumazine compounds, 7-hydroxy-6-methyl-8-D-ribityllumazine and 6,7-dimetyl-8-D-ribityllumazine (**Figure 1.6**), have also proven to act as MR1 ligands which led to strong MAIT cell stimulation (Meermeier et al. 2016; Patel et al. 2013). Despite RF metabolites being the main metabolites to induce activation of MAIT cells, there is evidence that these cells can be activated by other ligands; for example, Meermeier et al. illustrated TRAV12-2^{+} MR1- restricted T cell recognition from a bacterial *Streptococcus pyogenes* strain which was incapable of synthesizing RF (Meermeier et al. 2016) but were not able to identify the non-RF substrate responsible for activation.

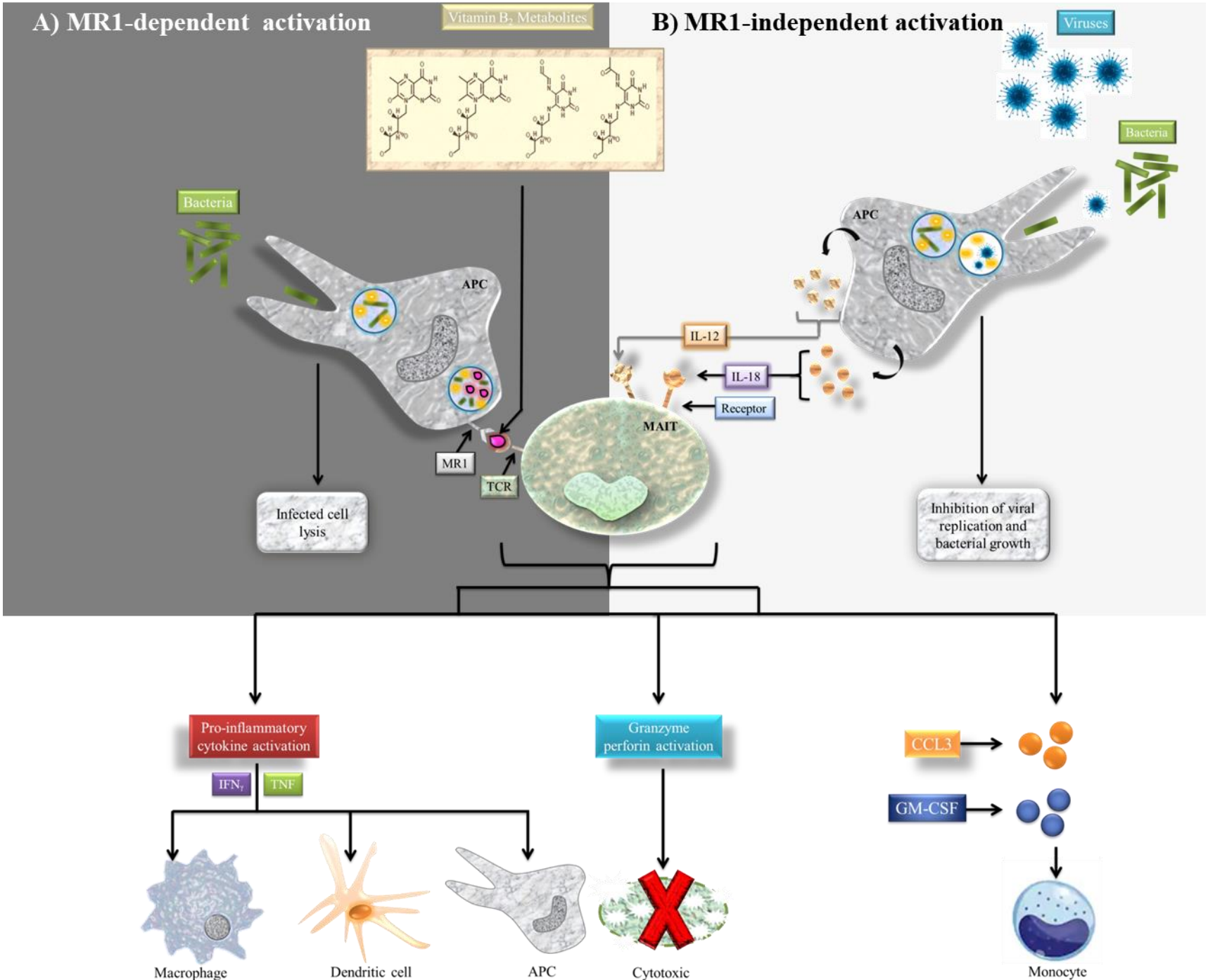
A) MR1-dependent activation
Vitamin B_2 Metabolites
Bacteria
APC
MR1
TCR
MAIT
Infected cell lysis
B) MR1-independent activation
Viruses
Bacteria
APC
IL-12
IL-18
Receptor
MAIT
Inhibition of viral replication and bacterial growth
Pro-inflammatory cytokine activation
IFN_γ
TNF
Granzyme perforin activation
CCL3
GM-CSF
Macrophage
Dendritic cell
APC
Cytotoxic
Monocyte

Figure 1.7: Schematic diagram of the MR1-dependent and MR1-independent cytokine-dependent MAIT cell activation pathways. (**A**) During bacterial infections, MAIT cells can be stimulated in a MHC class 1-related molecule (MR1)-dependent manner as a result of their T cell receptors recognizing the MR1-presented bacterial RF ligands; 7-Hydroxy-6-methyl-8-ribityllumazine, 6,7-Dimethyl -8-ribityllumazine, 5-OE-RU or 5-OP-RU. (**B**) Alternatively, the MR1-independent pathway could be activated and is primarily governed by inflammatory cytokines such as IL-18 and -12 produced by the infected APC which are sensed by MAIT cells via the cytokine-receptor interaction. As a result of MAIT cell activation, a cascade of immune responses is stimulated and ultimately suppresses viral replication or bacterial growth. APC, antigen presenting cell; CCL3-CC, chemokine ligand 3; GM-CSF, granulocyte-macrophage colony stimulating factor; IL-R, interleukin receptor; IFN_{γ}, interferon gamma, TNF, tumour necrosis factor.

MAIT cell activation is dependent on two pathways, either the MR1-dependent or the MR1-independent pathway. According to the prevailing model, during bacterial infections, the invading pathogen is engulfed by an APC which is degraded by cell lysis. As the pathogen is disintegrated, the intracellular contents are made available to the APC along with selected RF metabolites (**Figure 1.7**) which are presented via the MR1 protein to the MAIT cell TCR to induce MAIT cell activation. Upon MAIT cell activation, various cellular responses will be activated such as cytotoxic responses, MAIT cell proliferation and infected cell lysis.

Viruses and certain bacteria cannot synthesize RF, but have nevertheless been shown to be capable of robustly stimulating MAIT cells. This suggests that there is another pathway at play, termed the MR1-independent cytokine-dependent activation pathway. This pathway does not rely on RF metabolite derivatives but instead depends on cytokines released by the infected APC as a result of APC-pathogen intracellular lysis. Generally, MAIT cells express abundant levels of IL-18 and IL-12 which have surfaced as major cytokines that activate MAIT cells upon cytokine-receptor binding as a result of viral or bacterial infection (Chua et al. 2012; Meierovics, Yankelevich, and Cowley 2013; Jesteadt et al. 2018). In contrast, IL-18 is not essential for MAIT cell IFN_{γ} production during *in vivo* infection (Jesteadt et al. 2018). Of importance, deletion of the IL-12p40 subunit resulted in insufficient control of *F. tularensis* and *M. bovis* intracellular growth reflecting the importance of MAIT cells in restricting pathogen growth (Meierovics, Yankelevich, and Cowley 2013; Jesteadt et al. 2018). However, *in vitro* studies have shown that, whether or not *F. tularensis* and *Enterococcus faecalis* produce RF, they are still able to evoke IFN_{γ} production by MAIT cells in a cytokine dependent manner (Jesteadt et al. 2018; Ussher et al. 2014). Furthermore, the examination of the MR1 binding pocket shows that known ligands do not have the capacity to fully occupy the binding pocket (Lopez-Sagaseta, Dulberger, McFedries, et al.

2013), which suggests that more conformed diversified ligands can be presented by MR1 but have yet to be discovered.

More recently, it was shown (Keller, Eckle, et al. 2017) that the MR1 pocket can present diverse chemical structures due to its high structural plasticity. Of note, several agonists have been identified: that is, diclofenac and the chemical inhibitors; 3-formylsalisylic acid, 5-formylsalisylic and 2,4-diamino-6-formylpteridine. Complex binding of the TCR from MAIT cells in complex with MR1 protein bound to stimulants and non-stimulants showed explicit ligand orientation and contacts within the MR1 binding pocket (Keller, Eckle, et al. 2017). The versatility of MR1 to capture diverse chemical structures capable of either MAIT cell activation or inhibition indicates the probability that certain drugs or drug-like molecules could regulate the normal functioning of MAIT cells in mammals. However, none of the endogenous mammalian ligands have been identified, although their existence is highly plausible.

The role of MAIT cells in detecting bacterial pathogens represents a strong motivator for studying the RF pathway in mycobacteria: we proposed that the depletion of *ribF*, the gene of interest in this study, should lead to an accumulation of a RF precursor which could act either as a MAIT cell activator or antagonist, (Azevedo et al. 1993), the implication of which requires further investigation (Harriff et al. 2018). To this end, the recently described CRISPR interference (CRISPRi) technique (Rock et al. 2017) was selected as the preferred method to downregulate the expression of *ribF* in mycobacteria.

1.7 Transcriptional repression using CRISPR interference (CRISPRi)

CRISPRi is a tool derived from the ability of some bacteria to specifically cleave foreign DNA in order to restrict pathogen survival (Makarova et al. 2011). This naturally occurring "bacterial immunity" pathway has been manipulated in CRISPRi to block the transcription of specified gene targets and is now widely employed as a tool to mediate the downregulation of essential genes or to knockout non-essential genes (Janssen 2018). This system requires three major components: a single deactivated CRISPR-associated protein-9 endonuclease, dCas9, and two short RNAs, CRISPR RNA (crRNA) and a trans-activating crRNA (transcrRNA) which is partially complementary.

These two RNAs combine to form a single guide RNA (sgRNA) comprising ~20 nucleotides complementary to the target sequence (Deltcheva et al. 2011). The specificity is

determined by the protospacer adjacent motif (PAM) sequence, 5'-NNAGAA-3', and Watson-Crick base pairing of the sgRNA to the target DNA (Wright, Nunez, and Doudna 2016; Horvath et al. 2008; Deveau et al. 2008). To induce transcriptional repression and prevent cleavage of the target region (*i.e.*, to enable transcriptional inhibition via steric hindrance rather than gene editing), the Cas9 protein activity has been deactivated (dCas9) through targeted point mutations within the HNH (H840A) and RuvC (D10A) nuclease domains (Qi et al. 2013a; Bikard et al. 2013). On expression, dCas9 binds to the target sequence forming a $dCas9_{Sth}$ (this enzyme originates from ***S****treptococcus* ***th****ermophilus*) - sgRNA complex which efficiently represses the gene of interest, ensuring complete obstruction of transcription elongation (**Figure 1.8**).

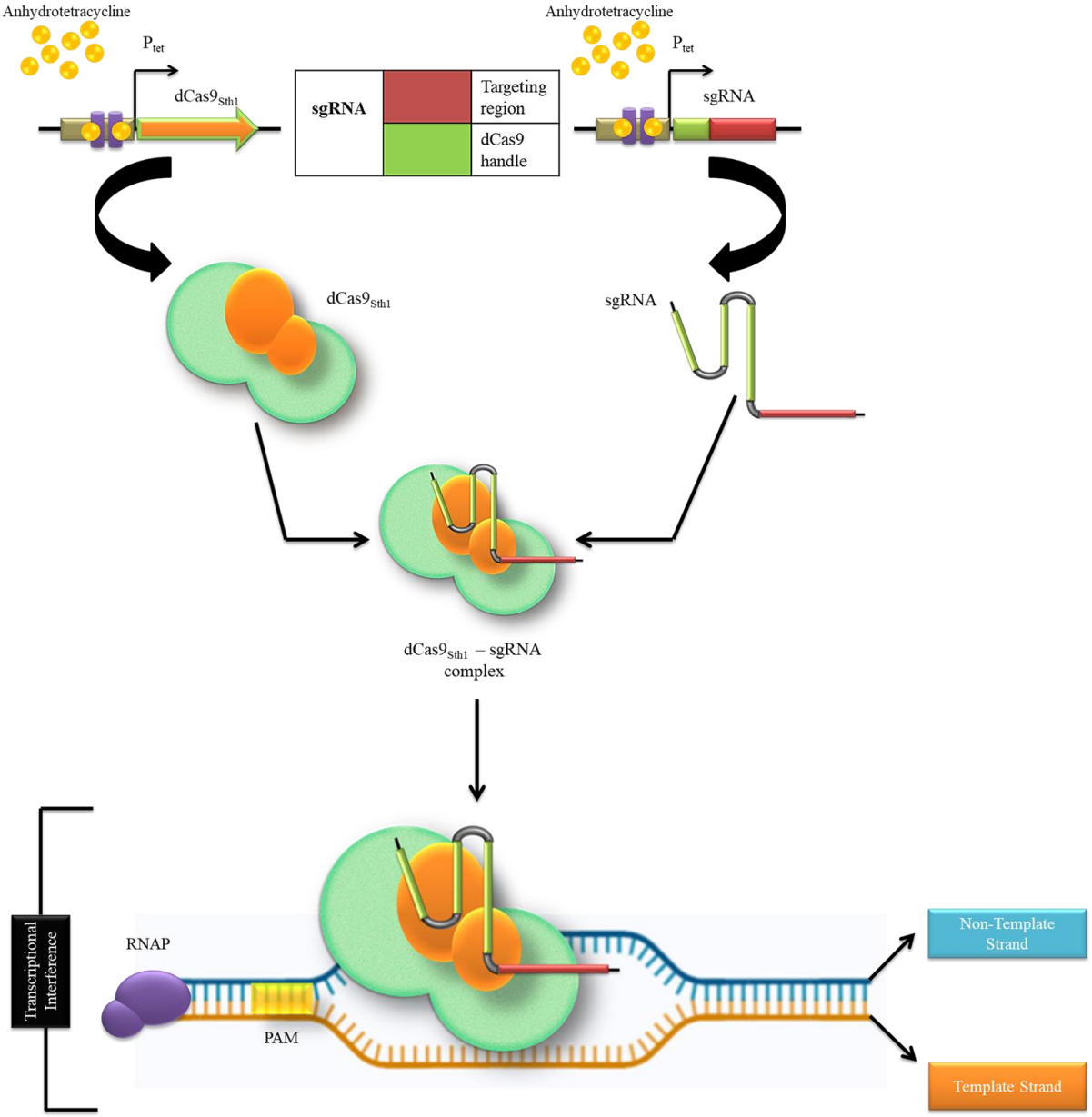

Figure 1.8: CRISPRi prevents transcription of the target gene. The sgRNA made up of the target region (red) and dCas9 handle (green) directs the dCas9 enzyme to the sequence of interest causing obstruction of the RNA polymerase (RNAP; purple) (*adapted and modified from* Rock et al. 2017).

Notably, the production of $dCas9_{Sth}$-sgRNA is under the control of an inducible anhydrotetracycline (ATc) promoter hence to initiate gene knockdown cells are exposed to ATc. Additionally, the sgRNA is also regulated by a separate inducible ATc promoter. The sgRNAs can be specific for either one of the template strands when targeting the promoter, but obstruction of transcription by targeting the non-template strand notably produces up to 300-fold higher repression (Qi et al. 2013a; Bikard et al. 2013). This technique initially

proved to be more successful in *E. coli* and *B. subtilis*, reducing gene expression by a thousand-fold, whereas testing in mycobacteria yielded poor results, producing just four-fold knockdown of gene expression (Choudhary et al. 2015; Singh et al. 2016), and was associated with toxic effects (Nielsen and Voigt 2014).

The *S. pyogenes* Cas9 is most commonly used in genomic engineering based on its ability to produce DNA double stranded breaks to sequences that are adjacent to -NGG- PAM sequences (Doudna and Charpentier 2014; Sontheimer and Barrangou 2015; Terns and Terns 2014). However, pioneering work by Jeremy Rock and Sarah Fortune and colleagues (Rock et al. 2017) involving the testing of codon optimized dCas9 proteins from either the type IIA or type IIC subfamilies identified dCas9Sth1 as optimal for mycobacterial use. This system has subsequently been validated in our laboratory in generating large-scale *Msm* knockdown libraries (de Wet et al. 2018) and was used here to inducibly inhibit *ribF* transcription.

1.8 Rationale and hypothesis

The overall aim of this study was to assess the function of *ribF* in *Msm*, a fast growing and non-pathogenic mycobacterial model organism (Shiloh and Champion 2010). RibF is annotated as encoding a bifunctional protein responsible for the generation of the flavins, FMN and FAD. It was hypothesized, therefore, that this enzyme plays a role in regulating the *rib* operon either directly or indirectly by influencing the riboswitch, precedent for which exists in *B. subtilis* where *ribR* has been shown to overpass repression withheld by the FMN riboswitch (Mack, van Loon, and Hohmann 1998a; Solovieva et al. 1999; Lee et al. 2001).

Given the role of this predicted essential enzyme (DeJesus et al. 2017; Sassetti, Boyd, and Rubin 2003a; Griffin et al. 2011a) in the operation of numerous flavoproteins which require cofactors for their functioning, it was expected that depletion of *ribF* would cripple numerous critical processes within the mycobacterial cell, validating RibF as a potential drug target.

1.9 List of objectives

The specific objectives for this proposed study were therefore:

i) To knock down the expression of *ribF* in *Msm* by inducible CRISPRi.

ii) To measure the efficacy of each sgRNA in the *ribF* knockdown mutants.

iii) To determine the most efficient inoculum concentrations needed to potently induce knockdown.

iv) To determine the minimal inhibitory concentration of ATc sufficient to induce the same inhibitory effect as the commonly used 100 ng/ml ATc standard.

v) To investigate whether depletion of RibF was bacteriostatic or bactericidal.

vi) To quantify the *ribF* transcript levels in the knockdown strain to verify transcriptional depletion in this system.

vii) To determine if the *ribF* hypomorph could be rescued by substrates: RF, FMN or FAD.

viii) To determine whether the depletion of RibF increased susceptibility to specific anti-mycobacterial agents and proposed FAD synthetase inhibitors.

ix) To investigate the influence of RibF depletion on the expression of the *rib* operon.

x) To investigate the consequence of *ribF* depletion on various metabolites of the RF biosynthetic pathway; namely ribulose-5-phosphate, 6,7-dimethyl-8-ribityllumazine (DMRL), riboflavin, FMN, FAD and vitamin B_{12}.

Chapter 2: Methodology

2.1 Materials and methods

2.1.1 Bacterial strains, plasmids and growth conditions

To create hypomorphs (targeted gene knockdown mutants), single guide RNAs (sgRNAs) comprising short oligonucleotides of ~ 21 bases were synthesized and cloned into the pLJR962 vector backbone (Rock et al. 2017) for transformation into *E. coli* and subsequently electroporated into *Msm* for targeted gene repression, the details of which are outlined below.

All *E. coli* and *M. smegmatis* (*Msm*) strains used in this study are derivatives of DH5α and mc^{2}155 respectively (**Table 2.1**) and were kept at -80ºC in 35% (v/v) glycerol for storage. All *Msm* strains were grown in Middlebrook 7H9 (Difco^{TM}) supplemented with 0.02% (v/v) glycerol, 10% (v/v) Middlebrook Oleic Acid Dextrose Catalase (OADC) enrichment (Difco^{TM}), 0.02% (v/v) of 25% Tween80 and 25 µg/ml kanamycin (Kan) where appropriate. In liquid culture, the strains were grown in 50 ml Erlenmeyer flasks at 37ºC in a shaking incubator (IncoShake incubator, Labotec). In contrast, on solid media, strains were grown on Middlebrook 7H10 agar supplemented with 0.05% (v/v) glycerol and 10% (v/v) OADC containing 25 µg/ml Kan where appropriate, incubated in a 37ºC stationary incubator (IncoCool incubator, Labotec).

All *E. coli* strains used for propagating vectors were grown in Luria-Bertani (LB); 0.5% (v/v) yeast extract, 1% (v/v) tryptone and 0.5% (v/v) NaCl broth containing 50 µg/ml Kan and grown overnight at 37ºC in a shaking incubator. Transformants were plated onto Luria-Bertani agar (LA) and incubated overnight at 37ºC in a stationary incubator.

Table 2.1: List of bacterial strains used in this study

Strains	Genotypic Composition	References
Escherichia coli		
DH5α	*supE44ΔlacU169* (F80*LacZΔM15*) *hsdR17 recA1 endA1 gyrA96 thi-1 relA1*	Promega
Mycobacterium smegmatis		

MSM_WT	High frequency transformation mutant of *Msm* ATCC 706	Snapper et al., 1990
CRISPR vector	Strain carrying CRISPRi vector backbone pLJR962	This study
MSM_RibF1	CRISPRi *ribF*1 knockdown strain	This study
MSM_RibF2	CRISPRi *ribF*2 knockdown strain	This study
MSM_RibF3	CRISPRi *ribF*3 knockdown strain	This study
MSM_RibF4	CRISPRi *ribF*4 knockdown strain	This study
MSM_RibF5	CRISPRi *ribF*5 knockdown strain	This study
MSM_RibF6	CRISPRi *ribF*6 knockdown strain	This study
MSM_RibF7	CRISPRi *ribF*7 knockdown strain	This study
MSM_RibF8	CRISPRi *ribF*8 knockdown strain	This study
MSM_RibF9	CRISPRi *ribF*9 knockdown strain	This study
MSM_RibF10	CRISPRi *ribF*10 knockdown strain	This study
MSM_MmpL3	CRISPRi *mmpL3* knockdown strain	This study

2.1.2 Plasmids used in this study

The list of sgRNA constructs generated is tabulated below and their respective sequences are shown in **Table 3.1**

Table 2.2: List of plasmids used this study

Plasmid	Composition	References
pLJR962	Anhydrotetracycline inducible Tet^R expressing Sth1 and dCas9, a single-copy L5 integrating backbone, Kan^R	Rock *et al*., 2017
pLJR962_*ribF*1	*ribF* knockdown construct created by insertion of sgRNA1 oligo	This study
pLJR962_*ribF*2	*ribF* knockdown construct created by insertion of sgRNA2 oligo	This study
pLJR962_*ribF*3	*ribF* knockdown construct created by insertion of sgRNA3 oligo	This study
pLJR962_*ribF*4	*ribF* knockdown construct created by insertion of sgRNA4 oligo	This study
pLJR962_*ribF*5	*ribF* knockdown construct created by insertion of sgRNA5 oligo	This study
pLJR962_*ribF*6	*ribF* knockdown construct created by insertion of sgRNA6 oligo	This study
pLJR962_*ribF*7	*ribF* knockdown construct created by insertion of sgRNA7	This study

	oligo	
pLJR962_*ribF*8	*ribF* knockdown construct created by insertion of sgRNA8 oligo	This study
pLJR962_*ribF9*	*ribF* knockdown construct created by insertion of sgRNA9 oligo	This study
pLJR962_*ribF*10	*ribF* knockdown construct created by insertion of sgRNA10 oligo	This study
pLJR962_*mmpL3*	*mmpL3* knockdown construct created by insertion of *mmpL3*_sgRNA oligo	This study

2.1.3 DNA extraction

2.1.3.1 Mini-prep plasmid DNA isolation

Purified plasmid was isolated according to instructions of the Zyppy plasmid miniprep kit (ZYMO RESEARCH). Positive *E. coli* transformants harbouring desired plasmids were allowed to grow overnight at 37ºC and cells were centrifuged at 4000 rpm for 5 minutes (min) (Allegra™ X-22R Centrifuge, BECKMAN COULTER). The supernatant was discarded and the pellet was resuspended in 600 µl of sterile H_2O. The entire contents were transferred into a 1.5 ml Eppendorf tube and 100 µl of 7X Lysis buffer was added and gently mixed by inversion. Afterwards 350 µl of cold neutralization buffer was added and thoroughly mixed. The supernatant was aliquoted into the preassembled Zymo-Spin™ IIN filter column and centrifuged at 11 000 rpm for 4 min (Centrifuge 5418, Eppendorf). The flow through was discarded and the column was washed twice using 200 µl Endo-Wash buffer and 400 µl Wash buffer with one min centrifugations at 11 000 rpm respectively. The flow-through was discarded and the column was transferred to a clean 1.5 ml microcentrifuge tube. Finally, 50 µl of the Zyppy™ Elution buffer was added directly onto the column matrix

and was incubated at room temperature for one min. Ultimately, the plasmid DNA was eluted by centrifugation at 10 000 rpm for two min. Approximately 500 ng of each sample was sent for sequencing for confirmation of sgRNA inserts at the Central Analytical Facilities (CAF), University of Stellenbosch. Verified constructs were electroporated into *Msm*.

2.1.4 DNA manipulations

Standardized protocols were adopted from (Sambrook *et al.*, 1989; Sambrook &Russell 2001) for all DNA manipulations and biological molecular techniques.

2.1.4.1 Agarose gel electrophoresis

The pLJR962 CRISPRi backbone was digested with *Bsm*BI and run on a 1% agarose gel for purification. The gel was prepared by dissolving 0.8 g agarose (Sigma-Aldrich) powder with 100 ml of 1 x TAE (40 mM Tris-acetic acid, 1 mM Na_2EDTA pH 8.0) buffer with 1 µl of 10 mg/ml ethidium bromide (EtBr). Approximately 1000 ng of the vector DNA was combined with loading dye (0.025% bromophenol-blue in 30% glycerol) for tracking. A DNA molecular weight marker (Roche Applied Science, Germany) was used to approximate the DNA fragment size of the template DNA. Electrophoresis was carried out using the Mini-Sub® cell GT with a submerged horizontal unit (Bio-Rad) set at 90 V and run for 40 min. The gel was viewed using the Gel dock (WealTech Ketagalan Imaging System) under ultraviolet (UV) light.

2.1.4.2 Gel extraction and quantification

The desired DNA fragment was cut out using a scalpel and purified following the manufacturer's instructions using the NucleoSpin® Extraction II kit, Macherey Nagel. The excised DNA fragment from the agarose gel was resuspended and incubated in DNA-binding buffer for 20 min at 50ºC. The dissolved gel solution was loaded on the NucleoSpin® Gel and PCR Clean-Up Midi column which was washed twice with wash buffer. Finally, the purified and digested pLJR962 vector backbone was eluted in 50 µl of elution buffer and quantitated using the NanoDrop ND-1000 spectrophotometer (Thermo Scientific).

2.1.4.3 Restriction digests

The vector backbone was digested with the restriction enzyme *Bsm*BI (NEB) and incubated at 55ºC. Approximately 1 µg of the plasmid DNA was digested for 1 hour incubated on a compact thermomixer (Eppendorf) with 10 µl of 1 x CutSmart® buffer containing 1 µl of the restriction enzyme. This particular enzyme does not produce compatible ends, hence self-re-

ligation was limited and dephosphorylation was unnecessary. Desired fragments were analysed and validated by running the digest on a 0.8% agarose gel.

2.1.4.4 SgRNA oligo annealing

4 µl of the forward and reverse oligo were added to 42 µl of annealing buffer (50 mM Tris, 50 mM NaCl and 1 mM of EDTA, pH 7.5) to obtain a total volume of 50 µl. The annealing conditions were set at a denaturation phase of 95ºC for 2 min followed by an annealing step incorporating a decline in temperature from 95ºC to 25ºC at a 0.1ºC per second interval (**T100**^{TM} Thermal cycler, BioRad).

2.1.4.5 Ligation

0.5 µl ($2.7x10^{-7}$ nmol) of the annealed complementary sgRNA targeting oligos were added to 9 ng ($1.56x10^{-9}$ nmol) of the *Bsm*BI digested vector. The ligation mixture was set up as follows; 0.5 µl of annealed oligos, 1 µl of digested vector, 2.5 µl of 1 x Quick buffer and 0.5 µl of Quick ligase (NEB) were added to a microtube and incubated at room temperature for 30 min followed by ligase inactivation on ice.

2.1.5 Bacterial transformation

2.1.5.1 *Escherichia coli*

2.1.5.1.1 Preparation of competent cells

E. coli DH5α cells were made transformation competent using rubidium chloride. Briefly, 100 µl of an *E. coli* freezer stock was inoculated in 5 ml of LB broth and incubated at 37ºC in a shaking incubator overnight. One ml of the overnight culture was inoculated into 99 ml of LB broth and allowed to grow at 37ºC to reach an OD_{600} of 0.8. The cultures were then incubated on ice for 15 min prior to being centrifuged at 4000 rpm for 5 min at 4ºC (Allegra^{TM} X-22R Centrifuge, BECKMAN COULTER). The pellet was resuspended in 40 ml of Transformation buffer I (30 mM potassium acetate, 100 mM rubidium chloride, 50 mM manganese chloride and 15% (v/v) glycerol, pH 5.8) (Tfb I) and incubated on ice for 15 min. The cells were spun down at 3000 rpm for 5 min and resuspended in 4 ml of Tfb II (10 mM MOPS, 75 mM calcium chloride,10 mM rubidium chloride and 15% (v/v) glycerol, pH 6.5. Competent cells were quick frozen in 500 µl aliquots and stored at -80ºC until required.

2.1.5.1.2 Transformation of plasmid DNA into competent *E. coli* cells

Competent DH5α cells were allowed to thaw and 500 ng of recombinant plasmid (sgRNA + pLJR962) was added to 100 µl of cells and incubated on ice for 15 min. The cells were

briefly heated to 42ºC for 90 seconds and were immediately placed back on ice for 2 min. The cells were rescued by the addition of 200 µl of 2 x TY (Tryptone Yeast) broth and incubated at 37ºC for 1 hour in a standing incubator (IncoCool incubator, LaboTech). The entire contents were plated onto LA agar containing 50 µg/ml Kan for selection. The plates were then incubated at 37ºC overnight in a stationary incubator (IncoCool incubator, LaboTech).

2.1.5.2 *Mycobacterium smegmatis*

2.1.5.2.1 Preparation of *Msm* electro-competent cells

A MSM_WT mc2155 culture was inoculated in 7H9-OADC and incubated overnight at 37ºC to reach an OD_{600} of ~ 0.6 (Incoshake incubator, LaboTech). The cells were spun down in a centrifuge (Allegra^{TM} X-22R Centrifuge, BECKMAN COULTER) at 4000 rpm at 4ºC for 10 min and washed three times using cold 10% (v/v) glycerol. Washes were carried out sequentially resuspended in 25 ml, 10 ml and 5 ml, respectively. Finally, the pelleted cells were resuspended in 1.8 ml of 10% (v/v) glycerol and distributed in 300 µl aliquots and stored at -80ºC until required.

2.1.5.2.2 Electroporation of recombinant plasmid into *Msm* cells

The competent *Msm* cells were gently thawed and aliquoted into pre-chilled electroporation cuvettes (0.2 cm electrode gap, Bio-Rad) containing ~ 500 ng of recombinant plasmid DNA. The GenePulser^{TM} (Bio-Rad) was set at 2.5 kV, 1000 Ω resistance and 25 µF capacitance. Cells were rescued after pulsing by adding 600 µl of 2 x TY to the cuvette and incubated at 37ºC overnight in a stationary incubator (IncoCool incubator, LaboTech). The following day, the contents were transferred into a clean 1.5 ml microcentrifuge tube and pelleted down at 10 000 rpm for 2 min (Centrifuge 5418, Eppendorf). The cells were then resuspended in 100 µl of 7H9-OADC and the entire contents plated on 7H10-OADC agar containing 25 µg/ml Kan and incubated at 37ºC for 3-5 days in a stationary incubator.

2.1.6 DNA sequencing

The presence of all sgRNA inserts in respective constructs was validated by sequencing, conducted by the Central Analytical Facility (CAF) at the University of Stellenbosch. Sequencing reads were conceptualized using FinchTv 1.4.0 free software (https://digitalworldbiology.com/finchTv) and compared to the predicted sgRNA sequence to verify the absence of mutations.

Table 2.3: Primer used in this study for sequencing sgRNA insert

Primer ID	Primer sequences (5'-3')	Application
CRISPR_Seq_Primer_1834	-TTCCTGTGAAGAGCCATTGATAATG-	Desired CRISPRi sgRNA construct validation

2.1.7 qRT-PCR

2.1.7.1 Sample preparation for detecting transcript levels

Strains were inoculated at an initial inoculum concentration of an OD_{600} of 0.016 in 7H9-OADC media containing either no ATc or 100 ng/ml ATc, including 25 µg/ml Kan where relevant. The cultures were allowed to grow for 24 hours in a shaking incubator at 37ºC (Incoshake incubator, LaboTech). The entire contents were transferred into Falcon tubes post-incubation and centrifuged at 4500 rpm for 10 min (Allegra™ X-22R Centrifuge, BECKMAN COULTER). The supernatant was discarded and the pellet resuspended in 1 ml of 7H9-OADC and transferred into clean 2 ml Eppendorf tubes. The cultures were washed twice by spinning down at 10 000 rpm for 10 min in a microcentrifuge (Centrifuge 5418, Eppendorf). Finally, the supernatant was discarded and remaining cells were resuspended in 500 µl of LBP Lysis buffer (Nucleospin® RNA plus kit) and stored at -80ºC in preparation for RNA extraction.

2.1.7.2 RNA isolation

The resuspended LBP lysis buffer samples were processed according to the manufacturer's protocol using the Nucleospin® RNA plus kit (Macherey-Nagel). Briefly, the samples were allowed to gently thaw on ice and transferred into 2 ml Homogenization microtubes containing silica lysing matrix (ZIRCONIA/SILICA 0.1 mm in diameter, BioSpec). Samples were sealed with parafilm and lysed using the cell disrupter (FastPrep™ FP120, BIO 101 Savant) set at speed 5 for 30 seconds. This was repeated three times separated by 2 min incubations on ice. The samples were spun down at 10 000 rpm for 10 min using a microcentrifuge and the supernatant was transferred into a genomic DNA removal tube before transferral into an RNA selective binding column (NucleoSpin® RNA Plus kit, Macherey-Nagel). The sample was eluted in 60 µl of RNAse-free water and residual genomic

DNA contaminants were digested with TURBO DNAse treatment (Invitrogen). Briefly, the eluent was treated by adding 0.1 the volume of TURBO DNAse buffer and 2 units of enzyme and incubated at 37°C for 1 hour. Following the incubation, 0.1 the volume of Inactivation reagent was added to the mixture, briefly centrifuged and the supernatant transferred to a new tube. The resultant DNA-free RNA was used to synthesize cDNA by addition of 1 µl of 50 µM random hexamers, 1 µl of 10 mM dNTP and 12 µl of 250 ng template RNA including 0.5 µl of SuperScript® IV Reverse Transcriptase, added to appropriate samples in preparation for qRT-PCR (SimpliAmp Thermal Cycler, Thermo Fisher Scientific). A no reverse transcriptase control was included to verify the absence of DNA contamination.

2.1.7.3 Junction amplification method used to identify single transcriptional units via junction primers

To establish if the RF genes constitute a single transcriptional unit, RNA was extracted and converted to cDNA as previously described in section 2.1.7.2 from MSM_WT and primers were designed to amplify the junctions between two genes. Five primers were designed to amplify the region between genes: MSMEG_3070-*ribE* (147 bp), *ribE-ribAB* (166 bp), *ribAB-ribH* (110 bp), *ribH*-MSMEG_3074 (306 bp) and MSMEG_3074-MSMEG_3075 (250 bp). The constitutive and highly expressed *sigA* gene was amplified as a positive control.

Table 2.4: List of junction primers used to validate genes constituting a single transcriptional unit

Junction name	Primer ID	Primer sequences (5'-3')
MSMEG_3070-*ribE*	qRT_*MSM*3070-*ribE* FWD	-CCAGTACGCCCAGTTCTTCAA-
	qRT*MSM*3070-*ribE* REV	-GAACAAGGACTGGACTGCGAA-
ribE-ribAB	qRT*MSM ribE-ribAB* FWD	-GGGTACGGGTCGGTAAGAG-
	qR*MSM ribE-ribAB* REV	-CGCCCTCTCGACGGAATC-
ribAB-ribH	qRT*MSM ribAB-ribH*	-CGGTGAGCATGGACGACT-

	FWD	
	qRT*MSM ribAB-ribH* REV	-TCTCGGGCAGATCGGGGA-
ribH-MSMEG_3074	qRT*MSM ribH*-MSM_3074 FWD	-GACCACCAACACCGAGGAG-
	qRT*MSM ribH*-MSM_3074REV	-GATGGCCACCTGATCCTCG-
MSMEG_3074-MSMEG_3075	qRT*MSM* 3074-MSM_3075 FWD	-GGTGGGCACGGATCGATC-
	qRT*MSM* 3074-MSM_3075 REV	-CACGCAGCATCTACGAGGATC-

2.1.7.4 Quantitative measurement of transcript levels of target genes by qRT-PCR

The Power SYBR® Green PCR Master mix was used in a 96-Well Piko PCR Fast Plate‡ with the forward and reverse primer constituting a final concentration of 0.3 µM in conjunction with cDNA template DNA, which resulted in a 20 µl volume per reaction. The thermal cycling parameters were set as follows: AmpliTaq Gold® Enzyme Activation was on hold for 10 min at 95ºC followed by denaturation at 95ºC for 15 seconds. The annealing and extension steps occurred at 60ºC for 60 seconds for 40 PCR cycles (PikoReal 96 Real-Time PCR System, Thermo Scientific). The absolute transcript expression levels of target genes were calculated in copies/µl and normalized to *sigA*. Comparable ratios between the normalized transcript levels of ATc induced versus non ATc induced strains were used to infer differences in the expression levels.

Table 2.5: List of primers used for qRT-PCR reactions to study transcriptional expression levels.

Gene	Primer ID	Primer sequences (5'-3')
sigA	qRT_*MSM_sigA*FWD	-ACCAAGGGCTACAAGTTCTCG-
	qRT_*MSM_sigA*REV	-CATCTCCTTGGCGAGCTCTTC-
*d*Cas9	qRT_*MSM*_dCas9FWD	-TCGGTGAAGCTGATGATGGAG-
	qRT_*MSM*_dCas9REV	-TGTAGATCTCCTCGGTCAGCA-
ribF	qRT_*MSM_ribF*FWD	-GATCGACGTGTTCCTGGTGAT-
	qRT_*MSM_ribF*REV	-CAGCATGTCGACGTTGCC-
mmpL3	qRT_*MSM_mmpL3*FWD	-AACGATCCGGAGAAGATGTGG-
	qRT_*MSM_mmpL3*REV	-CGCAACTCGTCGATCTTCTTG-

Table 2.6: List of primers used for qRT-PCR of the proposed *rib* operon, quantified by transcript expression levels

Gene	Primer ID	Primer sequences (5'-3')
ribE (MSMEG_3071)	qRT_*MSM_ribE*FWD	-TTGGTGATGACTGGTTTGAGA-
	qRT_*MSM_ribE*REV	-ATGACGTCCACTTCCAGGTTC-
ribAB (MSMEG_3072)	qRT_*MSM_ribAB*FWD	-GCCGACGATTTCACCAAGC-
	qRT_*MSM_ribAB*REV	-GTCCTTCTGGCTGACGATCTC-
ribH (MSMEG_3073)	qRT_*MSM_ribH*FWD	-GACCACCAACACCGAGGAG-
	qRT_*MSM_ribH*REV	-ACGGCGGTGGACAGTG-

2.1.8 Transcriptional downregulation of target genes by CRISPRi

A wide range of sgRNAs targeting *Msm* genes were designed and described by (de Wet et al. 2018) which were adopted for use in this study. Each individual sgRNA constituted a top and

bottom oligo usually 20 to 25 bases in length which targeted *ribF*, involved in the RF pathway. The oligos were ligated into the *Bsm*BI-digested vector backbone. Ligated recombinant plasmids were transformed into DH5α *E. coli* cells and plated on 50 µg/ml Kan LA agar containing plates. Plasmid DNA extraction was performed from single colonies and were sequenced using sequencing primer 1834 (**Table 2.3**) via Sanger sequencing to validate the presence of the insert. A control construct was also generated targeting *mmpL3*, an essential gene involved in the biosynthesis of the mycobacterial cell wall, also shown to be highly susceptible to transcriptional depletion. As a negative control, the CRISPRi vector without a sgRNA was used to illustrate that the plasmid itself does not have an effect on the growth or viability of the cells. Validated sgRNA carrying constructs were electroporated into competent *Msm* cells. Single colonies were grown in 7H9-OADC supplemented media containing 25 µg/ml Kan. An ATc MIC was performed to induce gene knockdown where growth was measured using alamar blue as described in the MABA assay (Collins & Franzblau, 1997). A detailed explanation of this procedure is provided below in section **2.1.9.1 Determination of ATc MIC in liquid media**.

2.1.9 Phenotypic Characterization

2.1.9.1 Determination of ATc MIC in liquid media

Cultures were grown in 7H9-OADC containing 25 µg/ml Kan where relevant to reach an OD_{600} of 0.5 and incubated at 37ºC in a shaking incubator (Incoshake incubator, LaboTech). Using a U-bottom 96 well microtiter plate (Greiner bio-one, CELLSTAR®), the assay was set up as follows; 50 µl of 7H9-OADC was added to columns 2 to 12. 100 µl of 7H9-OADC containing 400 ng/ml ATc stock was added to column 1. A two-fold dilution was carried out, 50 µl of the contents in column 1 were mixed 5-8 times by suctioning up and down with a multi-channel pipette before being transferred into column 2 and so forth until the end of the plate was reached and the remaining 50 µl was discarded. Each plate included a media only control row to confirm the absence of contamination. Finally, 50 µl of each 1: 1000 diluted culture was added to its respective row and plates were covered in foil and incubated at 37ºC in a stationary incubator for 24 hours (IncoCool incubator, LaboTech). Ten µl of a 0.01% Alamar blue solution (Resazurin) was added to each well using a 12-way multichannel pipette and plates were re-incubated for an additional 8 hours. Lastly, fluorescent readings were measured using a plate reader (FLUOstar Optima, BMG LabTech) set at an emission

and excitation wavelength of 590 nm and 544 nm, respectively, and images were captured using an inverted mirror.

In addition, a similar assay was carried out to demonstrate if the hypomorphs could access and survive by scavenging exogenous riboflavin metabolites. The metabolites tested were riboflavin (RF), flavin mononucleotide (FMN) and flavin adenine dinucleotide (FAD) (Sigma-Aldrich). The U-bottom 96 well microtiter plate was prepared as follows; 50µl of 200 ng/ml ATc diluted in 7H9-OADC media was added to columns 2 to 12. One hundred µl of a 1 mg/ml RF or FMN or FAD stock was added to each respective row in column 1. As described previously, a two-fold dilution was conducted and the plates processed in the same way as mentioned above. Similarly, the MIC_{90} analysis was used to determine the minimum inhibitory concentration of proposed FAD synthetase inhibitors against MSM_WT and starting concentrations of drugs used in this assay were as follows; 200 µM alexidine dihydrochloride, 200 µM benzethonium chloride, 200 µM roseoflavin, 200 µM ribocil-C, 200 µM PAS, 200 µM verteporfin, 200 µM thonzonium bromide and 552 µM vancomycin.

2.1.9.2 Spotting assay to assess growth inhibition on solid media

Cultures were allowed to grow at 37ºC overnight to reach an OD_{600} of 0.5 (Incoshake incubator, LaboTech). A 1:1000 dilution was performed and 100 µl of each sample was added to the first column of each respective row. The diluted cultures were then serially diluted in a 2-fold dilution series. Approximately 5 µl of each dilution was spotted on 7H10-OADC containing 100 ng/ml ATc or no ATc (0 ng/ml). The spotted cultures were allowed to fully absorb prior to incubation. Finally, plates were covered in foil and incubated at 37ºC for 2-3 days (IncoCool incubator, LaboTech) and images were captured.

2.1.9.3 2D Checkerboard Assay

This assay was used to demonstrate any potential synergy between the gene knockdown mutants and potential FAD synthetase inhibitors. The 96-well U-bottom plate was prepared as follows; 50 µl of 7H9-OADC media was added to all wells using a 12-way multichannel pipette.

	1	2	3	4	5	6	7	8	9	10	11	12
A	50µl	50µl	50µl	50µl	50µl	50µl	50µl	50µl	50µl	50µl	50µl	50µl
B	50µl	50µl	50µl	50µl	50µl	50µl	50µl	50µl	50µl	50µl	50µl	50µl
C	50µl	50µl	50µl	50µl	50µl	50µl	50µl	50µl	50µl	50µl	50µl	50µl
D	50µl	50µl	50µl	50µl	50µl	50µl	50µl	50µl	50µl	50µl	50µl	50µl
E	50µl	50µl	50µl	50µl	50µl	50µl	50µl	50µl	50µl	50µl	50µl	50µl
F	50µl	50µl	50µl	50µl	50µl	50µl	50µl	50µl	50µl	50µl	50µl	50µl
G	50µl	50µl	50µl	50µl	50µl	50µl	50µl	50µl	50µl	50µl	50µl	50µl
H	50µl	50µl	50µl	50µl	50µl	50µl	50µl	50µl	50µl	50µl	50µl	50µl

An additional 50 µl of media was added to column 2 and 12 as well as B2 to B11. Lastly, 50 µl of media was added to well B2 to obtain a final volume of 200 µl.

	1	2	3	4	5	6	7	8	9	10	11	12
A	50µl	100µl	50µl	50µl	50µl	50µl	50µl	50µl	50µl	50µl	50µl	100µl
B	50µl	200µl	100µl	100µl	100µl	100µl	100µl	100µl	100µl	100µl	100µl	100µl
C	50µl	100µl	50µl	50µl	50µl	50µl	50µl	50µl	50µl	50µl	50µl	100µl
D	50µl	100µl	50µl	50µl	50µl	50µl	50µl	50µl	50µl	50µl	50µl	100µl
E	50µl	100µl	50µl	50µl	50µl	50µl	50µl	50µl	50µl	50µl	50µl	100µl
F	50µl	100µl	50µl	50µl	50µl	50µl	50µl	50µl	50µl	50µl	50µl	100µl
G	50µl	100µl	50µl	50µl	50µl	50µl	50µl	50µl	50µl	50µl	50µl	100µl
H	50µl	100µl	50µl	50µl	50µl	50µl	50µl	50µl	50µl	50µl	50µl	100µl

4 µl of $drug_x$ was added to B2 and 2 µl of the same drug added to B3 to B11 and serially diluted in 2-fold dilutions by thoroughly mixing 5-8 times before transferring 100 µl contents from B2 into C2 until H2. Similarly, 50 µl of contents of B3-B11 were serially diluted in 2-fold dilutions until H3-H11 using a 12-way multichannel pipette and the residual 50 µl was discarded. 2 µl of 2500 ng/ml ATc was added to the entire column 3 and 50 µl of contents from column 2 were serially diluted in 2-fold dilutions until column 11.

	1	2	3	4	5	6	7	8	9	10	11	12
A	50µl	50µl	50µl	50µl	50µl	50µl	50µl	50µl	50µl	50µl	50µl	100µl
B	50µl	50µl	50µl	50µl	50µl	50µl	50µl	50µl	50µl	50µl	50µl	100µl
C	50µl	50µl	50µl	50µl	50µl	50µl	50µl	50µl	50µl	50µl	50µl	100µl
D	50µl	50µl	50µl	50µl	50µl	50µl	50µl	50µl	50µl	50µl	50µl	100µl
E	50µl	50µl	50µl	50µl	50µl	50µl	50µl	50µl	50µl	50µl	50µl	100µl
F	50µl	50µl	50µl	50µl	50µl	50µl	50µl	50µl	50µl	50µl	50µl	100µl
G	50µl	50µl	50µl	50µl	50µl	50µl	50µl	50µl	50µl	50µl	50µl	100µl
H	50µl	50µl	50µl	50µl	50µl	50µl	50µl	50µl	50µl	50µl	50µl	100µl

Finally, 50µl of a 1: 1000 dilution of an OD_{600} 0.5 culture was added to all 8 rows besides the media only control, column 12. The plates were then covered in foil and placed in a zippy bag (SIGMA) to prevent liquid evaporation. Lastly, the plates were incubated at 37ºC for 24 hours in a stationary incubator (IncoCool incubator, LaboTech). Post incubation, 10 µl of 0.01% Alamar blue was added to each well and plates were re-incubated at 37ºC for an additional 8 hours. The metabolic activities of live versus dead cells were measured using the plate reader (FLUOstar Optima, BMG LabTech) and images were captured using an inverted mirror.

Starting concentrations of drugs used in this assay per plate were as follows; 2500 ng/ml anhydrotetracycline (ATc), 80 µM alexidine dihydrochloride, 2500 µM benzethonium chloride, 10000 µM thonzonium bromide and 552 µM vancomycin.

2.1.9.4 Assessment of mycobacterial growth and viability

Cultures were incubated at 37ºC and allowed to grow overnight to reach exponential phase OD_{600} of 0.5 (Incoshake incubator, LaboTech). 25 ml of 7H9-OADC media was added to Erlenmeyer flasks containing 25 µg/ml Kan and no ATc or supplemented with 100 ng/ml ATc. A 0.004 starting inoculum per strain was added to relevant flasks and incubated at 37ºC in a shaking incubator for 24 hours. The OD_{600} readings were measured in 3 hour intervals over a 24 hour period using a spectrophotometer (Novaspec Plus visible spectrophotometer, Amersham Biosciences). Simultaneously, 1 ml of each sample was harvested, washed twice and resuspended in the same volume of media prior to plating (Centrifuge 5418, Eppendorf). Samples were serially diluted in 10-fold dilutions and 100 µl of each dilution factor was plated on a 7H10-OADC plate containing 25 µg/ml Kan where relevant. Finally, plates were

allowed to fully absorb overnight and placed in bags and incubated at 37ºC for 3-5 days (IncoCool incubator, LaboTech). Colonies were manually counted post 5-days of incubation and CFUs recorded.

2.1.9.5 Assessment of gene knockdown mutants exposed to varying concentrations of ATc

Cultures were incubated at 37ºC and allowed to grow overnight to reach exponential phase OD_{600} of approximately 0.5 (Incoshake incubator, LaboTech). 25 ml of 7H9-OADC media was added to Erlenmeyer flasks containing 25 µg/ml Kan and supplemented with decreasing concentrations of ATc set at 100 ng/ml, 50 ng/ml, 25 ng/ml, 12.5 ng/ml, 6.3 ng/ml, 3.125 ng/ml, 1.6 ng/ml, 0.8 ng/ml, 0.4 ng/ml, 0.2 ng/ml and 0.1 ng/ml, and no ATc. A 0.004 starting inoculum was inoculated into relevant flasks and incubated at 37ºC in a shaking incubator for 24 hours. The OD_{600} readings were measured in 3 hour intervals over a 24 hour period using a Novaspec Plus visible spectrophotometer (Amersham Biosciences).

2.1.9.6 Assessment of inoculum effect on the CRISPRi system

Cultures were incubated at 37ºC and allowed to grow overnight to reach stationary phase at an OD_{600} of approximately 1.0 (Incoshake incubator, LaboTech). 25 ml of 7H9-OADC media was added to Erlenmeyer flasks containing 25 µg/ml Kan either in the presence of 100 ng/ml ATc or absence of ATc. Increasing starting inoculum concentrations of an OD_{600} of 0.004, 0.016, 0.06 and 0.25 per strain were added to relevant flasks and incubated at 37ºC in a shaking incubator for 12 hours to induce transcriptional knockdown. The OD_{600} readings were measured in 3 hour intervals over a 12-24 hour period using a Novaspec Plus visible spectrophotometer (Amersham Biosciences).

2.1.9.7 LC-MS sample preparation

Cultures were grown to log-phase overnight at 37ºC in a shaking incubator (Incoshake incubator, LaboTech). A starting inoculum of 0.016 was inoculated in 10 ml of 7H9-OADC supplemented media containing 25 µg/ml Kan. Each strain was exposed to either 100 ng/ml or 0 ng/ml ATc and incubated at 37ºC to induce CRISPRi-mediated gene silencing. Each sample was washed twice and resuspended in 1000 µl of 50 mM sodium acetate (NaOAc pH 4.5) following a 10 min centrifugation at 10 000 rpm. This was stored at -80ºC until metabolite extraction was to be performed.

2.1.9.7.1 Metabolite extraction

The samples were allowed to gently thaw on ice. Each sample was sonicated at the following settings; amplitude of 30, process time of 5 min and pulse-on and off time of 15 seconds (Q700 Qsonica, Sonicators). The samples were spun down at 13 000 rpm for 5 min and the supernatants transferred into falcon tubes topped with 4 ml of sodium acetate buffer. The mixture was loaded onto a pre-equilibrated C_{18} cartridge and washed using 10 ml of sterile water. Seventy-five percent of ethanol (EtOH) was used to elute ~ 15 drops of each sample into a clean 1.5 ml Eppendorf tube and dried for approximately 2 hours at 50ºC in a miVac DNA concentrator, GeneVac. All dried samples were appropriately stored at -20ºC in preparation for LC-MS analysis.

2.1.9.7.2 LC-MS analysis of RF metabolites in *Msm*

The pellet was reconstituted in (A:B at 1:1 ratio) whereby A represents H_2O (0.02 % Formic Acid; 2mM Ammonium Formate) and B refers to Methanol (0.02 % Formic Acid; 2mM Ammonium Formate). Three ul of each reconstituted sample was injected into the high performance liquid chromatography mass spectrophotometer (SHIMADZU 8040) on a reverse-phased (C_{18}) column run at a flow rate of 0.8 ml/min with ESI detector run with A:B (1:1) mobile phase (Phenomenex Kinetex 2.6u phenyl-hexyl (4.6 X 100mm)) Multiple reaction monitoring (MRM) was assembled for each of the reference standards, *i.e.* FMN, FAD, RF, DMRL and vitamin B_{12}, at three sequential levels (high, medium and low). The difference of all tested RF metabolite peaks were compared in relation to *Msm* WT and no ATc *ribF* treated cells to validate metabolic differences in the pathway.

2.1.9.7.2.1 Bradford Protein assay to measure total protein content

2.1.9.7.2.1.1 Normalization of protein content between -/+ ATc CRISPRi KDs

Five dilutions of the protein standard, Bovine Serum Albumin (BSA) were prepared ranging from 1.8-0.05 mg/ml. One hundred µl of each standard was aliquoted separately into a clean falcon tube and resuspended in 5 ml of 1:4 diluted dye reagent (Bio-Rad Protein Assay Dye Reagent Concentrate). The samples were thoroughly mixed and incubated at room temperature for 5 min prior to absorbance measurement. Finally, 1 ml of each sample was aliquoted in a UV-cuvette and absorbance was measured at 595 nm using the spectrophotometer. Unknown concentrations of protein from crude extract samples were

likewise processed to obtain absorbance values; the standard curve was then used to enumerate the corresponding protein concentration (**Figure 2.1**).

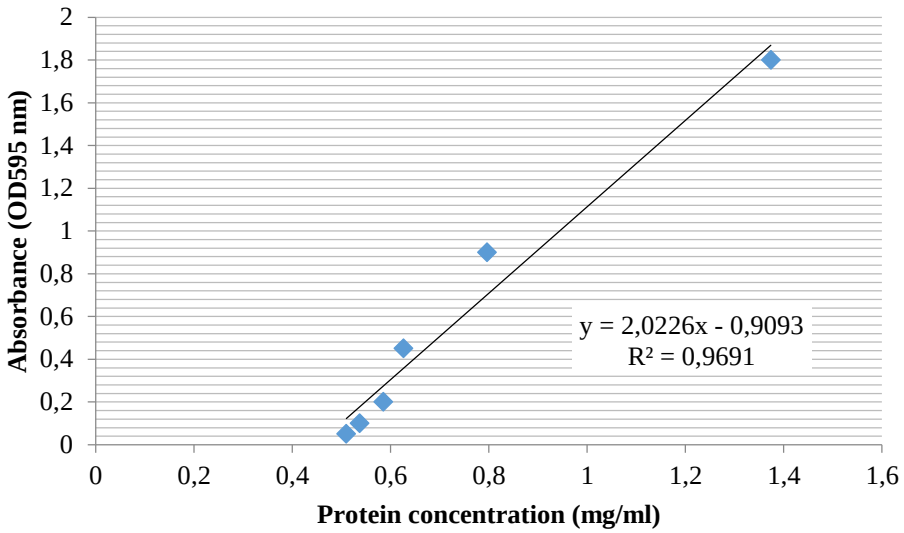

Figure 2.1: Bradford assay used to enumerate the protein concentration based on the equation generated from the standard curve. Protein concentrations of the uninduced and induced hypomorph strains were adjusted to approximately 1 mg/ml.

2.1.10 Whole Genome Sequencing

2.1.10.1 Sample preparation for genomic DNA extraction (gDNA)

Cultures were grown as mentioned in the assessment of mycobacterial growth and viability section **2.1.1 Bacterial strains, plasmids and growth conditions**. After a 5 day incubation, one colony from each plate was carefully picked and inoculated into 1 ml of 7H9 and allowed to grow at 37ºC to reach stationary phase (Incoshake incubator, LaboTech). These pre-cultures were used to inoculate into 50 ml of 7H9 containing 25 µg/ml Kan where appropriate and grown overnight. The cultures were centrifuged at 4000 rpm for 15 mins (Allegra^{TM} X-22R Centrifuge, BECKMAN COULTER) and resuspended in 500 µl of TE buffer (10 mM Tris, 1 mM EDTA, 25 mM NaCl, pH 8.0). Each of the resuspended cultures were transferred into 2 ml Eppendorf tubes and stored at -80ºC until isolation of gDNA from *Msm* was underway.

2.1.10.2 Cetyl Trimethyl Ammonium Bromide (CTAB) extraction of gDNA from *Msm*

This protocol was adapted from van Helden *et al*., 2001 where cells were allowed to gently thaw at room temperature and 50 µl of lysozyme (10 mg/ml) was added for digestion overnight at 37ºC on a thermomixer (**Thermomixer** compact, **Eppendorf**), rotating at a moderate speed of 300 rpm. Following lysozyme treatment, ~ 1.3 µl of RNAse (10 mg/ml) was added to each tube and incubated at 37ºC for an additional hour. Next, 70 µl of 10% SDS and 50 µl of proteinase K were simultaneously added and incubated at 65ºC for an hour. In addition, 100 µl of 5M NaCl and 10% of CTAB were added and incubated at 37ºC for 15 mins at low-mode shaking speed. Following the 15 mins incubation on the thermomixer, 700 µl of a (24:1) chloroform: isoamyl alcohol solution was added to each tube and pelleted down at 13 000 rpm for 10 mins, to harvest the DNA (Centrifuge 5418, Eppendorf). After centrifugation, approximately 700 µl of the aqueous phase was transferred into a new 2 ml Eppendorf tube and mixed with an equivalent volume of cold isopropanol to precipitate the DNA. The tubes were left at -20ºC overnight. The following day samples were centrifuged at 13 000 rpm for 10 mins and the supernatant was carefully discarded and the pellet washed in 800 µl of 70% EtOH. Lastly, the samples were drained of EtOH and dried at 40ºC in a Speed Vac (miVac DNA concentrator, GeneVac). All samples were quantitated using the Nanodrop to determine their concentration (NanoDrop ND-1000 spectrophotometer, Thermo Scientific) and run on an agarose gel using the same parameters as **2.1.4.1 Agarose gel electrophoresis** with a high molecular weight ladder , Marker III (Roche Applied Science, Germany).

2.1.11 Bioinformatics analysis tools

i) **Gene identifier***:* The Mycobrowser (http://mycobrowser.epfl.ch) database was used to identify the gene of interest, *ribF*, and homologs found in other mycobacterial species such as *M. leprae* and *Mtb* (**Supplementary table 1**). This database was also used to identify surrounding genes in close proximity to *ribF* to establish its genomic context (**Supplementary figure S1**) (Kapopoulou, Lew & Cole, 2011).

The GenoList – Institut Pasteur (http://genolist.pasteur.fr) genome browser database was used to identify *ribF* orthologs in model bacteria, *B. subtilis* and *E. coli*

ii) **Pathway predictor**: The KEGG: Kyoto Encyclopedia of Genes and Genomes – GenomeNet (www.genome.jp/kegg/) database was used to validate and map out all genes involved in the RF biosynthetic pathway.

iii) **Riboflavin chemical conversion identifier***:* The BioCyc Pathway/Genome Database Collection (https://biocyc.org/) was used to identify and reconstruct chemical conversions of RF to FMN and from FMN (Riboflavin-5'-phosphate) to FAD.

iv) **Secondary structure identifier***:* The psiprep: index – UCL (http://bioinf.cs.ucl.ac.uk/psiprep/) database was used to visualize secondary structures of RibF in *M. smegmatis* and *B. subtilis* (RibC and RibR).

v) **Chemical structure constructer**: The PubChem Sketcher V2.4 (https://pubchem.ncbi.nlm.nih.gov/edit2/index.html) database was used to construct any drug chemical compound structures

vi) **Clustal alignment identifier and phylogenetic tree constructer**: The Clustal Omega (https://www.ebi.ac.uk/Tools/msa/clustalo/ database was used to construct a phylogenetic tree to observe the relevance and evolutionary relatedness amongst *M. smegmatis*, *Mtb*, *M. leprae*, *E. coli*, and *B. subtilis ribF* homologs.

vii) **Protein domain predictor**: The InterPro protein sequence analysis & classification database (https://www.ebi.uk/interpro/) and the protein BLAST (https://blast.ncbi.nlm.nih.gov/Blast.cgi?PAGE=Proteins) database were used for the prediction of protein domains of RibF in model bacteria and Mycobacteria.

viii) **Statistical analysis**: Graphical representation of results and statistical variations in phenotypic features were analysed using the GraphPad Prism 7.04 software.

ix) **Protein structure predictor**: Protein Homology/analogY Recognition Engine version 2.0 was used to predict and analyse protein structures. The amino acid sequences of all tested mycobacterial proteins were accessed from Mycobrowser (*https://mycobrowser.epfl.ch*) with the human proteins obtained from NCBI. These sequences were pasted onto the amino acid sequence and the job was logged in after clicking the Phyre search tab. The server was accessed at *www.sbg.bio.ic.ac.uk › phyre2*

Chapter 3: Results

3.1 Selection and design of sgRNAs

Single guide RNAs (sgRNAs) are short oligonucleotides (oligos) that are complementary to the nucleotide sequence in the target gene of interest and are essential in mediating dCas9-sgRNA complex binding to the DNA to block RNA transcription by either occluding RNA polymerase access to the target promoter or steric blockage of transcription elongation (Rock et al. 2017). The sgRNAs were designed using a published algorithm (de Wet et al. 2018) which scans the length of the gene sequence, recognizing repetitive 2-6 bp protospacer adjacent motif (PAM) sequences that correlate with appropriate sgRNA binding sites. Ten potential targeting sites were identified within the *ribF* gene. The algorithm computationally assigned a score to each sgRNA sequence to predict the efficacy of transcriptional knockdown (Rock et al. 2017). Based on this scoring system, sgRNAs with low PAM scores were likely to cause the most efficient gene knockdown (**Table 3.1**; **Figure 3.1**).

Table 3.1: List of sgRNA oligos used to generate the constructs to knockdown the expression of *ribF* in this study.

CRISPR PRIMER SETS	SEQUENCES	PAM SCORE	DESCRIPTIVE sgRNA NAMES
MSMEG_2653_CrispRF1	3'-GGGAGCCGTCGAACACCCCGATGG-5'		
MSMEG_2653_CrispRR1	5'-AAACCCATCGGGGTGTTCGACGGC-3'	5	MSM_*ribF*_1
MSMEG_2653_CrispRF2	3'-GGGAGCAGGCCCGGATGTAGGTCGA-5'		
MSMEG_2653_CrispRR2	5'-AAACTCGACCTACATCCGGGCCTGC-3'	5	MSM_*ribF*_2
MSMEG_2653_CrispRF3	3'-GGGAGCCTCGACCGTGCGGGTGCGGCC-5'		
MSMEG_2653_CrispRR3	5'-AAACGGCCGCACCCGCACGGTCGAGGC-3'	5	MSM_*ribF*_3
MSMEG_2653_CrispRF4	3'-GGGAGAAGCGCTCACCGGCCTTGC-5'		
MSMEG_2653_CrispRR4	5'-AAACGCAAGGCCGGTGAGCGCTTC-3'	7	MSM_*ribF*_4
MSMEG_2653_CrispRF5	3'-GGGAAGCTGCGCCGGGTGGTTACC-5'		
MSMEG_2653_CrispRR5	5'-AAACGGTAACCACCCGGCGCAGCT-3'	11	MSM_*ribF*_5
MSMEG_2653_CrispRF6	3'-GGGAGTCGGAGGTGAACGGCATCAC-5'		
MSMEG_2653_CrispRR6	5'-AAACGTGATGCCGTTCACCTCCGAC-3'	11	MSM_*ribF*_6
MSMEG_2653_CrispRF7	3'-GGGAGGCGGTGCCACGTTGGCCGT-5'		
MSMEG_2653_CrispRR7	5'-AAACACGGCCAACGTGGCACCGCC-3'	11	MSM_*ribF*_7
MSMEG_2653_CrispRF8	3'-GGGAGTCTTGCCCACGCCAGCGTTGC-5'		
MSMEG_2653_CrispRR8	5'-AAACGCAACGCTGGCGTGGGCAAGAC-3'	13	MSM_*ribF*_8
MSMEG_2653_CrispRF9	3'-GGGAGACGACGTGCAGGTGCTCGA-5'		
MSMEG_2653_CrispRR9	5'-AAACTCGAGCACCTGCACGTCGTC-3'	13	MSM_*ribF*_9
MSMEG_2653_CrispRF10	3'-GGGAGTCGGAGGTGAACGGCATCA-5'		
MSMEG_2653_CrispRR10	5'-AAACTGATGCCGTTCACCTCCGAC-3'	14	MSM_*ribF*_10
MSMEG_0250_CrispRF	3'-GGGAGCGACAGACTGGCTGCCCTCGTC-5'		
MSMEG_0250_CrispRR	5'-AAACGACGAGGGCAGCCAGTCTGTCGC-3'		MSM_*mmpL3*

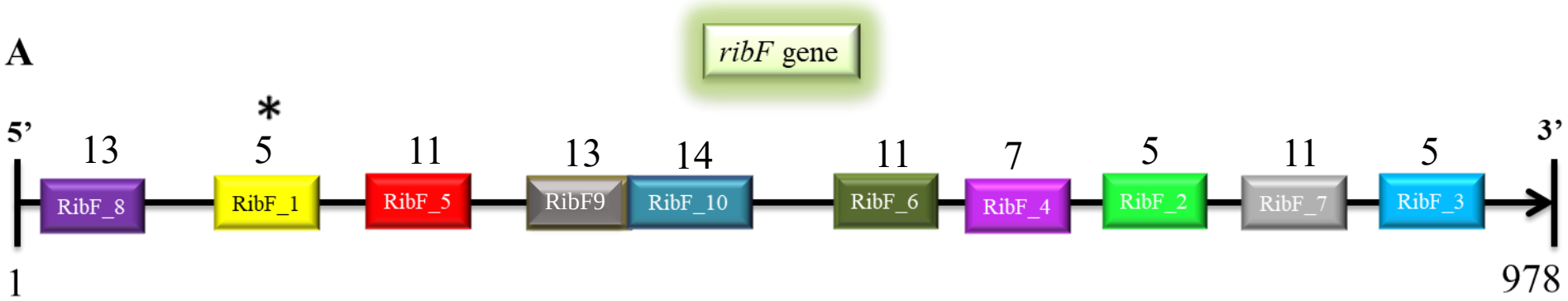

gtgcaacgctggcgtgggcaagacgagatccccacggactggggccggtgcgttctgaccatcggggtgttcgacggcgtccatcgtgggcatgcggagctgatcaaccacgcggt
caaggcgggccgggcccgtggagtccccgtggtgctgatgacgttcgatccccatccgatggaggtggtgttcccggtaaccacccggcgcagctgaccaccctgacccggcgcg
ccgagctggtcgaggaactcgggatcgacgtgttcctggtgatgccgttcacctccgacttcatgaagctgacccctgagcgctacatccacgagctgctcgtcgagcacctgcac
gtcgtcgaggtggtcgtgggggagaacttcacgttcggcaagaaggccgcgggcaacgtcgacatgctgcgcaaggccggtgagcgcttcgggttcgccgtcgaggcgatgtcgct
ggtcgccgagcatcaccgcaacgagacggtgacgttctcgtcgacctacatccgggcctgcgtcgacgcgggcgacatggtcgccgcggccgaggcgctgggccgtccccaccgcg
tcgaggggtcgtggtgcgcggcgacggccgtggccgggtgctcgggttcccgacggccaacgtggcaccgccatgtactcggcgatccccgccgacggcgtctacgcggcctgg
ttcacggtgctcggccagggaccgcaggtgggaaccgtcgtgccgggggagcggtatcaggccgcggtgtcggtggggaccaatccgacgttctcggggccgcacccgcacggtcga
ggcgttcgtgctcgacacgtttgccgacctgtacggacagcacgtcgcggtcgacttcgtgtcccgcatccgcggccaggagaagttcgattcggtcgacgacctcgtggtcgcga
tggaacgtgacgtcgagcgcgcccgcacgatcctgcgcgattctgtctag

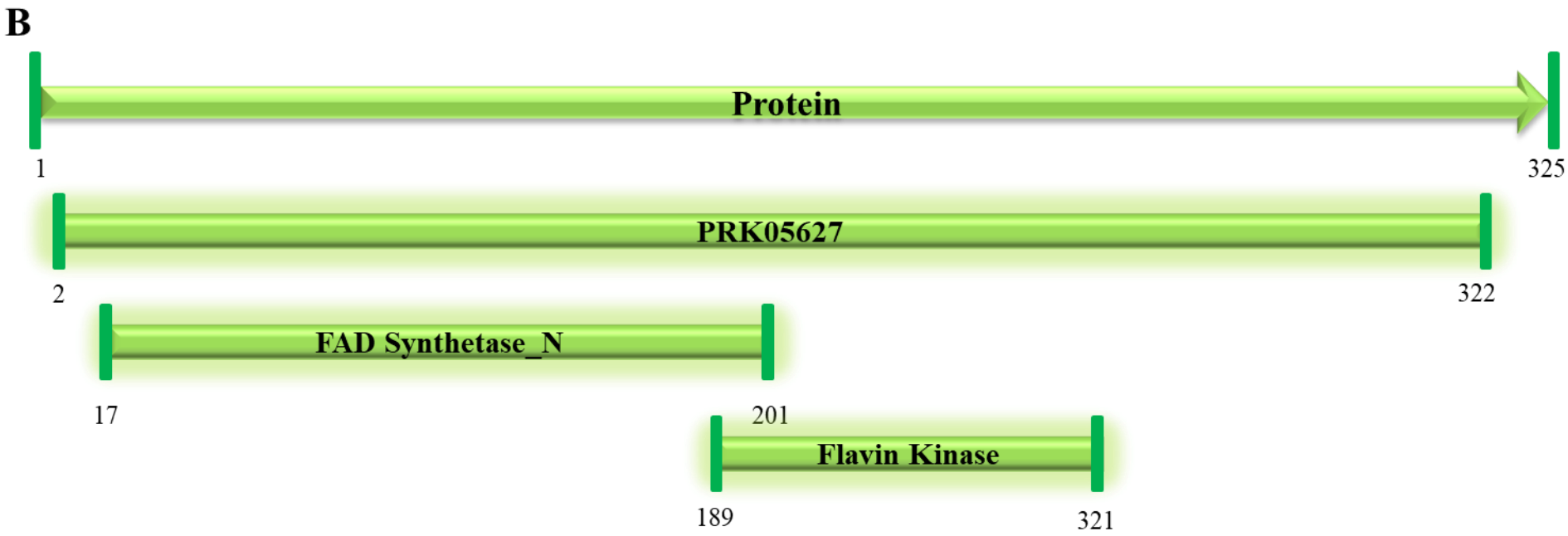

Figure 3.1: Distribution of sgRNAs designed to target *Msm ribF*. (A) The black line represents the length of the gene and each highlighted sequence represents an individual sgRNA in the DNA sequence of *ribF* annotated from 5` to 3`. The asterisk (*) indicates an sgRNA that was predicted to be the most effective targeting guide based on PAM score. Individual PAM scores are annotated above each sgRNA coloured box. (**B**) The bifunctional RibF comprises two domains, namely FAD synthetase_N and flavin kinase. Eight sgRNAs (RibF1, 2, 4, 5, 6, 8, 9 and 10) target the FAD_synthetase whereas the remaining two (RibF7 and 3) target the flavin kinase.

An optimized mycobacterial CRISPRi system (Rock et al. 2017) was used to investigate gene essentiality through transcriptional interference of *ribF* by monitoring the effect of its depletion on mycobacterial viability. To investigate the efficacy of the sgRNAs experimentally, each sgRNA (**Figure 3.1**) was used to create a gene knockdown construct, a 20 to 25 bp oligo constructed by a short PCR annealing of a Fwd and Rev primer. The sgRNA construct was cloned into a *Bsm*B1 digested CRISPRi (pLJR962) plasmid and transformed into DH5α *E. coli* cells. Sequence verification of positively incorporated sgRNAs was carried out by Sanger sequencing prior to electroporation into wild type *Msm* mc^2155 to generate inducible gene knockdown mutants or "hypomorphs" (**Figure 3.2**). Following electroporation, this plasmid integrates into the L5 site where it expresses both the sgRNA and the deactivated Cas9 (dCas9) under the control of the inducible anhydrotetracycline promoters. Phenotypic validation of the efficacy of knockdown and the level of gene repression associated with each guide was assessed using the microplate alamar blue assay (MABA).

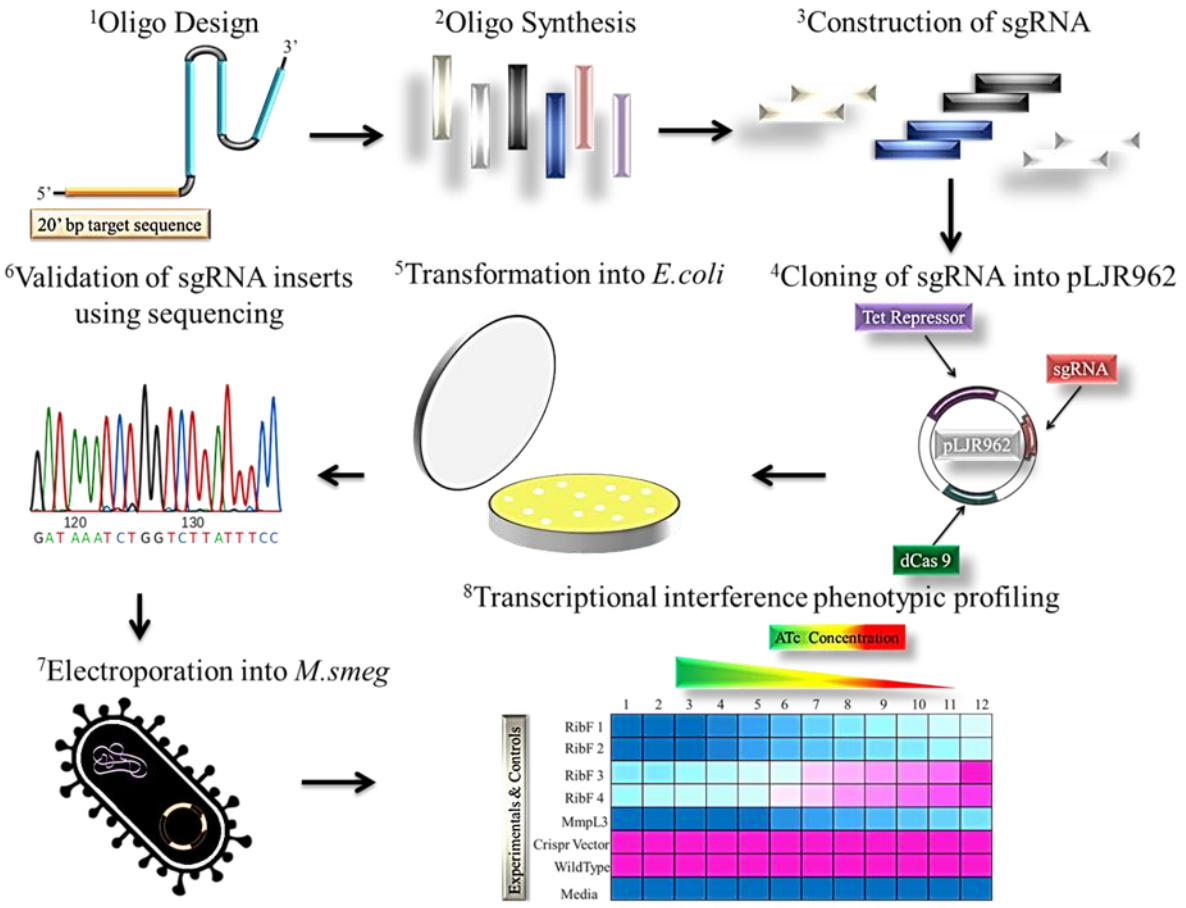

Figure 3.2: Tailoring CRISPRi knockdown mutants. Step 1 Oligos were designed to target *Msm ribF*. **Step 2** The oligos were commercially synthesized. **Step 3** sgRNAs were constructed through PCR annealing of the Fwd and Rev oligos. **Step 4** Each sgRNA was cloned into the pLJR962 plasmid**. Step 5** The recombinant plasmid was transformed into *E. coli*. **Step 6** Potential transformants carrying sgRNA constructs were validated by Sanger sequencing. **Step 7** Constructs were finally electroporated into *Msm*. **Step 8** Lastly an ATc MIC assay was carried out to measure the efficacy of each sgRNA.

3.2 Utilization of CRISPRi to probe the essentiality of *Msm ribF*

The sgRNAs were used to generate 10 hypomorphs (gene knockdown mutants) (**Figure 3.2**). In addition, 3 control strains were used throughout this project: (i) a hypomorph targeting *mmpL3* (MSM_MmpL3), a known essential gene required for trehalose mono-mycolate transportation across the inner membrane (Xu et al. 2017a), which was used as to demonstrate efficient gene repression using the CRISPRi system (McNeil and Cook 2019a),(ii) a vector-only *Msm* control strain (MSM_Vector) with no targeting sgRNA to ensure that the vector backbone had no adverse effects on cell growth and (iii) the wild type mc^2155 parental strain (MSM_WT) which was expected to phenocopy the vector-only control.

3.2.1 Phenotypic validation of transcriptional downregulation as a result of CRISPRi induction in *Msm*

It was critical to investigate the strength of transcriptional repression of each sgRNA to identify the most efficient guides and to establish if these correlated to that which had been predicted computationally. To test this, mycobacterial cultures were grown to an exponential phase of an OD_{600} of 0.5 (hereafter referred to as exponential phase) and were serially diluted in 2-fold increments before spotting onto media either without ATc (uninduced) or containing 100 ng/ml ATc to induce CRISPRi-mediated repression. These results demonstrated that, as predicted, the strength of transcriptional knockdown was inversely proportional to the calculated PAM score: 7 of the guides (RibF1-7) with PAM scores ranging from 5-11 elicited the most effective growth repression. The remaining 3 guides, RibF8-10, did not result in discernible growth inhibition. Notably, no clear trend relating guide efficacy to position within the gene was detected; that is, as reported previously (Rock et al. 2017; de Wet et al. 2018), location closer to either the 5` or 3` terminus did not yield any bias towards better transcriptional repression. As expected, the growth of the MSM_Vector and MSM_WT

controls were unaffected, in contrast, the growth of MSM_MmpL3 was potently inhibited (**Figure 3.3**).

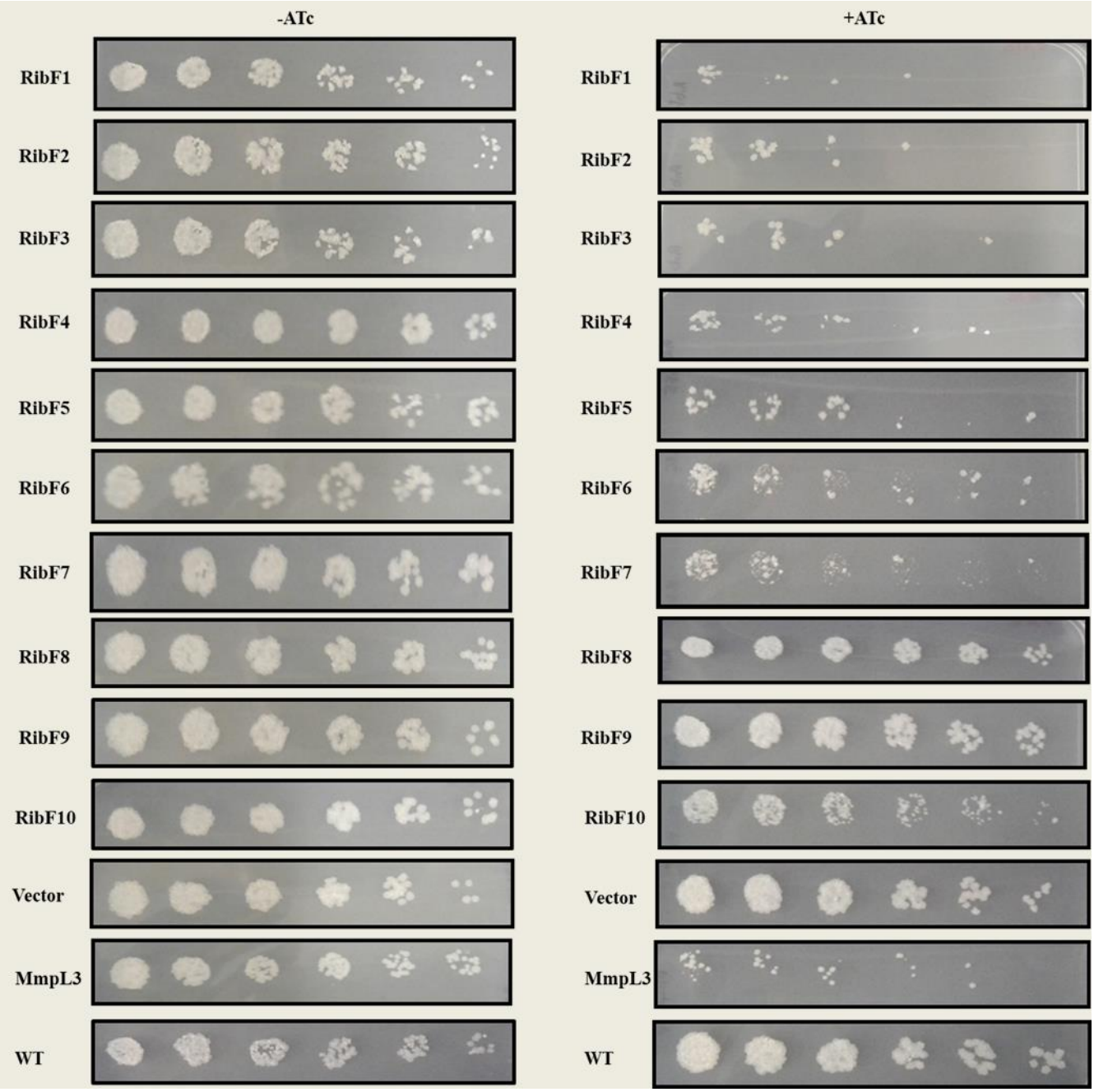

Figure 3.3: CRISPRi-mediated growth inhibition via *ribF* repression. Spotting assays of exponential phase cultures in 2-fold dilutions on standard 7H10 medium without ATc (-ATc) (Left) and with ATc (+ATc) (Right). Strain names are indicated on the left of the images. Results represent one of the three biological replicates. The first spot in each case contains approximately 5000 mycobacterial cells.

This assay was also performed in liquid medium in a broth microdilution assay in which all strains were again grown to exponential phase and exposed to a range of ATc concentrations. In this assay, the first 5 strains, RibF1-5, were highly repressed in the presence of ATc (as evident from the reduction in fluorescence) and were responsive to ATc concentrations as low as 1.6 ng/ml. RibF6 and RibF7 were not as responsive to ATc in the liquid assay. Based on the solid and liquid phenotypes observed with the 10 hypomorphs, MSM_RibF1 (hereafter referred to as MSM_RibF) was selected for use in all further experiments (**Figure** 3.4).

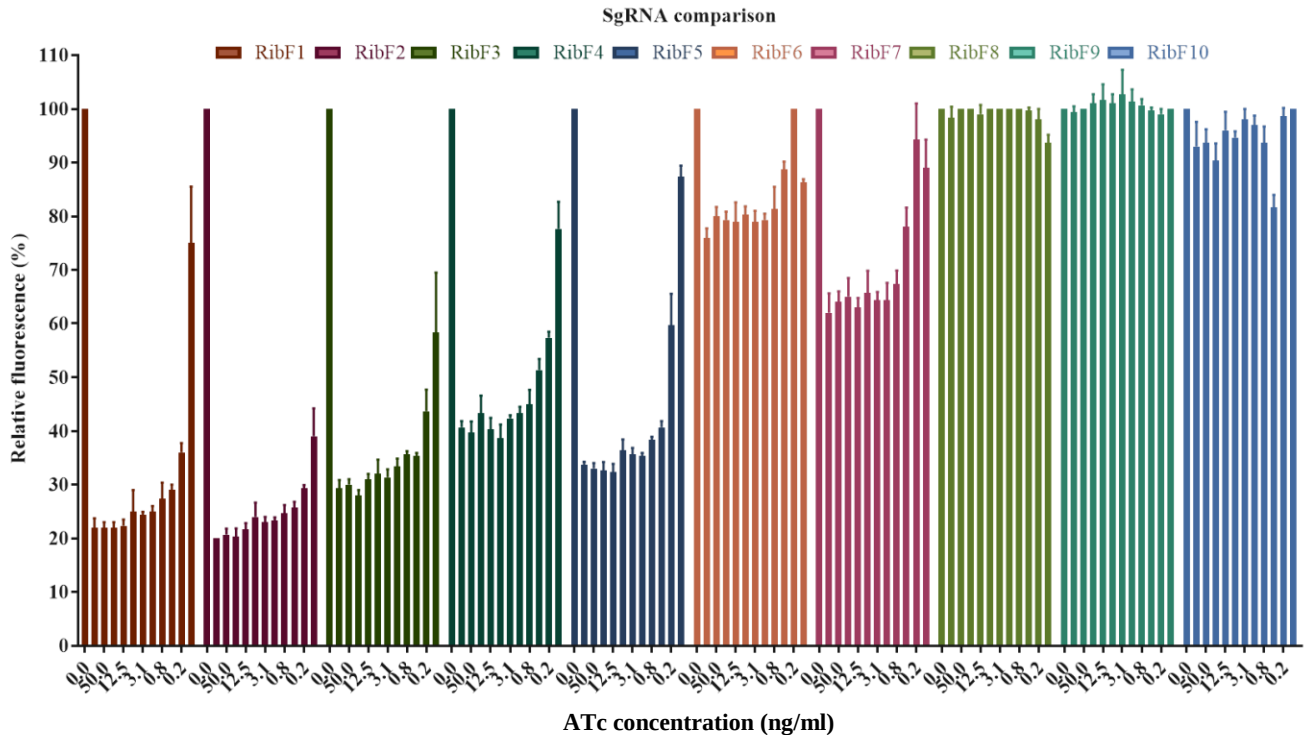

Figure 3.4: Growth responsiveness of RibF hypomorphs to different concentrations of ATc. Each bar represents the relative fluorescence percentage (%) determined at the corresponding ATc concentration. Relative fluorescent percentages were calculated such that the raw experimental values were divided by the average row of the uninduced cells only control and multiplied by 100 to enumerate percentages, based on microplate alamar blue assay (MABA) readings. Error bars represent standard deviations and were derived from three technical replicates.

We speculated that the extent of gene repression might depend on the inoculum used in setting up the microdilution assay; that is, the total number of cells applied in each well of the microwell plate. This was investigated by monitoring the growth of liquid cultures at starting inoculums of 0.004, 0.016, 0.06 and 0.25 in the absence and presence of ATc. At the starting inoculum of 0.004, the growth of MSM_RibF was reduced by 11-fold compared to

the uninduced control. As the inoculum was increased from 0.016 to 0.06 and 0.25, growth was less effectively repressed. That is, an increase in the inoculum caused the growth inhibition to be reduced by 7-fold, 3-fold and 1-fold, respectively, compared to the ATc unexposed control (**Figure 3.5**). All inocula concentrations revealed statistical significance in growth repression at 21 and 24 hours, $P < 0.0001$.

As expected, the MSM_Vector and MSM_WT control strains showed negligible differences in growth at all inoculum concentrations under induced and uninduced conditions. The repression of *mmpL3* expression led to a 20-fold decrease in growth at the lowest inoculum. As the starting inocula were adjusted to 0.016, 0.06 and 0.25, growth inhibition was less effective, resulting in 18-fold, 6-fold and 2-fold reduction, respectively, compared to the untreated culture. Similarly, all tested inoculum concentrations showed robust statistical significant differences in growth inhibition as early as 15 hours until 24 hours at the high inocula starting cultures of 0.06 and 0.25. In addition, the lowest inoculum revealed abundant differences at 24 hours and at 18, 21 and 24 hours using a 0.016 inoculum culture, $P < 0.0001$ (**Figure 3.5**). These results demonstrated that gene repression, judged as the greatest log fold difference between ATc treated and untreated at the lowest starting inoculum had the greatest impact on bacterial growth. Consequently, a starting inoculum of 0.004 was utilized for all subsequent growth kinetic experiments (**Figure 3.6 and 3.7**).

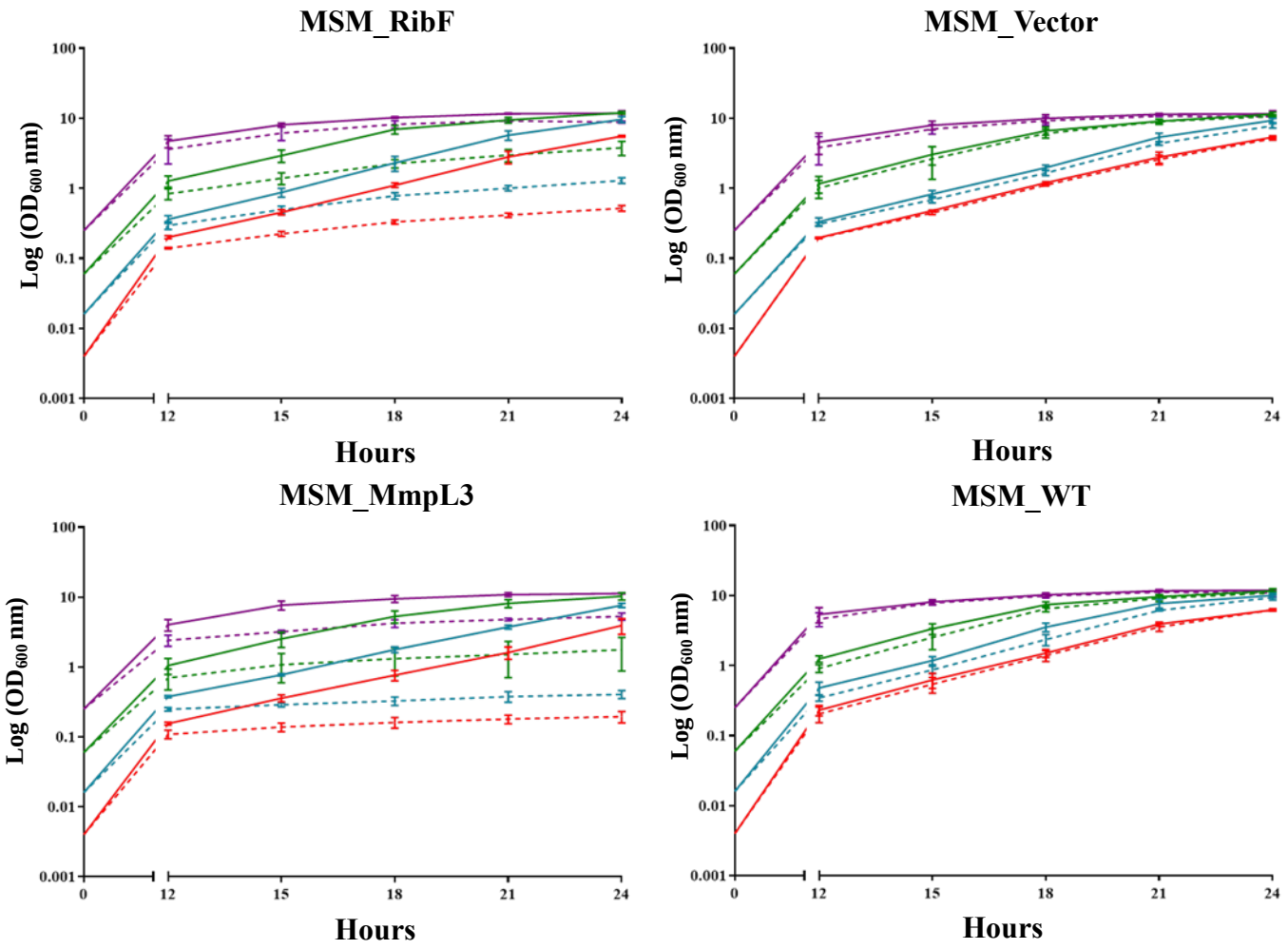

Conditions	Varying inoculum concentrations under tested conditions			
	0.004	0.016	0.06	0.25
Uninduced (-ATc)				
Induced (+ATc)				

Figure 3.5: CRISPRi-dependent growth repression is inoculum dependent. Growth kinetics of MSM_RibF, MSM_Vector, MSM_MmpL3 and MSM_WT in 7H9-OADC medium with varying inoculum concentrations: 0.004, 0.016, 0.06 and 0.25. Cells were incubated for 24 hours with optical density (OD_{600}) measurements taken at 3 hour intervals. The solid lines represent no ATc addition whereas the dashed lines represent the addition of 100 ng/ml ATc. The inset shows the growth at different starting inocula in the first 12 hours. Each colour corresponds to a specific inoculum concentration and the data represent standard deviations (SDs) of 3 biological replicates. Statistical comparisons were performed using Sidak's multiple comparison test using a 2way ANOVA multiple comparison analysis.

We next determined the minimum inhibitory concentration of ATc (ATc "MIC") required to induce effective transcriptional knockdown; *i.e.* that which manifested as above 80% reduction in growth relative to the untreated control. Briefly, cultures were inoculated at

a starting OD_{600nm} of 0.004 and exposed to serial 2-fold dilutions of ATc starting from 0.1-100 ng/ml, and OD_{600nm} readings were recorded at 3 hourly intervals for 24 hours (**Figure 3.6**). The results demonstrated that MSM_RibF required a minimum of 18 hours for growth inhibition to become evident (this observation is consistent with other CRISPRi-mediated essential gene knockdowns in *Msm*; (de Wet et al. 2018) and that 3.125 ng/ml ATc represented the lowest concentration required to induce significant growth repression, $P < 0.0001$. Overall, all ATc concentrations above 3.125 ng/ml were sufficient to mediate knockdown equivalent to exposure to 100 ng/ml ATc, whereas those below 3.125 ng/ml were less efficient in inducing knockdown (**Figure 3.6**).

As expected, MSM_Vector and MSM_WT exhibited no significant differences in growth from 0 till 18 hour time points. However, unexpected significant differences were observed between the uninduced and ATc exposed MSM_Vector strains at 21 and 24 hours after exposure to 100, 50, 25, 12.5 and 6.3 ng/ml ATc concentrations, $P < 0.0001$, with no observable significance in MSM_WT at any time point (**Figure 3.6**). It is possible that the slight reduction in growth of this strain in the presence of ATc at 21 and 24 hours can be attributed to prolonged incubation with ATc which has been shown to affect the electron transport chain (Moullan et al. 2015). Further work is required to demonstrate this unequivocally. The growth of both MSM_MmpL3 and MSM_RibF were unaffected from 0 till 15 hours, consistent with the inferred time lag required for the cell to exhaust the target proteins as a result of protein utilization or degradation. This suggests that a number of factors (including mRNA and protein turnover rates) likely determine how quickly a growth phenotype is detectable. MSM_MmpL3 growth was also reduced significantly in the presence of 3.125 ng/ml ATc at 21 and 24 hours, $P < 0.0001$ (**Figure 3.6**). Therefore, it appears that, in this system, more than 3.125 ng/ml ATc is required for full transcriptional repression and potent growth inhibition.

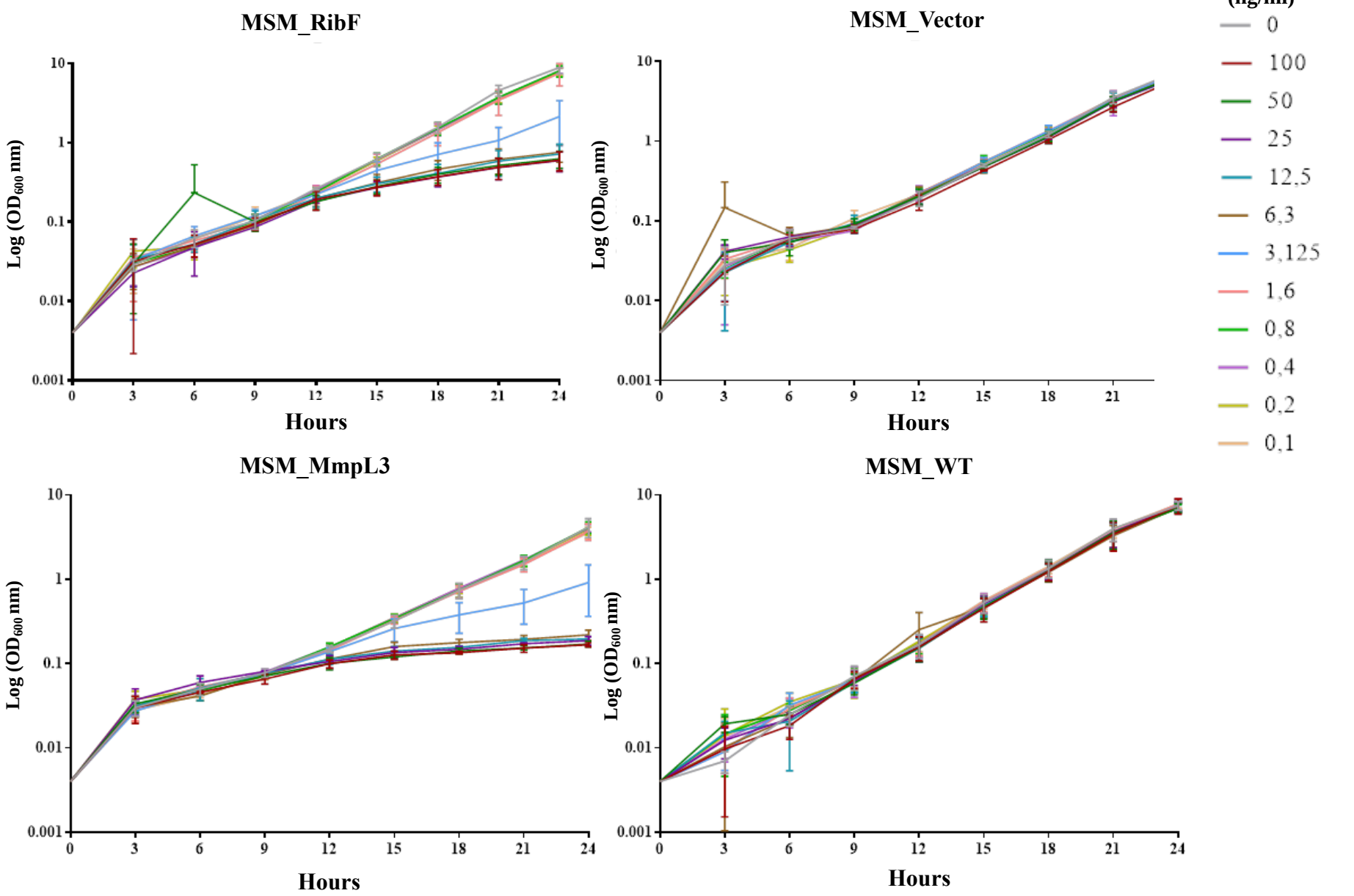
MSM_RibF
MSM_Vector
MSM_MmpL3
MSM_WT
Log (OD600 nm)
Hours
ATc concentration (ng/ml)
0
100
50
25
12,5
6,3
3,125
1,6
0,8
0,4
0,2
0,1

Figure 3.6: CRISPRi efficacy is ATc concentration dependent. Growth kinetics of MSM_RibF, MSM_Vector, MSM_MmpL3 and MSM_WT in 7H9 media. Cultures were started from an initial inoculum of an OD_{600nm} of 0.004 and readings were taken at 3 hour time intervals over 24 hours. Coloured lines represent the different concentrations of ATc used ranging from 100 to 0 ng/ml. Data are representative of 3 biological replicates with SDs shown as error bars. Statistical analysis was conducted using the Dunnett's multiple comparison test using a 2way ANOVA analysis test.

It was noteworthy that the ATc MIC of 3.125 ng/ml inferred from OD readings (**Figure 3.6**) to some degree varied from the MIC of 0.4-0.8 ng/ml suggested by fluorescence readings (**Figure 3.4**) in the sgRNA efficacy comparison. It seemed likely that this difference could be ascribed to the fact that the two assays employed different growth parameters of stationary growth in microtitre plate assay versus aerobic culturing in the flask. Previous observations also indicate that optical density does not necessarily directly correspond to viable fluorescence output (Arora et al. 2014).

3.3 Consequence of *ribF* depletion on cell growth and viability in *Msm*

Next, we determined the effect of *ribF* depletion on the growth and viability of the MSM_RibF strain by measuring optical density and CFUs during liquid culture. An adverse effect on bacterial growth could be detected as early as 12-15 hours post ATc induction (**Figure 3.7**). As expected, repression of *ribF* resulted in a 10-fold difference in growth at 24 hours between the ATc-induced and uninduced strains. In addition, the corresponding CFU counts at this timepoint reflected no reduction in CFUs, indicating that *ribF* is essential for bacterial growth and that its depletion results in bacteriostasis. Furthermore, different colony morphotypes of RibF were observed from the ATc induced culture after plating (**Supplementary figure S6**). Noticeably, large colonies similar to MSM_WT were observed, however a smaller colony phenotype was also evident. Individual colonies were isolated and the genomic DNA extracted as outlined in **2.1.10**. These samples were sent for whole genome sequencing analysis to identify the genetic basis for the observed colony morphologies; however results of this analysis are still pending. MSM_Vector and MSM_WT controls exhibited no observable impairment of bacterial growth in induced and uninduced cultures, indicating that the vector backbone alone had no effect on bacterial growth and no gene in the MSM_Vector strain was non-specifically targeted.

The repression of *mmpL3* resulted in a robust 20-fold reduction in growth in liquid media when induced with ATc and a subsequent 2.5 log-fold drop in CFUs at 24 hours, confirming that targeting this gene was bactericidal. *MmpL3* is highly susceptible to depletion

as has been previously demonstrated (Degiacomi et al. 2017), a minimal time of just 3 hours was sufficient to detect a reduction in CFUs indicating cell vulnerability as a consequence of MmpL3 deficiency (**Figure 3.7**).

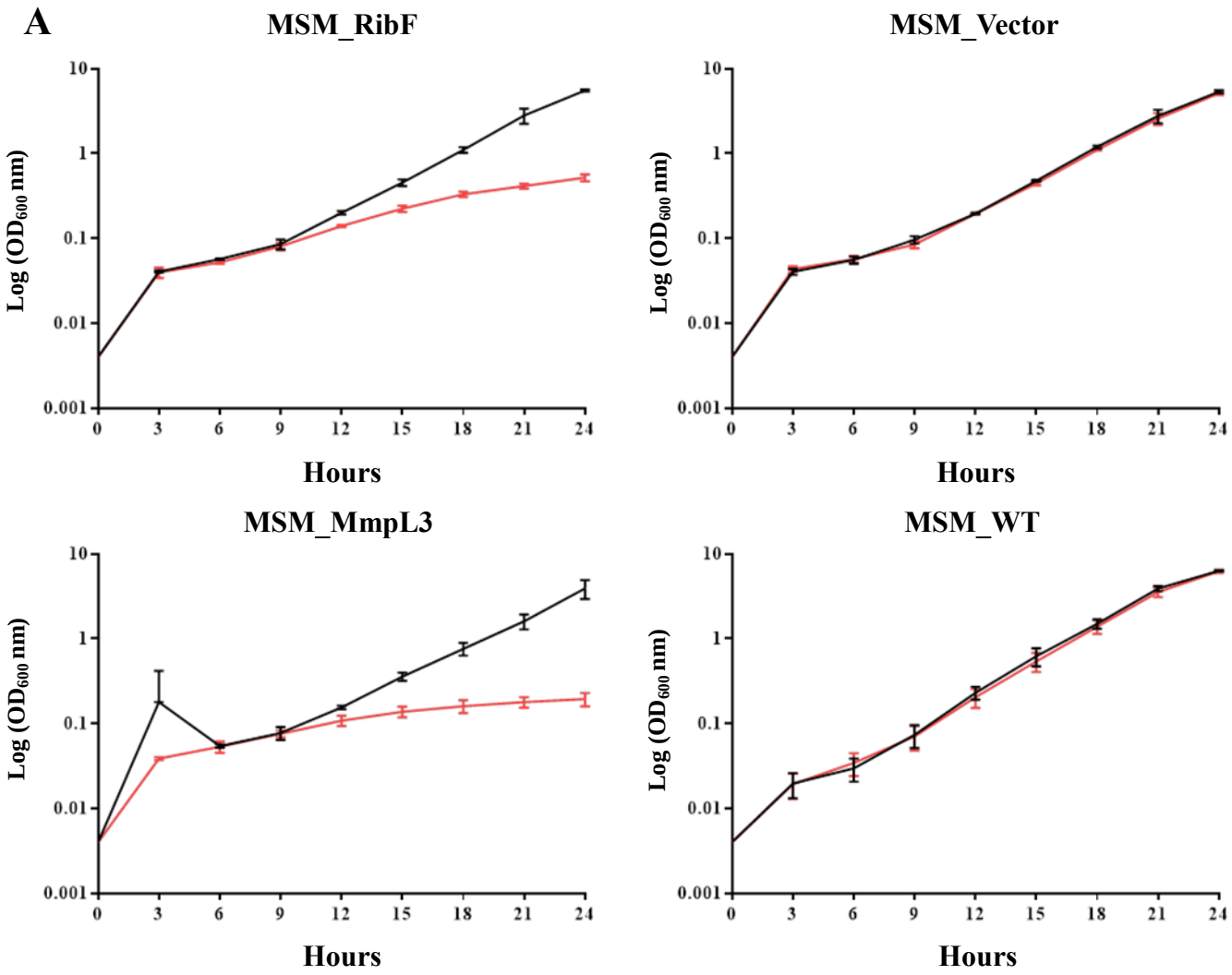

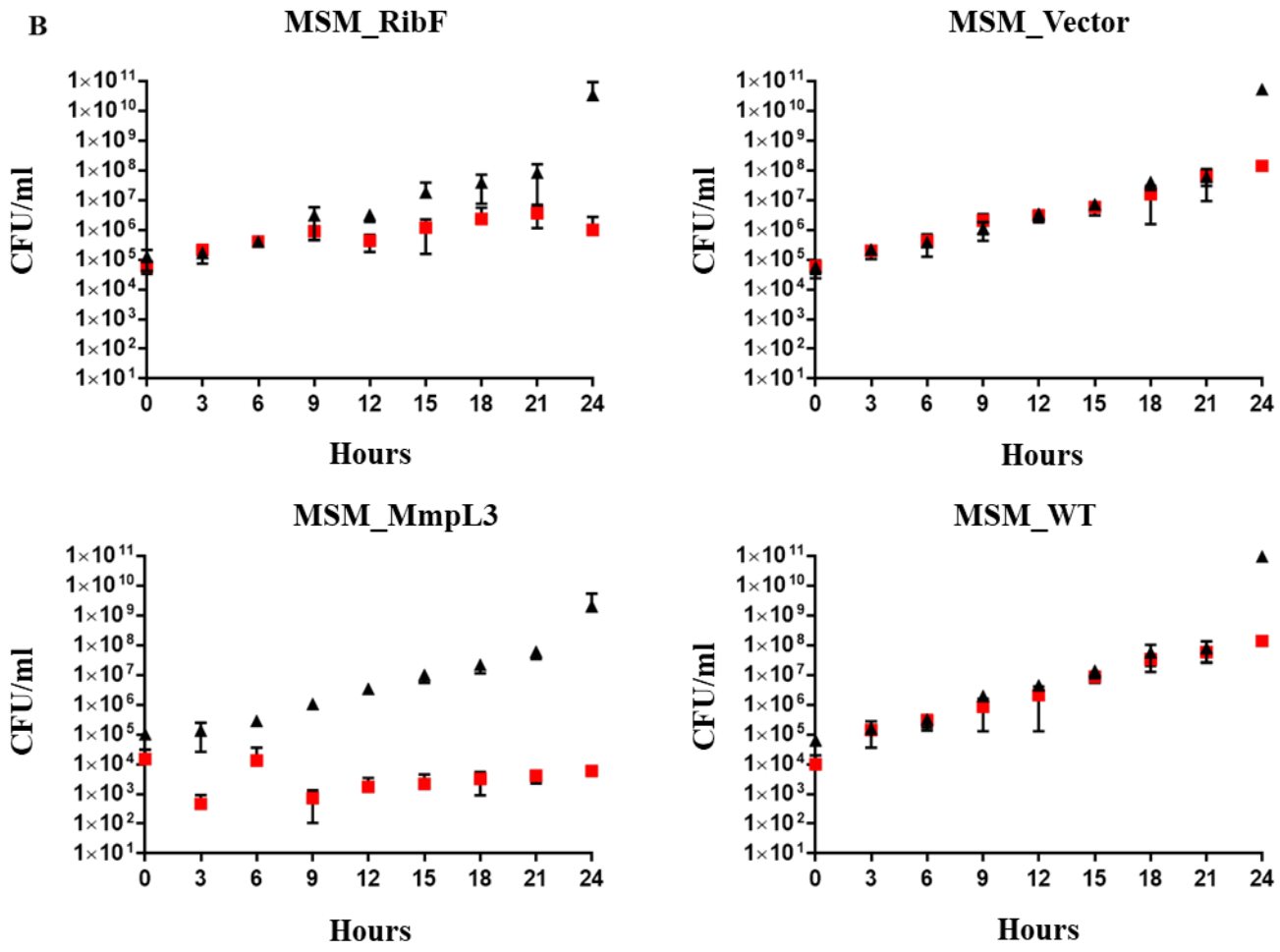

Figure 3.7: CRISPRi mediates inducible knockdown of essential genes in *Msm* with measurable consequences on growth viability. (A) Growth curves and **(B)** corresponding CFU counts of MSM_RibF, MSM_Vector, MSM_MmpL3 and MSM_WT exposed to 0 (black line/triangle) or 100 ng/ml ATc (red line/square) for 24 hours. OD readings were taken every 3 hours and aliquots plated for CFU determination. Plotted lines represent OD readings while triangles and squares are CFU/ml counts. Error bars represent standard deviations of 3 biological replicates and the limit of detection is 10^2 CFU/ml.

3.4 Transcriptional downregulation of *ribF* by CRISPRi induction in *Msm*

To confirm that the observed phenotypes could be equated to downregulation of *ribF* and were not a consequence of an off-target effect (Kim et al. 2015), the transcript levels of *ribF* were measured. Cultures were inoculated at an initial OD_{600nm} of 0.016 into 7H9-OADC liquid medium. This inoculum concentration was chosen primarily to induce efficient knockdown while allowing for sufficient biomass for RNA extraction. RNA was extracted from induced and uninduced cultures at 24 hours. Synthesis of cDNA and qRT-PCR analysis was performed as detailed in 2.1.7. The results indicated effective knockdown in the induced strains when compared to the uninduced strains at 24 hours. Following ATc induction,

MSM_MmpL3 revealed a 14-fold drop in transcript levels and similarly, there was a 11-fold reduction in transcript levels in MSM_RibF, $P < 0.0001$ (**Figure 3.8**).

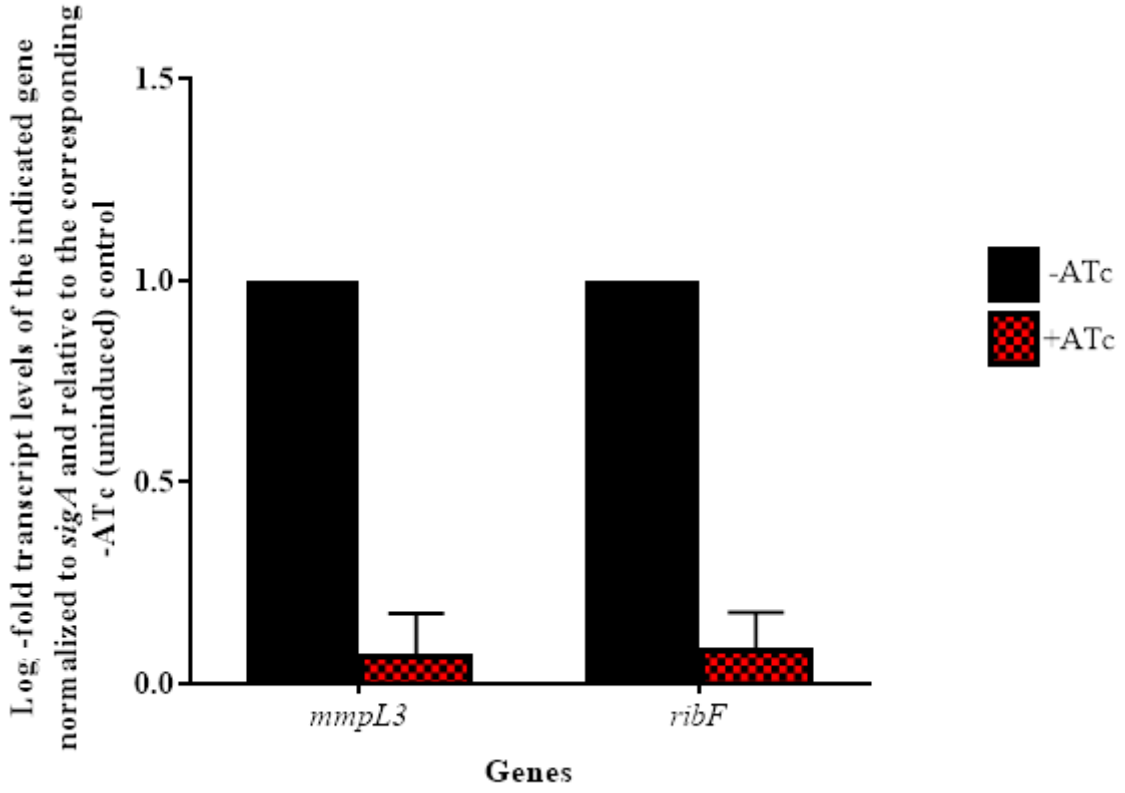

Figure 3.8: CRISPRi-mediated transcriptional depletion of *mmpL3* and *ribF*. Black bars represent transcripts measured in strains grown in the absence of ATc (-ATc) while red bars indicate transcript levels in the presence of the inducer (+ATc). Error bars are SD of 3 technical replicates. Statistical analysis was conducted using Sidak's multiple comparison in a 2way ANOVA multiple comparison analysis test.

3.5 MSM_RibF lethality cannot be rescued by riboflavin, FMN or FAD

The possibility that host-derived metabolites might rescue antibiotic-mediated nutrient auxotrophy is a key concern in targeting metabolic pathways for new TB drug development. For this reason, we tested the potential for uptake and assimilation of exogenous riboflavin (RF), FMN or FAD to rescue *ribF* depletion. To this end, the hypomorph strains were grown in 7H9-OADC medium to exponential phase before exposure to ATc (50 ng/ml) in combination with decreasing concentrations of each of the three potential metabolites of riboflavin biosynthesis: RF, FMN, or FAD (column 2 to 12). In this assay, the ability of each substrate to mitigate *ribF* depletion would result in improved growth relative to the unsupplemented ATc-exposed culture. Exposure to the individual metabolites alone did not

inhibit growth (**Figure 3.9**, **column 1**), establishing that none was toxic at the concentrations applied. However, there was complete absence of growth in ATc-exposed cultures irrespective of the metabolite concentration provided, apparently eliminating the capacity in *Msm* for salvage or assimilation of these metabolites when RibF was depleted (**Figure 3.9**). As expected, MSM_Vector and MSM_WT were unaffected in all conditions and moreover, MSM_MmpL3 was not rescued by any of the additives.

To validate these results, an equivalent spotting assay was performed. Briefly, cultures were grown to exponential phase in 7H9 and diluted serially in 2-fold increments prior to being spotted onto solid 7H10 medium containing any of the three metabolites alone or in combination with 100 ng/ml ATc. Again, the phenotypes observed, verified that none of the metabolites was capable of rescue (**Supplementary figure S5**).

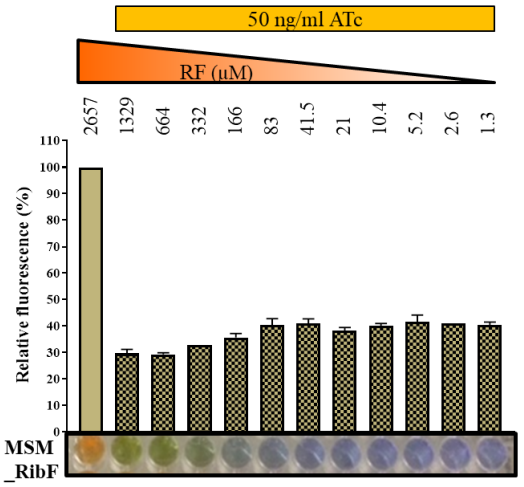
50 ng/ml ATc
RF (µM)
2657 1329 664 332 166 83 41.5 21 10.4 5.2 2.6 1.3
Relative fluorescence (%)
MSM _RibF

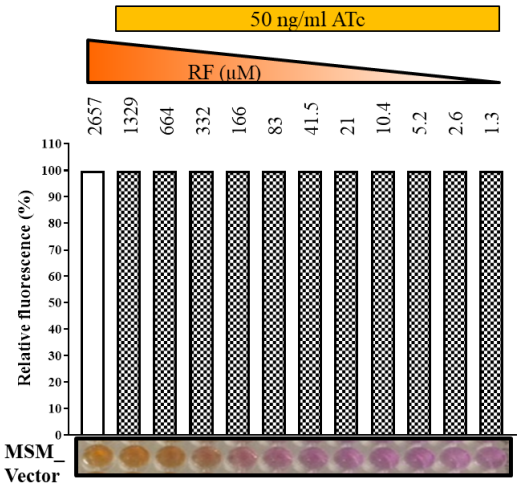
50 ng/ml ATc
RF (µM)
2657 1329 664 332 166 83 41.5 21 10.4 5.2 2.6 1.3
Relative fluorescence (%)
MSM_ Vector

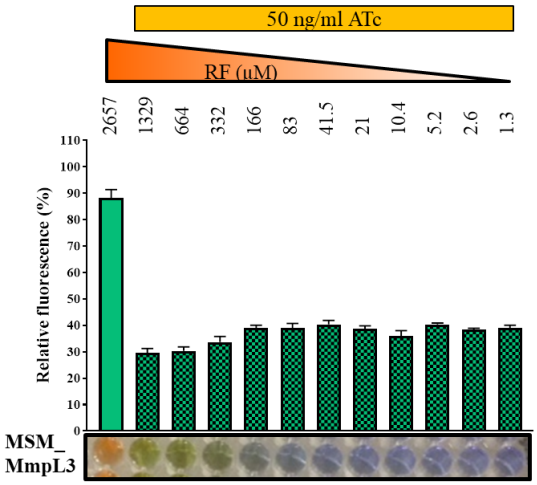
50 ng/ml ATc
RF (µM)
2657 1329 664 332 166 83 41.5 21 10.4 5.2 2.6 1.3
Relative fluorescence (%)
MSM_ MmpL3

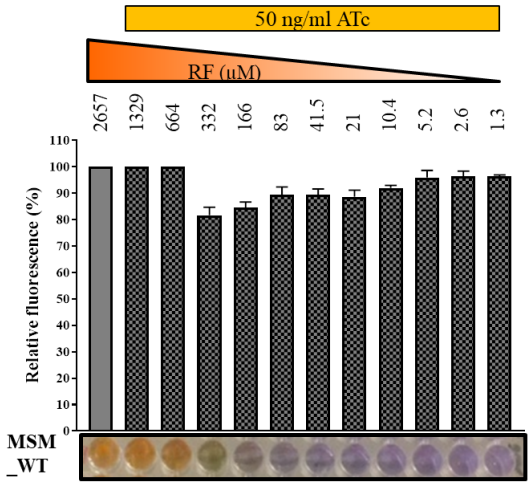
50 ng/ml ATc
RF (µM)
2657 1329 664 332 166 83 41.5 21 10.4 5.2 2.6 1.3
Relative fluorescence (%)
MSM _WT

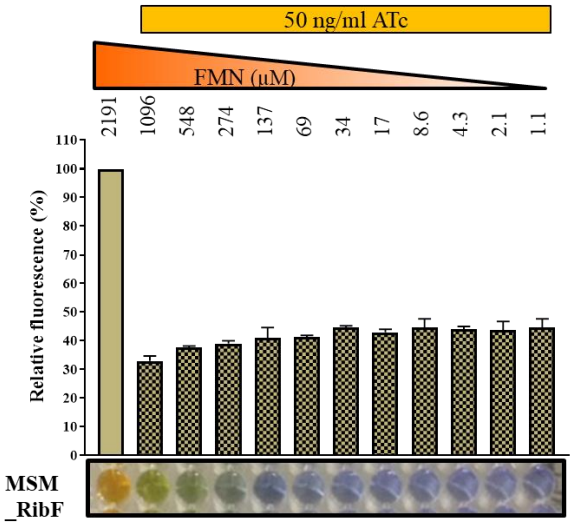
50 ng/ml ATc
FMN (µM)
2191 1096 548 274 137 69 34 17 8.6 4.3 2.1 1.1
Relative fluorescence (%)
MSM _RibF

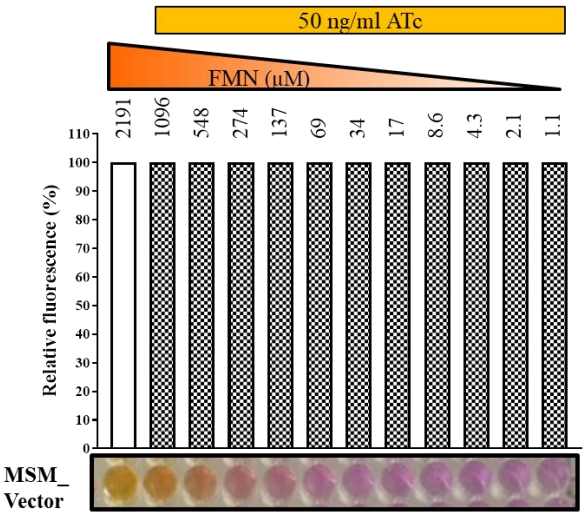
50 ng/ml ATc
FMN (µM)
2191 1096 548 274 137 69 34 17 8.6 4.3 2.1 1.1
Relative fluorescence (%)
MSM_ Vector

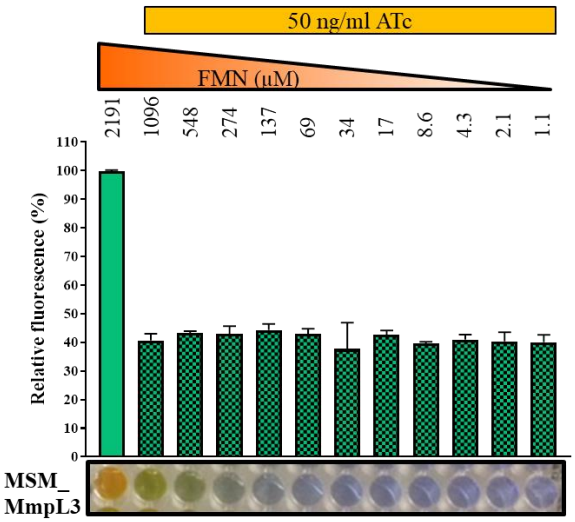
50 ng/ml ATc
FMN (µM)
2191 1096 548 274 137 69 34 17 8.6 4.3 2.1 1.1
Relative fluorescence (%)
MSM_ MmpL3

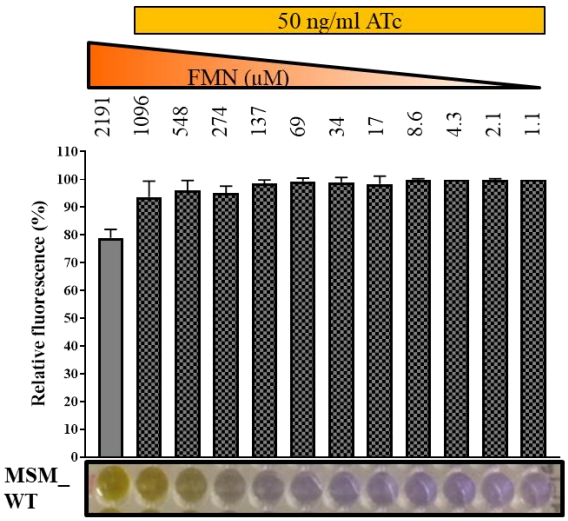
50 ng/ml ATc
FMN (µM)
2191 1096 548 274 137 69 34 17 8.6 4.3 2.1 1.1
Relative fluorescence (%)
MSM_ WT

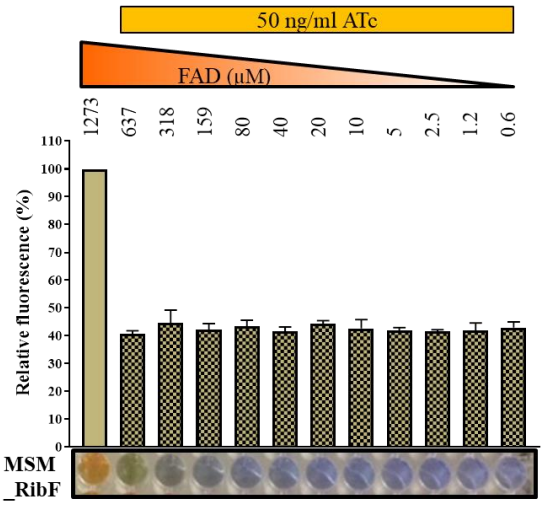
50 ng/ml ATc
FAD (µM)
1273 637 318 159 80 40 20 10 5 2.5 1.2 0.6
Relative fluorescence (%)
MSM _RibF

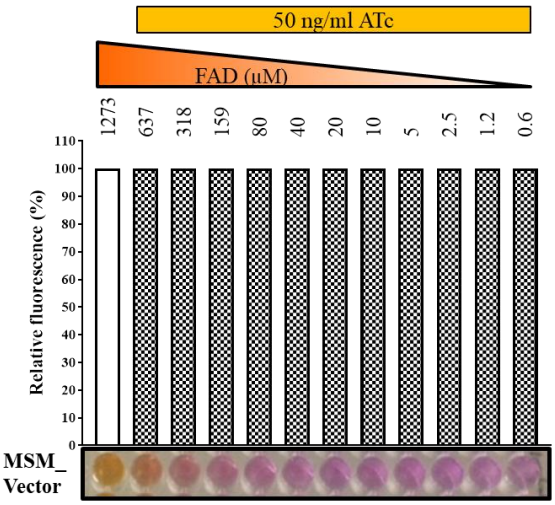
50 ng/ml ATc
FAD (µM)
1273 637 318 159 80 40 20 10 5 2.5 1.2 0.6
Relative fluorescence (%)
MSM_ Vector

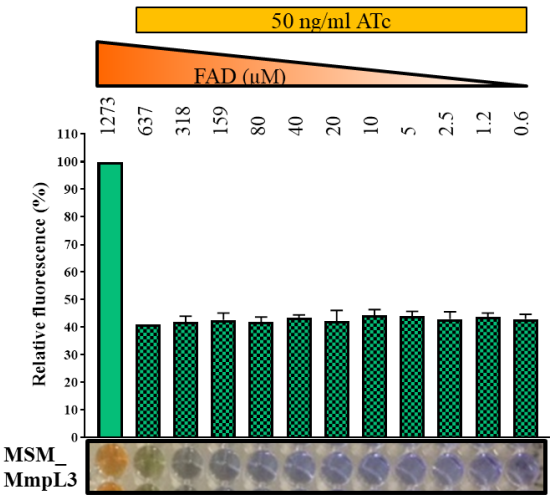
50 ng/ml ATc
FAD (µM)
1273 637 318 159 80 40 20 10 5 2.5 1.2 0.6
Relative fluorescence (%)
MSM_ MmpL3

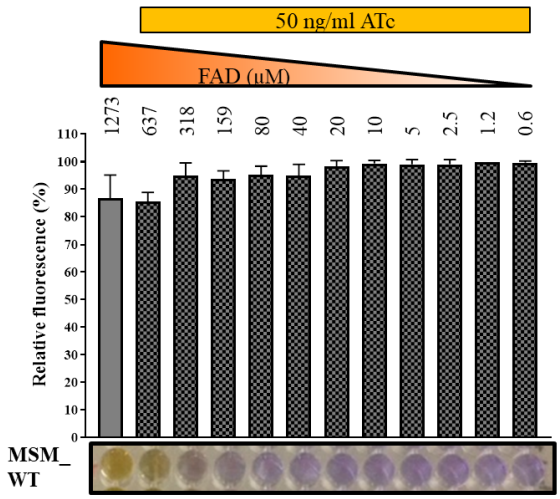
50 ng/ml ATc
FAD (µM)
1273 637 318 159 80 40 20 10 5 2.5 1.2 0.6
Relative fluorescence (%)
MSM_ WT

Figure 3.9: **RF metabolites cannot rescue *ribF* depletion.** Broth microdilution assays comprising 2-fold serial dilutions of each substrate with growth measured in relative fluorescence percentage. The concentrations of each substrate including the constant 50 ng/ml ATc are stipulated above each graph. Solid bars represent wells without ATc (-ATc) and patterned bars represent wells containing substrate with constant ATc (50 ng/ml) concentration. Each colour corresponds to a specific *Msm* strain and error bars are SD of three technical replicates.

3.6 Comparison of the mycobacterial and human RibF protein

The fact that *ribF* depletion could not be rescued by any of the tested metabolites (which are likely present in the human host) supported the notion that RibF could serve as an attractive target for new TB drug development. To determine the potential for selectivity, the mycobacterial RibF and its human RibF homolog structures were predicted using a protein computational modelling publicly available database; **P**rotein **H**omology/analog**Y** **R**ecognition **E**ngine version 2 (**Phyre**[2]). Full details of its use are provided in **2.1.11.3**. Despite the inability of humans and other mammals to synthesize RF, humans do possess a RibF homolog which is required to convert RF acquired from the diet to the essential derivative cofactors. In contrast to most bacteria, the human homolog is not bifunctional and humans instead possess separate RF flavokinase (RFK/FMN1) and FAD synthetase (FLAD1) proteins (Brizio et al. 2006; Barile et al. 2000).

Mtb RibF was used as the scaffold protein to model *Msm* RibF since the intention was to use this work to lay a foundation for follow-up investigations in the human pathogen. At both primary and tertiary levels, the *Msm* and *Mtb* proteins retained high sequence and structural similarity. Hence, the *Mtb* RibF protein scaffold was used to superimpose both the RFK and FLAD1 human proteins. These analyses indicated significant overlap between the *Mtb* RibF flavokinase and human flavokinase domains. In contrast, the FAD synthetase domains were non-homologous (**Figure 3.10**), suggesting that the FAD synthetase domain of the *Mtb* RibF protein should be preferentially targeted owing to the reduced risk of affecting the human FLAD1 protein.

Numerous FAD synthetase inhibitors with different activities have been identified by (Sebastian et al. 2018) who optimised an activity-based high-throughput screening assay for compounds targeting *Corynebacterium ammoniagenes* FAD synthetase. The identified inhibitors include alexidine dihydrochloride, benzethonium chloride, thonzonium bromide and verteporfin. Favourable whole-cell antimicrobial properties of these inhibitors were also observed against *Streptococcus pneumonia* and *Mtb* (Sebastian et al. 2018). However, this does not necessarily validate the target since there is no evidence (in the absence of a hypomorph or resistant mutant) to confirm that the compound is actually interacting with the RibF protein. In principle, the compound could inhibit growth by an unrelated mechanism – a common observation in TB drug discovery. Therefore, in this instance, the creation of a

CRISPRi hypomorph provided a platform to validate if these compounds are primarily targeting RibF.

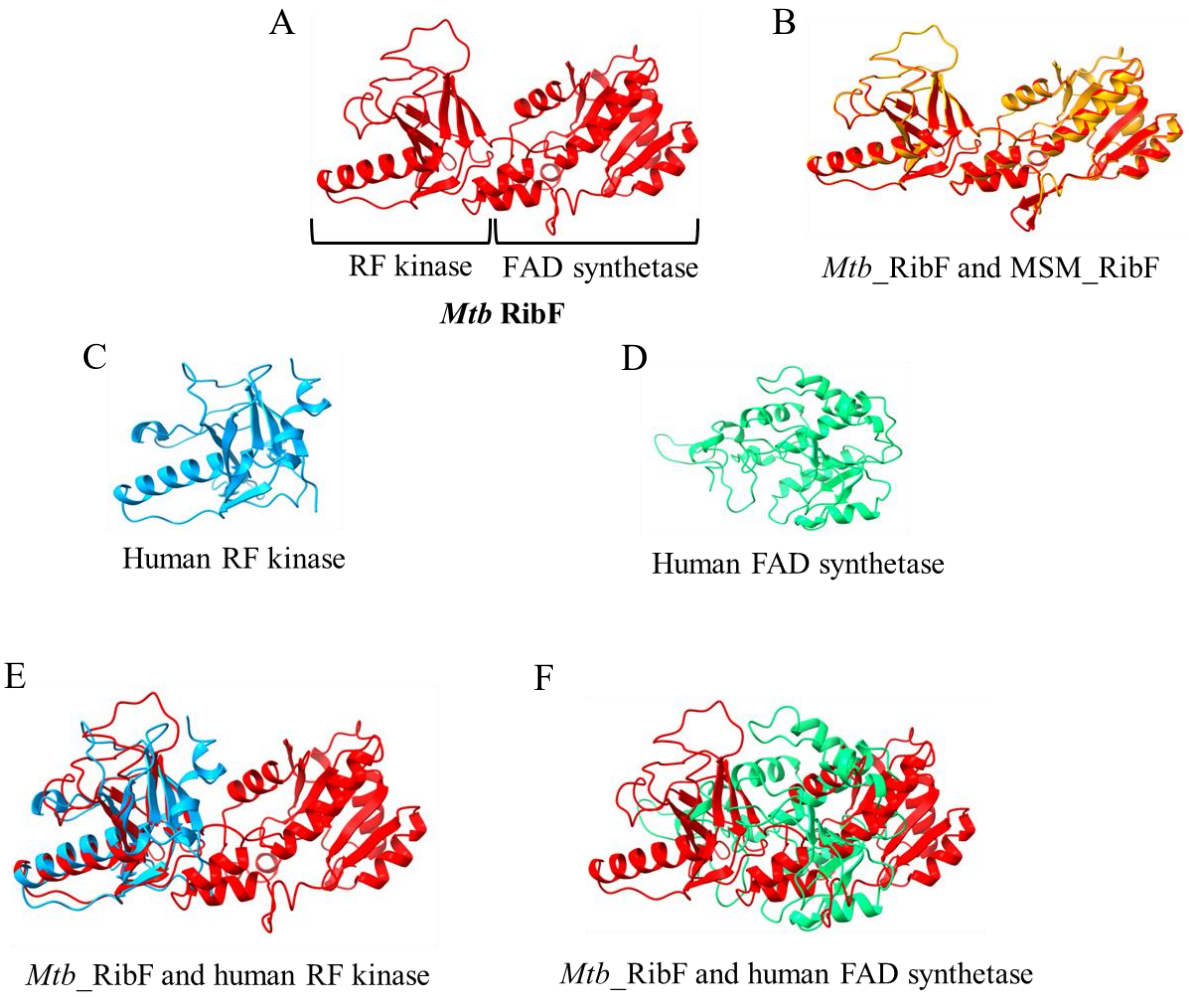

Figure 3.10: Structural homology between the *Mtb* and human RibF proteins. The red protein structure represents the *Mtb* RibF (**A**) whereas the yellow represents the *Msm* RibF (**B**). The blue represents the human RFK protein (**C**) and the green represents FLAD1, a FAD synthetase protein (**D**). Super-imposition of the *Mtb* RibF on the human RFK (**E**) and FLAD1 (**F**). All protein structures were adapted from Protein Homology/ analogY Recognition Engine V 2.0 (Phyre[2]).

3.7 Targeted depletion of *ribF* sensitizes *Msm* to putative FAD synthetase inhibitors and vancomycin

Hypomorphs have proven very useful in demonstrating on-target efficacy of compounds designed to inhibit mycobacterial growth in whole-cell assays (Evans and Mizrahi 2015). To evaluate the susceptibility of the MSM_RibF mutant to putative FAD synthetase inhibitors – alexidine dihydrochloride (ADD), benzethonium chloride (BZC) and thonzonium bromide (TZB) – the microplate alamar blue assay (MABA) (Franzblau et al. 1998) was used to assess hypersensitivity, manifested by any shift in MIC as a consequence on *ribF* depletion. Several compounds with distinct mechanisms of action were also included to identify any increased susceptibility to known antimycobacterial agents, consequent on RF pathway disruption and include rifampicin, ethambutol, para- aminosalicylic acid (PAS) and vancomycin. In addition, riboswitch inhibitors ribocil-C and roseoflavin were also tested.

First, the MIC of each compound was determined against MSM_WT to be used as a reference in order to establish if any shift in MICs that could be detected when testing MSM_RibF. Briefly, cultures were inoculated into 96-well microtitre plates, containing compounds diluted 2-fold and inhibition was determined colorimetrically via alamar blue reduction. The results demonstrated that MSM_WT was intrinsically resistant to roseoflavin, ribocil-C, verteporfin and para-aminosalicyclic acid (PAS), with MICs not determined at the concentrations used. In contrast, alexidine dihydrochloride, benzethonium chloride and thonzonium bromide returned weak MIC_{90} values of 80 µM, 12.5 µM, 25 µM, respectively except vancomycin which revealed an exceptionally low MIC_{90} of 0.0000055 µM, against MSM_WT (**Table 3.2**). MICs against known antimycobacterials was also determined (data not shown), only vancomycin was of interest and pursued further.

Table 3.2: Minimal inhibitory concentrations and structures of proposed FAD synthetase inhibitors against *Msm* mc^{2}155.

Compound name	Chemical structure	MIC_{90}
Alexidine dihydrochloride	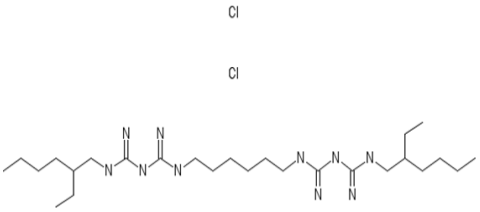	80 µM
Benzethonium chloride	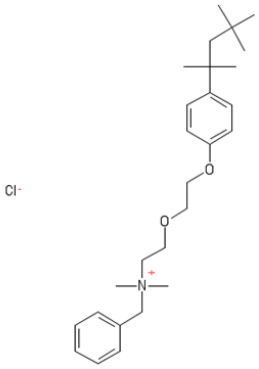	12.5 µM
Thonzonium bromide	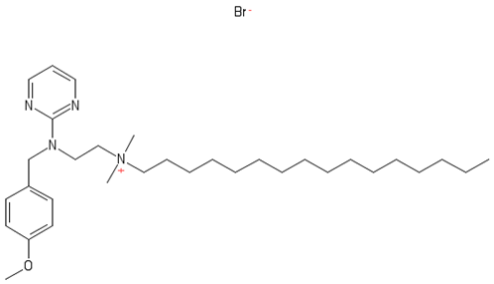	25 µM
Verteporfin	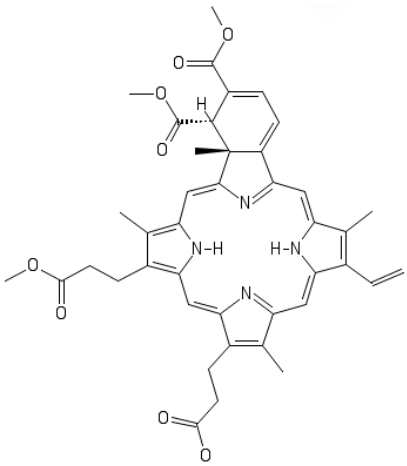	>200 µM

Roseoflavin	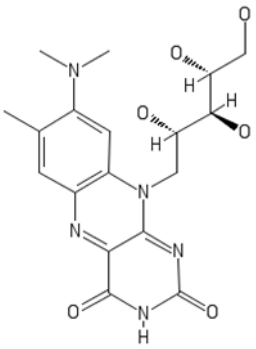	>200 µM
PAS	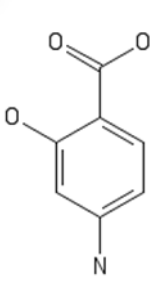	>3265 µM
Ribocil-C	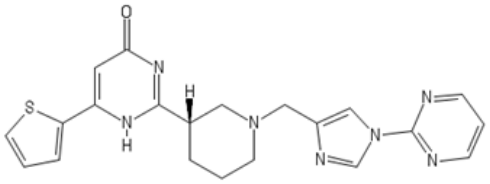	>200 µM
Vancomycin	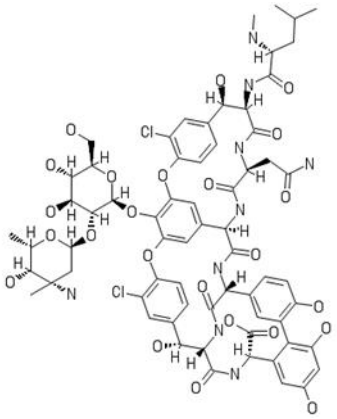	0.0000055 µM

Standard checkerboard assays are used to investigate possible synergistic drug-drug combinations that exhibit increased bacterial inhibition at sub MIC concentrations (Bhusal, Shiohira, and Yamane 2005; Berenbaum 1978). The method was adapted here using ATc as a known "on target" partner drug in combination with the other *Msm* active compounds to validate predicted compound mechanism of action involving RibF.

Recent work from our lab (Omollo et al. 2019) demonstrated a synergistic interaction between chlorpromazine and spectinomycin and the set-up used in that study was applied here as a template to illustrate interpretation of the checkerboard data (**Figure 3.11**). So, each 96 well plate was prepared such that column 1 and 12 represented "cell only" and "media only" controls, respectively. Row A represented drug X control with its specified MIC (light orange square (A5)) and similarly, well D2 (grey square) represented the MIC of drug Y in the drug Y control, column 2. The combination of the two drugs ranges from B3 diagonally to H11 (**Figure 3.11**).

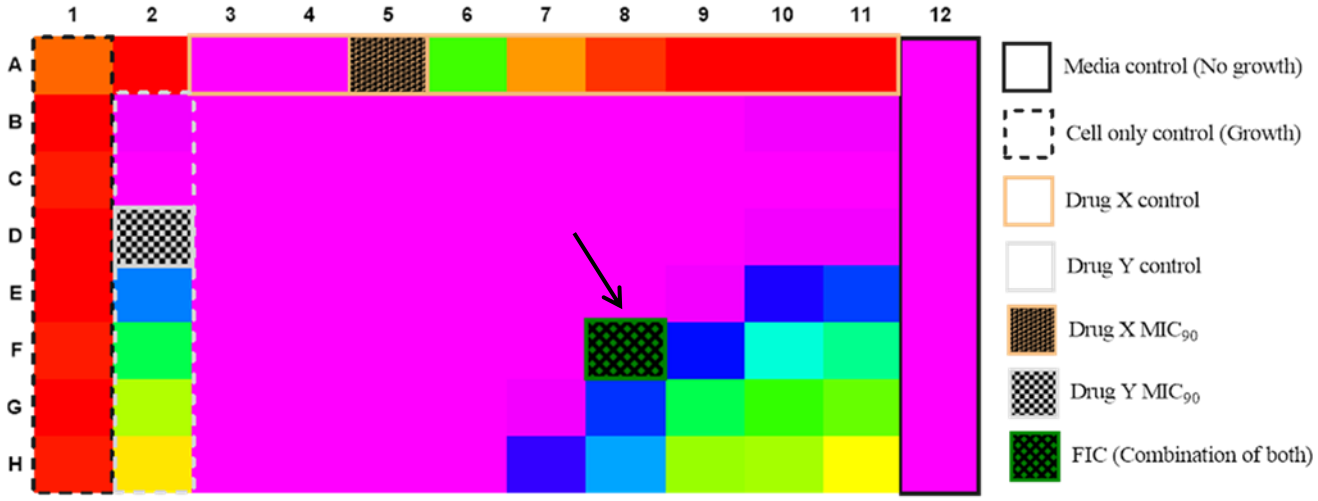

Figure 3.11: Evaluating synergistic interactions via checkerboard assay. Each square represents an individual well in a 96 well microtitre plate and representation of each borderline is listed under the legend on the right. The arrow points to the well that was used to calculate the fractional inhibitory concentration (FIC) index, where the two drugs inhibit more than 90% bacterial growth and elicited an FIC index (FICI) lower than 0.5. This result is based on the resazurin assay, where the colour red indicates bacterial growth and pink represents bacterial inhibition.

To calculate the FIC of drug X (FIC_{drugX}), a well that represents more than 90% inhibition below the combinatorial MIC of both drugs was considered and was divided by the MIC of drug X alone. The same method was used to calculate the FIC of drugY (FIC_{drugY}). To compute the fractional inhibitory concentration index (FICI), FICs of $drug_X$ and $drug_Y$ were summed; $\Sigma FICI = FIC_{drugX} + FIC_{drugY}$. Using this approach, the checkerboard assay reveals 3 potential outcomes: synergistic, antagonistic, or no drug-drug interaction. For synergy, this is defined by the combinatorial ability of two drugs to produce greater bacterial inhibition than the sum of their individual effects and the ΣFICI must be below the threshold of 0.5 (Odds 2003). No interaction refers to a combination where both drugs are working

independently of each other, the ΣFICI lies between 0.5 and 4. Lastly, antagonism defines a combination of two compounds that are counter-effective, so that the ΣFICI is above 4 (Odds 2003; Johnson et al. 2004).

After determination of MICs for the tested compounds, checkerboard assays were performed with the aim of investigating the utility of the CRISPRi tool to validate compound mode of action and to test for any synergistic interactions as a consequence of RibF depletion. Checkerboard experiments demonstrated no interaction for TZC and ATc-treated MSM_RibF (**Table 3.3**). Both ADD and BZC revealed no well with more than 90% bacterial inhibition below the sub MICs and no FIC index could be calculated suggesting that they are likely targeting a different protein in an unrelated pathway; hence they do not show specificity to the tested RibF knockdowns. No interaction was defined by an FICI that is greater than 0.5 but less than or equal to 4. In addition, no antagonistic interaction was observed from all the tested combinations. Surprisingly, vancomycin, a cell wall targeting agent (Watanakunakorn 1984) displayed synergistic interaction with depletion of RibF (**Figure 3.12**) despite being unrelated to the RF pathway. However, these features were also manifested in the MSM_MmpL3 hypomorph, which had enhanced susceptibility to vancomycin and to the proposed FAD synthetase inhibitors and yet are not related to the mycolic acid biosynthesis pathway either (**Supplementary figure S7**). This suggests these inhibitors either have multiple modes of action and are not specifically targeting RibF or that the depletion of *mmpL3* is increasing its susceptibility to these drugs as a consequence of an impaired bacterial cell wall.

Table 3.3: *In vitro* additive interactions between ATc and selected FAD synthetase inhibitors in the MSM_RibF depleted strain.

Compounds[a]	MIC[b] (μM) Solitary	MIC[b] (μM) combined	FIC	FICI[c]
ADD	80	N/A	N/A	N/A
ATc	0.008	N/A	N/A	N/A
BZC	12.5	N/A	N/A	N/A
ATc	0.008	N/A	N/A	N/A
TZB	25	12.5	0.5	0.57
ATc	0.008	0.0005	0.07	
VAN	0.0000055	0.0000014	0.25	**0.38**
ATc	0.008	0.001	0.125	

[a] Compounds selected for checkerboard *in vitro* experiments are as follows; ADD, Alexidine dihydrochloride; BZC, Benzethonium chloride; TZB, Thonzonium bromide; VAN, Vancomycin and ATc, Anhydrotetracycline.

[b] Minimum inhibitory concentration of each drug calculated as MIC_{90}. The MIC used for ATc was MIC_{80}.

[c] Represented FICI values reflect the lowest values obtained from the 3 biological replicates; where synergy is classified by FICI ≤ 0.5, no interaction, as FICI > 0.5 t and ≤4 and antagonism as FICI > 4.

Combinations that revealed synergistic interactions are highlighted in bold text and N/A represents absence of a well that exhibited more than 90% bacterial inhibition, hence the FIC of an individual compound and combinatorial FIC index could not be calculated as a result.

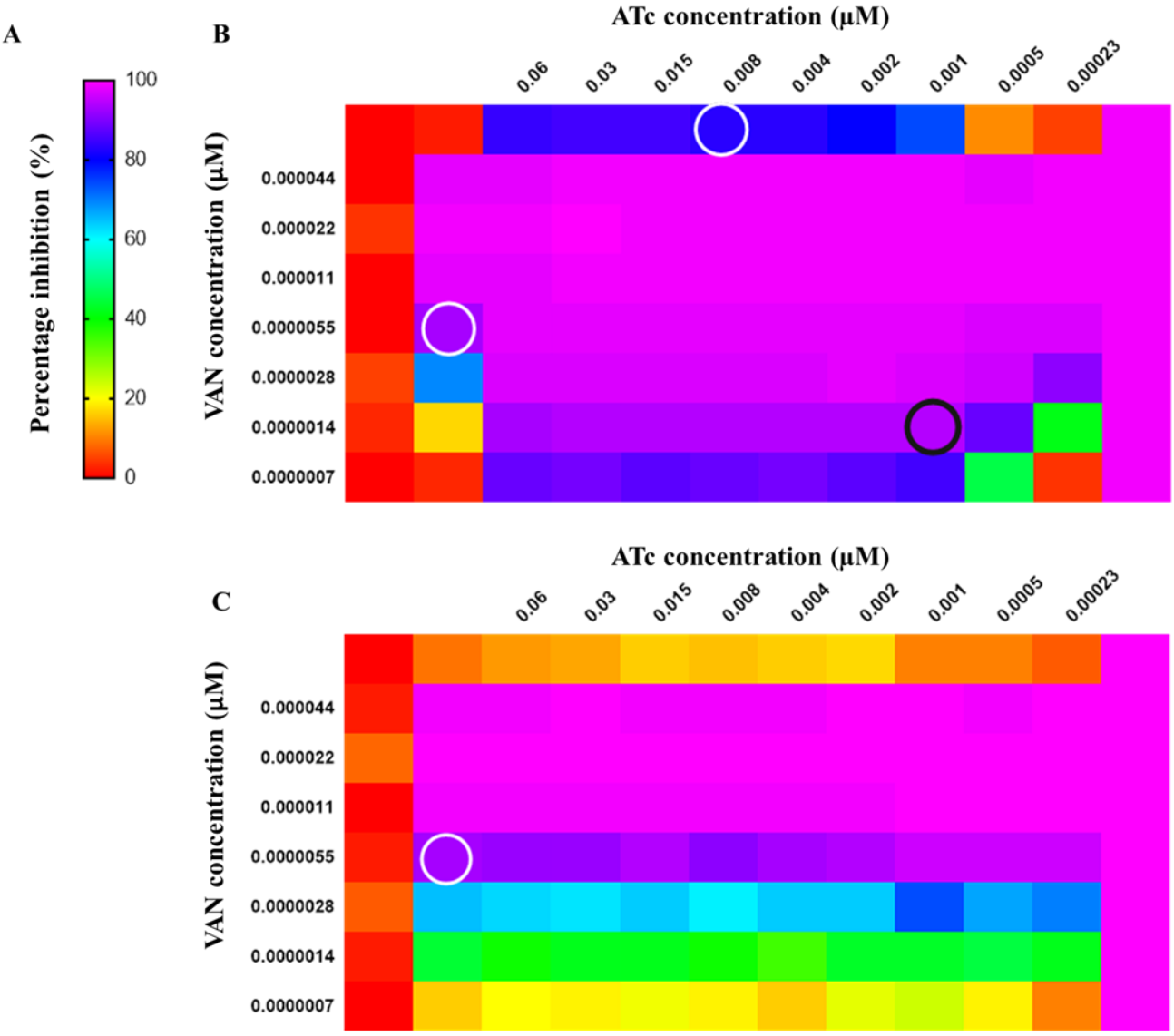
A
Percentage inhibition (%)
100
80
60
40
20
0
B
ATc concentration (µM)
0.06
0.03
0.015
0.008
0.004
0.002
0.001
0.0005
0.00023
VAN concentration (µM)
0.000044
0.000022
0.000011
0.0000055
0.0000028
0.0000014
0.0000007
C
ATc concentration (µM)
0.06
0.03
0.015
0.008
0.004
0.002
0.001
0.0005
0.00023
VAN concentration (µM)
0.000044
0.000022
0.000011
0.0000055
0.0000028
0.0000014
0.0000007

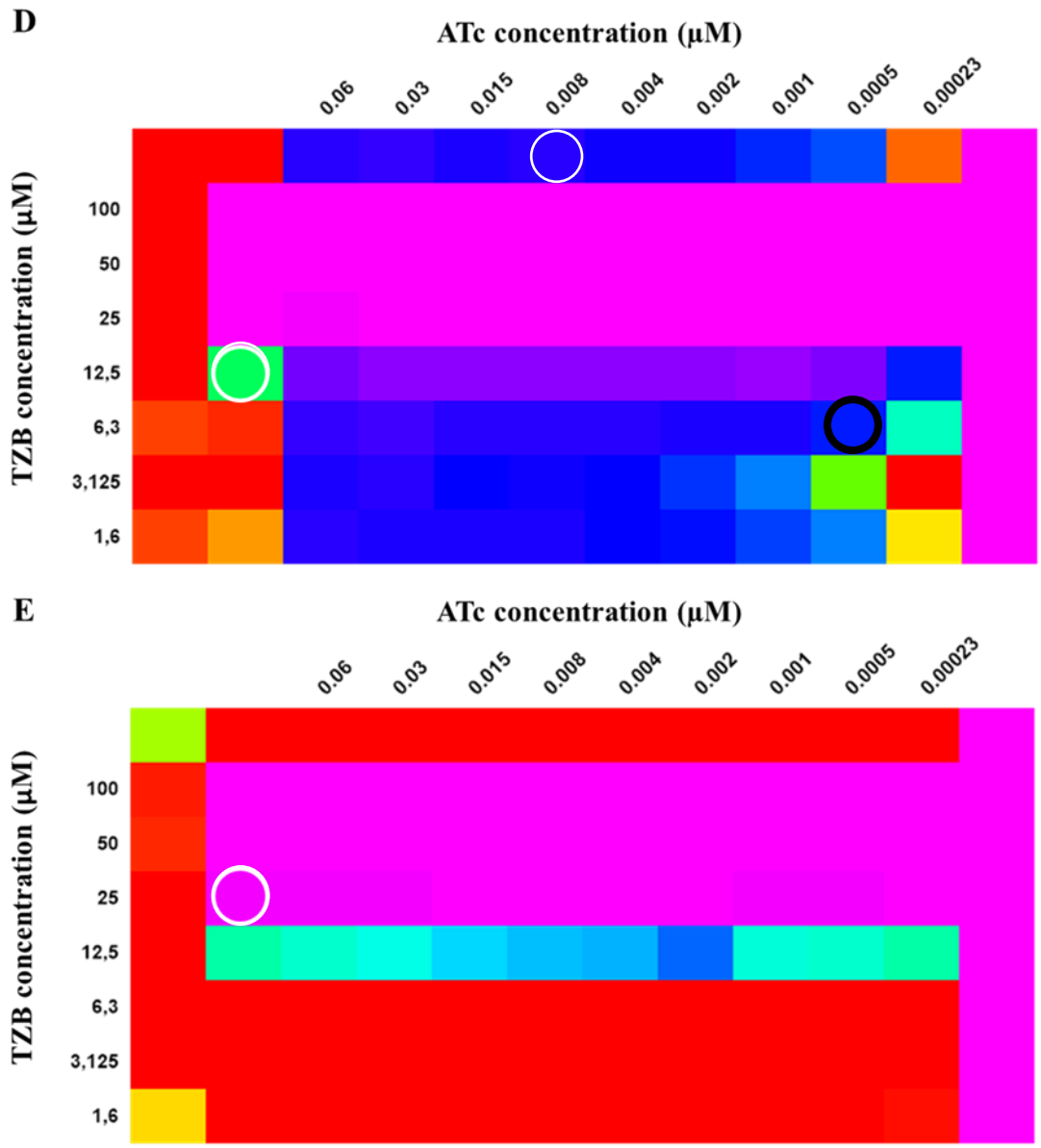

Figure 3.12: CRISPRi *ribF* knockdown strain demonstrates increased susceptibility to vancomycin and FAD synthetase inhibitors. A colour scale for percentage inhibition values is represented on the left (**A**), indicating maximal and minimal growth inhibition as pink (100%) and red (0), respectively. Standard checkerboard assays representing combinatorial data compiled in a 9 ATc x 7 drug matrix. Cells were treated with vancomycin and TZC against (**B** and **D**) *ribF* deficient and (**C** and **E**) WT control strains for 24 hours. The MICs for both ATc and VAN are represented in white ovals, with the well used to calculate the FICI indicated by a black circle.

A control was used to compare the increased susceptibility to tested compounds following *ribF* depletion. As expected, MSM_WT revealed no increased susceptibility to any compound with no observable interaction (**Figure 3.12 (C and E)**). Experimental data of VAN and TZB against the MSM_RibF hypomorph and MSM_WT are indicated as heat maps

(**Figure 3.12** (**B** and **D**) and (**C** and **E**)), and the additional tested compounds against MSM_MmpL3 and MSM_Vector are shown in **supplementary figure S7**. In addition, tested compound reliability was experimented by extending the standard checkerboard across two plates to ensure the integrity of the observed results (**Supplementary figure S8**).

3.8 Regulatory role of RibF in *Msm*

The flavin cofactor FMN has been shown to play a role in regulating the *rib* operon (*ribDG-E-AB-H*) directly by influencing the "*ribDG* FMN riboswitch" located the 5'-UTR of the single transcription unit of *ribDG-E-AB-H* mRNA, precedent for which exists in *B. subtilis* but in contrast, RibR, a mycobacterial RibF homolog that has been shown to supersede repression by directly interacting with the aptamer region mediated by the FMN riboswitch (Solovieva et al. 1999; Higashitsuji et al. 2007; Pedrolli, Kuhm, et al. 2015). In *E coli*, however, the essential 3,4-dihydroxy-2-butanone-4-phosphate enzyme, RibB, has been shown to regulate the FMN riboswitch at both the transcriptional and translational levels (Pedrolli, Langer, et al. 2015a).

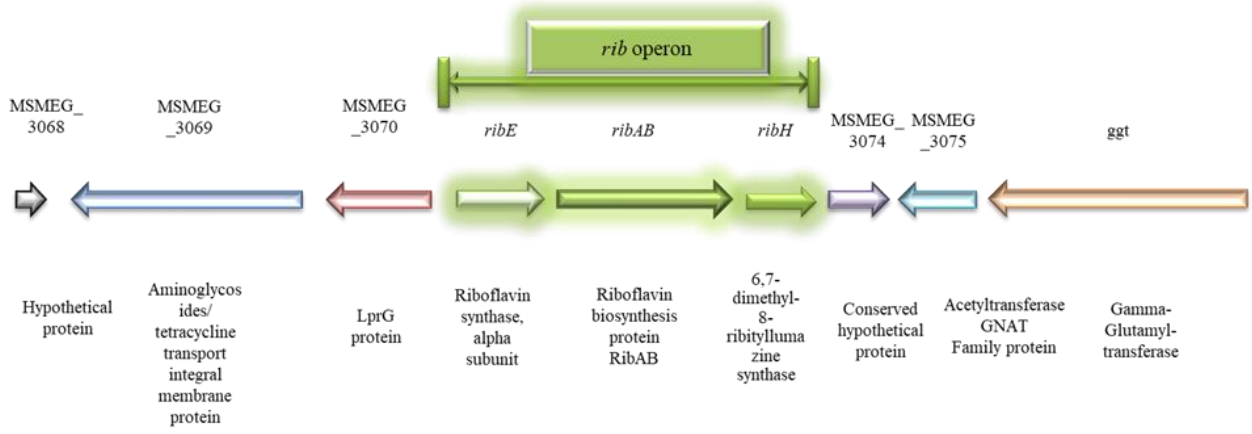

Figure 3.13: Genomic context of the proposed RF operon in *Msm*. Green highlighted arrows represent RF genes, *ribE*, *ribAB* and *ribH* within the operon. The three arrows on the left of the operon are genes located upstream of the operon; those on the right are genes located downstream (*adapted from Mycobrowser*).

To validate which genes constitute the *rib* operon, junction primers were used to amplify the region between two genes to confirm a single transcriptional unit. Results confirmed that *ribE* is the first gene in the operon followed by *ribAB* and *ribH*.

Unexpectedly, these results also indicated that the operon may extend beyond the RF biosynthesis genes into MSMEG_3074 and MSMEG_3075 (**Figure 3.14**). Whilst this suggests that *ribE-ribAB-ribH*-MSMEG_3074-MSMEG_3075 constitute a single transcriptional unit, this does not rule out the possibility of an overlapping transcriptional unit which may not span across the entire proposed *rib* operon and instead constitutes a subset of the operonic genes.

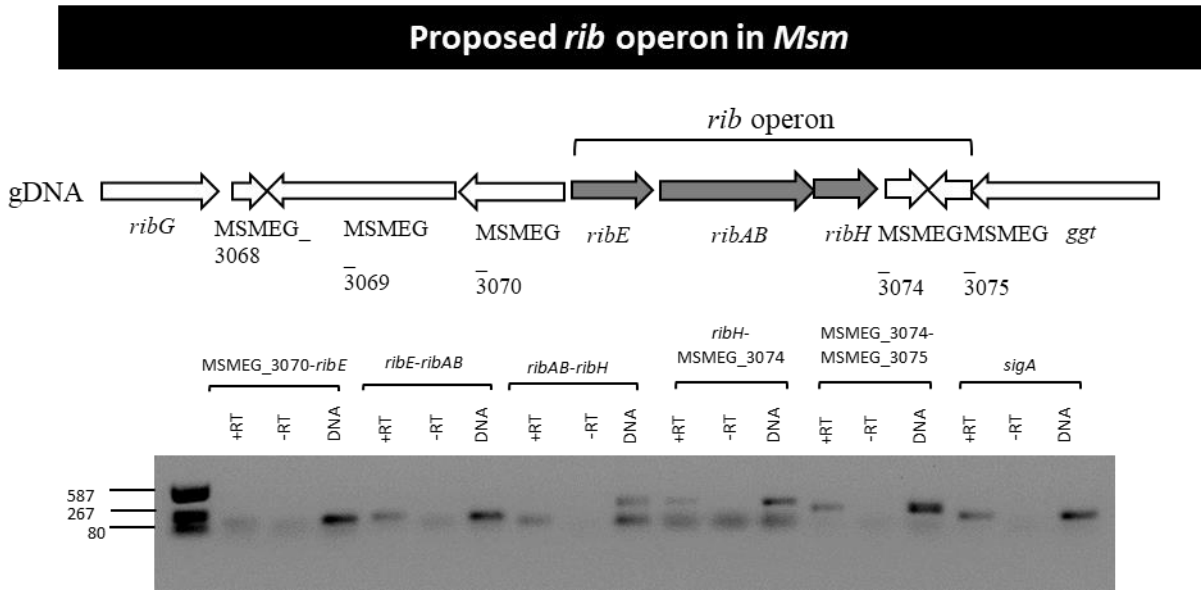

Figure 3.14: Confirmation of amplicons to determine the *rib* operon in *Msm*. The grey shaded arrows represent genes that are involved in RF biosynthesis while the non-shaded represent genes located upstream (left) and downstream (right) of the RF genes. Junction names between two genes are shown above each square bracket and RT represents presence (+RT) and absence (-RT) of reverse transcriptase. DNA represents presence of the template gDNA of *Msm* and the Molecular weight marker (Marker V) is shown on the left of electrophoresis gel image.

The transcript levels of *rib* operon genes - *ribE*, *ribAB* and *ribH* - in the uninduced MSM_RibF strain were determined (**Figure 3.13**) by qRT-PCR and compared to the *ribF* depleted strain (**Figure 3.15**). The qRT-PCR reactions were performed using the procedure detailed in **2.1.7**. The results demonstrated significant upregulation of *rib* operon genes, *ribE* and *ribAB* as a result of *ribF* depletion, $P < 0.0233$ and $P < 0.0130$ by 7-fold and 8-fold respectively. A 3-fold non-significant increase was observed for *ribH* (**Figure 3.15**). This strongly suggests that RibF could be a negative regulator of the operonic RF biosynthesis pathway genes. However, the exact mechanism of regulation still remains unknown; one possibility could be regulation through aptamer region binding by FMN or direct RibF

protein binding to the upstream region of the regulatory elements of the RF operon. Further work is required to test these possibilities, and is complicated by the fact that the RibF protein and FMN metabolite are both limited in the *ribF* deficient strain.

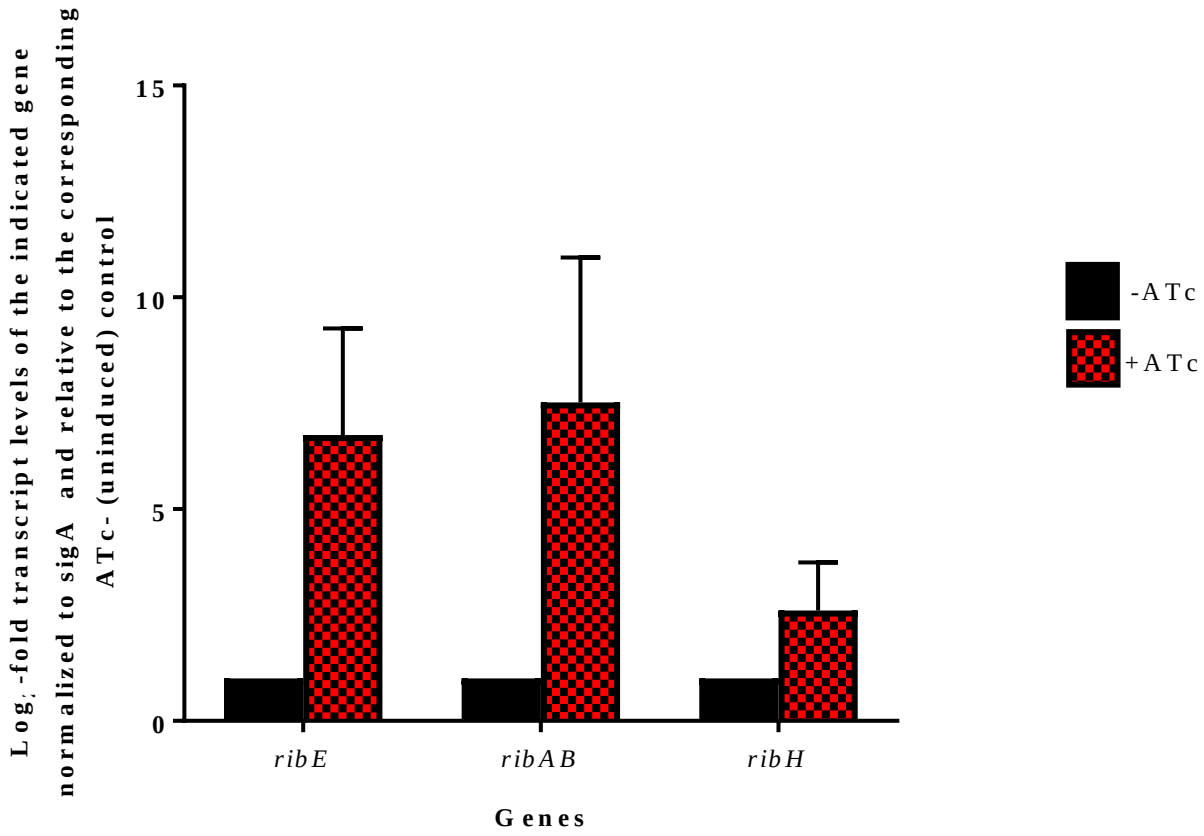

Figure 3.15: **Analysis of transcript levels of *rib* specific genes.** Expression of indicated *rib* operon genes was determined in ATc induced (red bar) and uninduced (black bar) MSM_RibF cultures by qRT-PCR at 24 hours post CRISPRi induction from a 0.016 inoculum. Transcript levels were normalized to the ATc uninduced strain. Error bars represent SD of three technical replicates. Statistical analysis was performed using Sidak's multiple comparison using a 2way ANOVA multiple comparison analysis.

3.9 The effect of RibF depletion on RF metabolite levels

We next sought to determine the effect of *ribF* transcriptional silencing on RF metabolite concentrations in the RibF deficient strain. To this end, cultures were inoculated to an initial OD_{600} of 0.016 in 7H9-OADC supplemented media containing either 0 or 100 ng/ml ATc. A crude extraction was performed using the procedure outlined in **2.1.9.7** prior to liquid chromatography mass spectrophotometry (LC-MS) analysis (**Supplementary figure S9**).

Results revealed that there was a three times increase in the upstream substrate 6,7-Dimethyl-8-ribityllumazine (DMRL) while the downstream metabolite FMN was below the

limit of quantification as was expected (**Table 3.4**) due to RibF being limited. The increase of DMRL could be attributed to the recycling route which converts one of the two DMRL molecules to 5-A-RU whilst the second molecule is converted to RF (**Figure 3.16**); however, this explains its enhanced abundance rather than the lack of RF substrate accumulation as would have been predicted to occur in the MSM_RibF hypomorph (**Table 3.4**). Furthermore, vitamin B_{12} synthesis is interconnected to RF biosynthesis, since an essential product from the RF pathway feeds into the vitamin B_{12} synthesis route. The substrate, dimethylbenzimidazole (DMB), is formed from reduced FMN ($FMNH_2$) by the enzyme *bluB* (**Figure 3.16**). Hence it was expected that vitamin B_{12} synthesis would be restricted due to the scarcity in FMN intracellular concentrations emanating from the RF pathway in the RibF hypomorph.

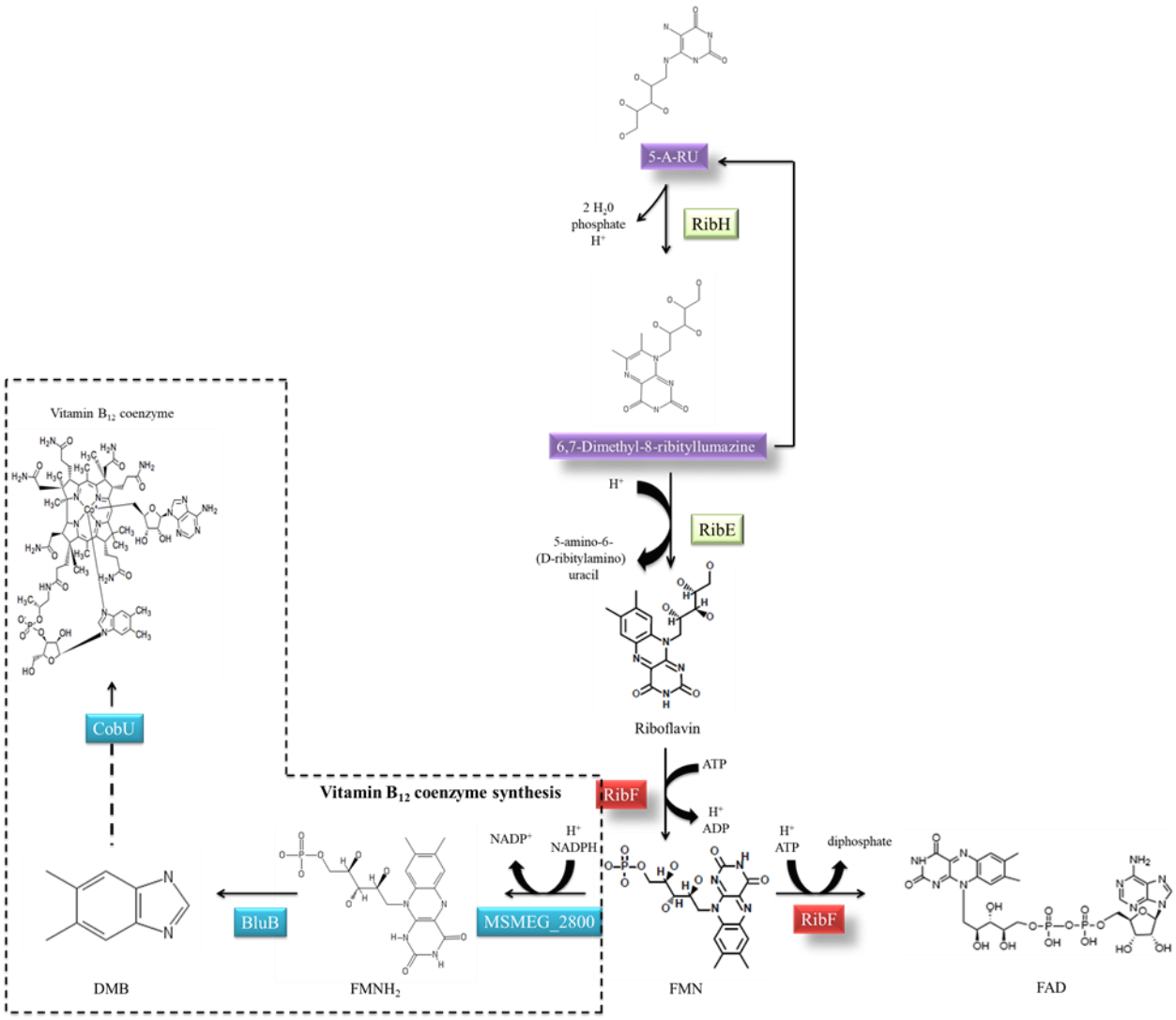

Figure 3.16: Biochemical reactions of RF metabolites carried out by RF enzymes. Enzymes that partake in specific reactions are highlighted in rectangles and each metabolite is listed below each chemical structure. The

solid line represents passive recycling of DMRL to 5-A-RU, both highlighted in purple rectangles. The blue rectangles represent the branch in the RF pathway to vitamin B_{12} synthesis surrounded by dotted lines.

Table 3.4: Summary of RibF metabolite concentrations obtained after 24 hour post ATc exposure (+ATc) and in the absence of ATc (-ATc).

Compound	Strain: RibF	
	+ATc	-ATc
DMRL	14.44	4.22
RF	0.039	0.031
FMN	0.018	0.245
Vitamin B_{12}	BLQ	0.081

BLQ: Below limit of quantification

Chapter 4: Discussion

Newly approved TB drugs are being integrated into current and experimental TB drug regimens based on their novel metabolic targets and ability to inhibit both replicating and non-replicating bacilli (Barry, Boshoff, and Dowd 2004) (WHO 2008). These include bedaquiline, delamanid and pretonamid which respectively target essential elements such as the ATP synthase proton pump, synthesis of methoxy- and keto-mycolic acid and biosynthesis of mycobacterial mycolic acids (Andries, Verhasselt, Guillemont, Göhlmann, et al. 2005; Xavier and Lakshmanan 2014; Manjunatha, Boshoff, and Barry 2009). However, resistance to these drugs has already been documented and reiterates the need to identify new drug targets by excavating unexplored territory of *Mtb* metabolism (Somoskovi et al. 2015; Hartkoorn, Uplekar, and Cole 2014; Baptista et al. 2018). Riboflavin (RF) biosynthesis, an essential pathway in *Mtb* and plays a role in the generation of flavin cofactors; FMN and FAD which contribute to 25% and 75% of essential cellular reactions, respectively through flavoenzymes (Macheroux, Kappes, and Ealick 2011). Since these cofactors are uniquely generated in the RF pathway without any possibility of being compensated by other enzymes, they represent potentially useful drug targets.

Interrogation of essential genes and their functions remains a priority as a means to identify possible drug targets. Conventional approaches to identify essential genes such as gene-deletion libraries (Baba et al. 2006; Winzeler et al. 1999) and saturating transposon mutagenesis (Goodman et al. 2009; Van Opijnen, Bodi, and Camilli 2009), cannot be used to characterize essential genes as, by definition, the cells do not survive in the absence of their essential functions and so are eliminated from libraries *ab initio* (Christen et al. 2011). However, new high-throughput tools have been developed to study essential genes namely destabilization of 3` UTR of mRNAs (DaMP alleles) (Breslow et al. 2008), CRISPR/Cas9 gene editing (Blomen et al. 2015; Wang et al. 2015), and CRISPRi/dCas9 transcriptional interference (Gilbert et al. 2014).

Here, we utilized a pioneering CRISPRi system optimized for mycobacteria (Rock et al. 2017). By evaluating several sgRNAs, we achieved inducible and dose-dependent transcriptional knockdown of *ribF* which varied depending on the sgRNA site within the target gene. As expected, sgRNAs that possessed the lower computationally calculated PAM scores elicited the most robust KD, while those with higher PAM scores showed reduced or partial KD (**Figure 3.3 & 3.4**) (Rock et al. 2017). This supports the potential tunability of the CRISPRi system by varying the PAM score selected (in turn, determining sgRNA-dCas9 binding affinity), or varying the concentration of the small molecule ATc inducer (**Figure**

3.6) (Peters et al. 2016). Other studies have also shown that the strength of sgRNA-target gene complementarity can be adjusted by sgRNA target region shortening (Qi et al. 2013b), with optimal repression obtained with sgRNAs of 20 bp and lower repression mediated by shortening the sgRNA guide length to ~10 bp (Vigouroux et al. 2018).

In bacteria, most bactericidal antibiotics exhibit potent bacterial killing when targeting actively growing cells, an effect which can be inoculum-dependent (Vandal et al. 2008). This is similar to what we have observed when CRISPRi strains at varying inoculum concentrations were challenged with a high ATc concentration of 100 ng/ml. Strikingly, the lowest inoculum concentration elicited the most potent transcriptional KD. This confirmed that the CRISPRi system is inoculum concentration dependent and its robustness relies on actively growing bacteria, preferably exponential phase cultures, while slow growing or stationary phase cultures seem to adversely affect the efficiency of the system by less-effectively repressing growth (**Figure 3.5**).

The notable bacterial growth cessation attained from moderate KD of *ribF* after approximately four generations (*i.e.* 12 hours) of growth suggests that, in *Msm*, these protein levels are not in excess in the cell. However, this is also dependent on the vulnerability of the functional target: targeting *ribF* led to a 10-fold reduction in growth whereas *mmpL3* depletion caused a greater than 20-fold reduction in bacterial growth in liquid media (**Figure 3.7**). In addition, 12 hours and 3 hours were identified as the minimal time required for the CRISPRi inducer to significantly affect growth as a consequence of *ribF* or *mmpL3* depletion, respectively (**Figure 3.7**). This suggests that a number of factors (including mRNA and protein turnover rates) likely determine how quickly a growth phenotype is detectable. MmpL3 in particular serves as an essential membrane protein required for the transportation of trehalose mono-mycolates across the inner membrane (Xu et al. 2017b), the disruption of which renders the bacillus susceptible to external factors.

It has also been shown that even where reduction in the levels of essential proteins such as dihydrofolate reductase (*DHFR*) and alanine racemase (*alr*) exceeds 97%, there might be no effect on mycobacterial growth and viability (Wei et al. 2011; Rock et al. 2017). This suggests that, in these cases, the amount of enzyme present was still adequate to fulfil its function without impeding growth (Wei et al. 2011). The results presented here indicate that RibF is a highly vulnerable target in mycobacteria, and possibly other pathogens with the capability to synthesize RF *de novo*.

The potential of the organism to scavenge essential nutrients can mitigate the lethality of antibiotic-mediated disruption of a targeted enzyme, ending the development aspirations of promising lead candidates (Brinster et al. 2009). This phenomenon was most clearly observed in *Mtb*, where toxicity mediated by GuaB2 depletion through VCC234718 drug treatment was rescuable by guanine (Singh et al. 2017). Highly efficient RF transporters have been identified in both Gram negative and Gram positive pathogenic bacteria, including *S. aureus*, *E. faecalis*, *S. pyogenes* and *Vibrio cholera*, all of which are unable to synthesize RF *de novo* (Sepúlveda Cisternas, Salazar, and García-Angulo 2018; Deka et al. 2013; Wang et al. 2017). Moreover, it has been shown that human serum contains enough RF to resuscitate a *S. aureus* RF auxotroph (Wang et al. 2017). To evaluate the possibility that mycobacteria might scavenge RF, we showed that genetic KD of *ribF* was not chemically complementable by the addition of RF, FMN and FAD (**Figure 3.9; Supplementary figure S5**). In contrast, in parallel work in our laboratory (Chengalroyen MD, personal communication), it has also been observed that a *Mtb* and *Msm ribAB* hypomorph – in which the first step of the RF pathway is silenced – are capable of rescue by exogenous RF, albeit at 43 µM and 11 µM respective RF concentrations, strongly supporting the capacity of the bacilli to assimilate exogenous RF. In turn, this observation supports the requirement for a functional RibF enzyme to enable conversion of RF to active flavin cofactors for use by flavoenzymes.

The inability of FMN and FAD to complement *ribF* depletion indicates that the notoriously complex, hydrophobic mycobacterial cell wall is impermeable to these phosphate-containing nucleotides. Another possibility could be the inability of mycobacteria to utilize the cofactors to synthesize RF through a reverse reaction, evidence for which exists in bacteria such as *Shewenella oneidensis*, *C. albicans* and *Pseudomonas aeruginosa***.** To our knowledge, no FMN nor FAD transporter has been identified in mycobacteria despite the conclusion from a genomic analysis of *Mtb* that phosphate importers are overly represented in comparison to model bacteria, *E. coli* and *B. subtilis* (Braibant, Gilot, and Content 2000b). Notably, it has been observed that the exporter-to-importer proteins ratio is distinctly higher in *Mtb* than *E.coli* (Braibant, Gilot, and Content 2000a) which may be another reason for the reduction in small molecule uptake.

The predicted tertiary structure of the bifunctional *Mtb* RibF protein was compared to the human homologs, RFK (flavokinase) and FLAD1 (FAD synthetase). This was done to determine the likelihood that drugs interacting with the *Mtb* RibF might also adversely affect the corresponding human enzymes. Superimposition of the *Mtb* flavokinase domain on that

of the human flavokinase, RFK, demonstrated that the structures were almost identical; in contrast, no structural homology with the human FAD synthetase was observed (**Figure 3.10**). This strongly suggests that the FAD synthetase domain of *Mtb* RibF can be targeted without affecting the human homolog. In fact, the structural and biochemical distinctness of the mammalian FAD synthetases compared to the prokaryotic FAD synthetase is widely documented (Barile et al. 1993; Serrano et al. 2012; Efimov et al. 1998; Mack, van Loon, and Hohmann 1998b). Moreover, the availability of an array of bacterial FAD synthetase structures might expedite the development and design of both inhibitory compounds and activity assays (Herguedas et al. 2009; Wang et al. 2005; Wang et al. 2003). Bacterial FAD synthetases can be perceived as promising antimicrobial drug targets since interruptions in the production of FMN and FAD interfere with all pathways that involve flavoproteins and biosynthesis of these cofactors in most bacteria is facilitated by a single bifunctional enzyme, simultaneously disrupting both processes (Sassetti, Boyd, and Rubin 2003b; Griffin et al. 2011b). The fundamental criteria for a good drug candidate stems from; (i) the essentiality of the target gene, (ii) the absence of off-target effects, iii) no opportunity for rescue by exogenous nutrient scavenging, and (iv) selective differences between the mammalian and bacterial target enzymes (Finberg et al. 2004; Copeland, Pompliano, and Meek 2006; Singh et al. 2017; Serrano et al. 2012). RibF appears to satisfy these criteria.

The putative FAD synthetase inhibitors (Sebastián et al. 2018) exhibited no synergistic activity when used in combination with *ribF* depletion. This suggests that they either target a different protein in an unrelated pathway or have multiple modes of action (MOA) and target RibF in addition to other enzymes. The synergistic interaction observed with the RibF hypomorph and vancomycin was unanticipated (**Figure 3.12**) owing to the conventional MOA of vancomycin as a cell wall-targeting inhibitor. This suggests that the depletion of RibF led to bacterial cell wall impairment in turn leading to increased susceptibility to the cell wall targeting agent or that VAN weakens the cell wall to allow more ATc influx. Notably, this was not observed when the hypomorph was tested with ethambutol, also a cell wall targeting antibiotic (data not shown). At a practical level, it is worth noting that the checkerboard approach adopted in this study allowed for a rapid and more comprehensive validation of on-target activity and compound MOA determination across a 9 by 7 compound concentration matrix as opposed to using a narrow 3 by 1 drug concentration matrix as demonstrated by (McNeil and Cook 2019b).

In bacteria, RF homeostasis is mediated by FMN riboswitches, one of the predominate classes of RNA regulatory elements (Gutiérrez-Preciado et al. 2015) which controls gene expression required for the synthesis and transport of this vitamin (Winkler, Cohen-Chalamish, and Breaker 2002b; Gelfand et al. 1999; Mack, van Loon, and Hohmann 1998b; Vitreschak et al. 2002b; Serganov, Huang, and Patel 2009; Pedrolli, Langer, et al. 2015b). Our observations strongly support the notion that RibF is a negative regulator of the *rib* operon which comprises three RF biosynthesis related genes - *ribE*, *ribAB*, *ribH* - and MSMEG_3074 and MSMEG_3075. MSMEG_3074 is a conserved hypothetical protein while MSMEG_3075 codes for an acetyltransferase, Gcn5-related N-acetyltransferases (GNAT) family protein; neither appears to function in the RF pathway (**Figure 3.13**). However, the total length to which the *Msm* operon extends and the regulatory mechanism is still unknown. Regulation of the RF genes can be affected either by riboswitches or regulatory promoter elements. It is known that, in *B. subtilis*, both negative and positive regulation exists through FMN and RibR, respectively. FMN negatively regulates the *rib* operon by binding to the aptamer region domain which reduces the formation of FMN. In contrast, RibR has the ability to counteract this effect by binding to the FMN riboswitch to allow upregulation of the genes. In a similar manner, the expression of *ribB* is mediated by a FMN riboswitch in *E. coli* but retains a bifunctional role, working at both the transcriptional and translational level (Pedrolli, Langer, et al. 2015a). Notably, *Msm* was completely resistant to FMN riboswitch inhibitors, ribocil-C and roseoflavin (**Table 3.2**), hence it is tempting to speculate that FMN riboswitches could be absent in *Msm*.

Concluding remarks

In this study, the utility of CRISPRi allowed for the rapid validation of target gene essentiality. This system was also used to characterize the effect of disrupting an essential gene by monitoring its effect on mycobacterial growth and evaluating the on-target activity of proposed inhibitors. It was demonstrated that the depletion of RibF was bacteriostatic, the nature of which was linked to a reduction in flavin cofactors. In addition, the adverse effect on the vitamin B_{12} biosynthesis pathway indicated that routes which rely on these essential cofactors are also affected. In accordance with this, RibF depletion led to enhanced susceptibility to vancomycin which we speculate could be attributed to the disruption of the activity of flavoproteins involved in cell wall biosynthesis such as DprE1 and DprE2 for which future prospects are to test against DprE1 inhibitors, most notably benzothiazinones (BTZ) (Makarov et al. 2015). Preliminary data in the laboratory strongly supports the existence of a RF transporter. However, neither RF, FMN nor FAD supplementation had the ability to rescue this lethal phenotype. These favourable attributes led to the evaluation of proposed FAD synthetase inhibitors to target RibF. However, the compounds tested revealed either an off-target effect or possible multiple action against RibF and a secondary target/ cellular processes. Nevertheless, this work has demonstrated a non-redundant and essential role for RibF in mycobacterial metabolism, making it an attractive drug target to investigate in the future. Silencing *ribF* also led to the upregulation of the *rib* operon providing strong evidence for its role in regulating mycobacterial RF biosynthesis (**Figure 4.1**).

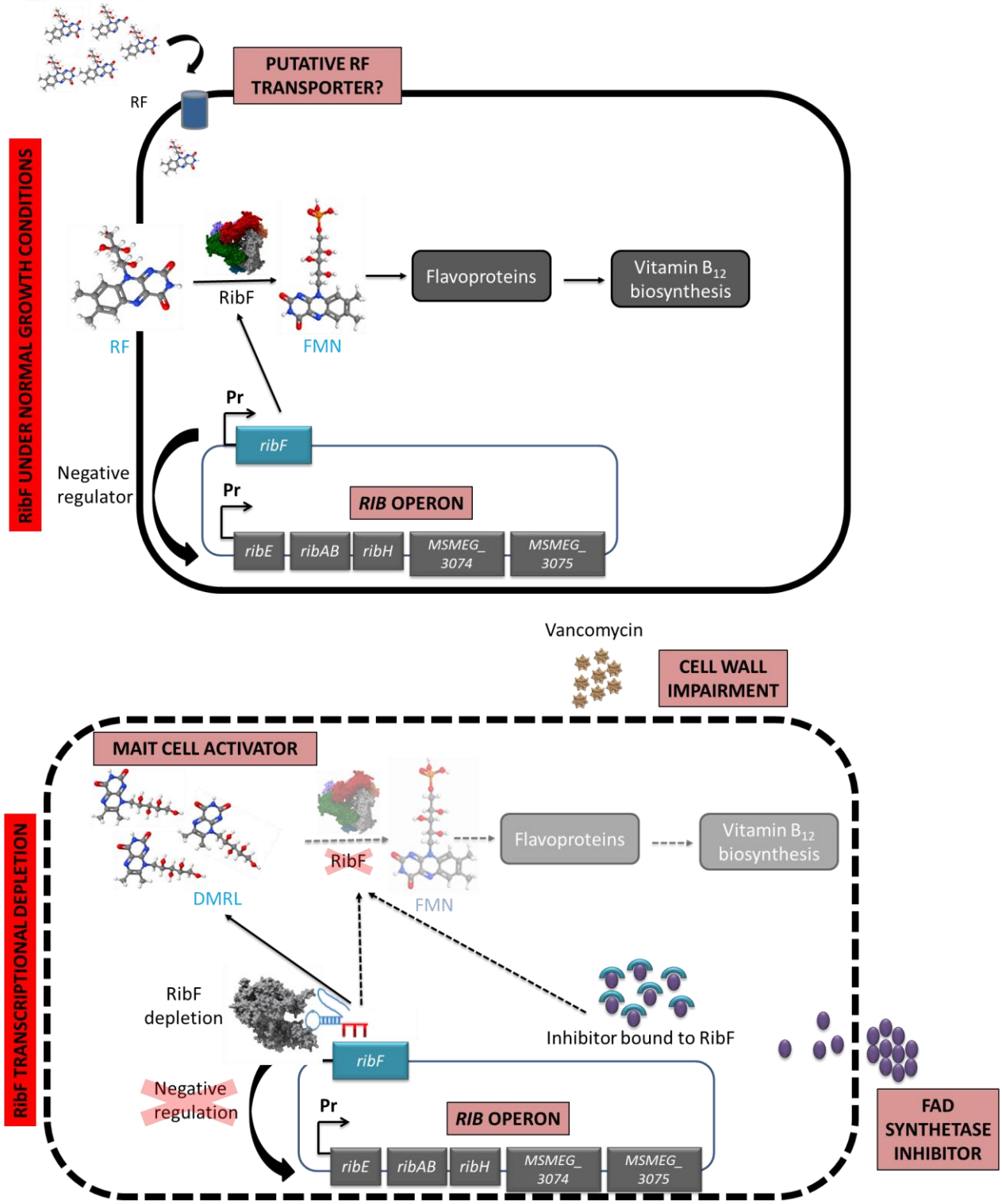

Figure 4.1: Consequence of RibF depletion in *Msm*. RF biosynthesis under normal conditions (left) and phenotypic and metabolite alterations resulting from RibF depletion (right). DMRL, 6,7-dimethyl-8-ribityllumazine; FAD, Flavin adenine dinucleotide; FMN, Flavin mononucleotide; *Msm*, *Mycobacterium smegmatis*; Pr, Promoter; RF, Riboflavin; MAIT, Mucosal associated invariant T.

Future work

Recent studies describe a pivotal role of MAIT cells in controlling TB progression (Le Bourhis et al. 2010; Gold et al. 2010; Kurioka et al. 2015). These cells are regarded as bridging cells that participate both in the innate and adaptive immunity. Like innate cells, they serve as the first line of defence against bacterial intruders yet like adaptive immune cells they are able to acquire effector memory. The most distinguishing feature comes from their unique ability to recognize pathogen derived RF metabolites presented by antigen presenting cells (APC) via an MR1 protein. The use of CRISPRi provided a platform to reduce the RibF enzyme, causing the accumulation of a specified RF precursor, 6,7-dimethyl-8-ribityllumazine (DMRL) which is associated with the ability to stimulate MAIT cell activity (Corbett et al. 2014). In the wider scope of this project, our collaborator Prof. David Lewinsohn and his research group at the Oregon Health & Science University (specialists in MAIT cell research) propose to comprehensively characterize immunological responses in relation to the RibF hypomorph generated in this study with the potential to provide insight into immunotherapeutic strategies.

References

Ahmed, F Hafna, Paul D Carr, Brendon M Lee, Livnat Afriat-Jurnou, A Elaaf Mohamed, Nan-Sook Hong, Jack Flanagan, Matthew C Taylor, Chris Greening, and Colin J Jackson. 2015. 'Sequence–structure–function classification of a catalytically diverse oxidoreductase superfamily in Mycobacteria', *Journal of molecular biology*, 427: 3554-71.

Andersen, P., and T. M. Doherty. 2005. 'The success and failure of BCG - implications for a novel tuberculosis vaccine', *Nat Rev Microbiol*, 3: 656-62.

Andries, K., P. Verhasselt, J. Guillemont, H. W. Gohlmann, J. M. Neefs, H. Winkler, J. Van Gestel, P. Timmerman, M. Zhu, E. Lee, P. Williams, D. de Chaffoy, E. Huitric, S. Hoffner, E. Cambau, C. Truffot-Pernot, N. Lounis, and V. Jarlier. 2005. 'A diarylquinoline drug active on the ATP synthase of Mycobacterium tuberculosis', *Science*, 307: 223-7.

Andries, Koen, Peter Verhasselt, Jerome Guillemont, Hinrich WH Göhlmann, Jean-Marc Neefs, Hans Winkler, Jef Van Gestel, Philip Timmerman, Min Zhu, and Ennis Lee. 2005. 'A diarylquinoline drug active on the ATP synthase of Mycobacterium tuberculosis', *Science*, 307: 223-27.

Arora, K., B. Ochoa-Montano, P. S. Tsang, T. L. Blundell, S. S. Dawes, V. Mizrahi, T. Bayliss, C. J. Mackenzie, L. A. Cleghorn, P. C. Ray, P. G. Wyatt, E. Uh, J. Lee, C. E. Barry, 3rd, and H. I. Boshoff. 2014. 'Respiratory flexibility in response to inhibition of cytochrome C oxidase in Mycobacterium tuberculosis', *Antimicrob Agents Chemother*, 58: 6962-5.

Ashoori, M., and A. Saedisomeolia. 2014. 'Riboflavin (vitamin B(2)) and oxidative stress: a review', *Br J Nutr*, 111: 1985-91.

Avorn, J. 2013. 'Approval of a tuberculosis drug based on a paradoxical surrogate measure', *JAMA*, 309: 1349-50.

Azevedo, V., A. Sorokin, S. D. Ehrlich, and P. Serror. 1993. 'The transcriptional organization of the Bacillus subtilis 168 chromosome region between the spoVAF and serA genetic loci', *Mol Microbiol*, 10: 397-405.

Baba, Tomoya, Takeshi Ara, Miki Hasegawa, Yuki Takai, Yoshiko Okumura, Miki Baba, Kirill A Datsenko, Masaru Tomita, Barry L Wanner, and Hirotada Mori. 2006. 'Construction of Escherichia coli K-12 in-frame, single-gene knockout mutants: the Keio collection', *Molecular systems biology*, 2.

Bair, Thomas B, Dale W Isabelle, and Lacy Daniels. 2001. 'Structures of coenzyme F420 in Mycobacterium species', *Archives of microbiology*, 176: 37-43.

Balasubramanian, R., B. T. Levinson, and A. C. Rosenzweig. 2010. 'Secretion of flavins by three species of methanotrophic bacteria', *Appl Environ Microbiol*, 76: 7356-8.

Baptista, R., D. M. Fazakerley, M. Beckmann, L. Baillie, and L. A. J. Mur. 2018. 'Untargeted metabolomics reveals a new mode of action of pretomanid (PA-824)', *Sci Rep*, 8: 5084.

Barile, M., C. Brizio, D. Valenti, C. De Virgilio, and S. Passarella. 2000. 'The riboflavin/FAD cycle in rat liver mitochondria', *Eur J Biochem*, 267: 4888-900.

Barile, Maria, Salvatore Passarella, Angela Bertoldi, and Ernesto Quagliariello. 1993. 'Flavin adenine dinucleotide synthesis in isolated rat liver mitochondria caused by imported flavin mononucleotide', *Archives of biochemistry and biophysics*, 305: 442-47.

Barry, Clifton E, Helena IM Boshoff, and Cynthia S Dowd. 2004. 'Prospects for clinical introduction of nitroimidazole antibiotics for the treatment of tuberculosis', *Current pharmaceutical design*, 10: 3239-62.

Bashiri, Ghader, Ellen F Perkowski, Adrian P Turner, Meghan E Feltcher, Miriam Braunstein, and Edward N Baker. 2012. 'Tat–dependent translocation of an F420–binding protein of Mycobacterium tuberculosis', *PloS one*, 7: e45003.

Behr, Marcel A., Paul H. Edelstein, and Lalita Ramakrishnan. 2018. 'Revisiting the timetable of tuberculosis', *BMJ*, 362: k2738.

Berenbaum, M. C. 1978. 'A method for testing for synergy with any number of agents', *J Infect Dis*, 137: 122-30.

Beztsinna, N., M. Sole, N. Taib, and I. Bestel. 2016. 'Bioengineered riboflavin in nanotechnology', *Biomaterials*, 80: 121-33.

Bhusal, Y., C. M. Shiohira, and N. Yamane. 2005. 'Determination of in vitro synergy when three antimicrobial agents are combined against Mycobacterium tuberculosis', *Int J Antimicrob Agents*, 26: 292-7.

Bikard, D., W. Jiang, P. Samai, A. Hochschild, F. Zhang, and L. A. Marraffini. 2013. 'Programmable repression and activation of bacterial gene expression using an engineered CRISPR-Cas system', *Nucleic Acids Res*, 41: 7429-37.

Blomen, Vincent A, Peter Májek, Lucas T Jae, Johannes W Bigenzahn, Joppe Nieuwenhuis, Jacqueline Staring, Roberto Sacco, Ferdy R van Diemen, Nadine Olk, and Alexey Stukalov. 2015. 'Gene essentiality and synthetic lethality in haploid human cells', *Science*, 350: 1092-96.

Boehm, T., and C. C. Bleul. 2007. 'The evolutionary history of lymphoid organs', *Nat Immunol*, 8: 131-5.

Boshoff, Helena IM, and Clifton E Barry 3rd. 2005. 'Tuberculosis—metabolism and respiration in the absence of growth', *Nature Reviews Microbiology*, 3: 70.

Braibant, M., P. Gilot, and J. Content. 2000a. 'The ATP binding cassette (ABC) transport systems of Mycobacterium tuberculosis', *FEMS Microbiol Rev*, 24: 449-67.

Braibant, Martine, Philippe Gilot, and Jean Content. 2000b. 'The ATP binding cassette (ABC) transport systems of Mycobacterium tuberculosis', *FEMS microbiology reviews*, 24: 449-67.

Breslow, David K, Dale M Cameron, Sean R Collins, Maya Schuldiner, Jacob Stewart-Ornstein, Heather W Newman, Sigurd Braun, Hiten D Madhani, Nevan J Krogan, and Jonathan S Weissman. 2008. 'A comprehensive strategy enabling high-resolution functional analysis of the yeast genome', *Nature methods*, 5: 711-18.

Brinster, S., G. Lamberet, B. Staels, P. Trieu-Cuot, A. Gruss, and C. Poyart. 2009. 'Type II fatty acid synthesis is not a suitable antibiotic target for Gram-positive pathogens', *Nature*, 458: 83-6.

Brizio, C., M. Galluccio, R. Wait, E. M. Torchetti, V. Bafunno, R. Accardi, E. Gianazza, C. Indiveri, and M. Barile. 2006. 'Over-expression in Escherichia coli and characterization of two recombinant isoforms of human FAD synthetase', *Biochem Biophys Res Commun*, 344: 1008-16.

Cheeseman, P., A. Toms-Wood, and R. S. Wolfe. 1972. 'Isolation and properties of a fluorescent compound, factor 420 , from Methanobacterium strain M.o.H', *J Bacteriol*, 112: 527-31.

Choi, Kwang-Pil, Nathan Kendrick, and Lacy Daniels. 2002. 'Demonstration that fbiC is required by Mycobacterium bovis BCG for coenzyme F420 and FO biosynthesis', *Journal of bacteriology*, 184: 2420-28.

Choudhary, E., P. Thakur, M. Pareek, and N. Agarwal. 2015. 'Gene silencing by CRISPR interference in mycobacteria', *Nat Commun*, 6: 6267.

Christen, Beat, Eduardo Abeliuk, John M Collier, Virginia S Kalogeraki, Ben Passarelli, John A Coller, Michael J Fero, Harley H McAdams, and Lucy Shapiro. 2011. 'The essential genome of a bacterium', *Molecular systems biology*, 7.

Christie, J. M., L. Blackwood, J. Petersen, and S. Sullivan. 2015. 'Plant flavoprotein photoreceptors', *Plant Cell Physiol*, 56: 401-13.

Chua, W. J., S. M. Truscott, C. S. Eickhoff, A. Blazevic, D. F. Hoft, and T. H. Hansen. 2012. 'Polyclonal mucosa-associated invariant T cells have unique innate functions in bacterial infection', *Infect Immun*, 80: 3256-67.

Cohen, J. 2013. 'Infectious disease. Approval of novel TB drug celebrated--with restraint', *Science*, 339: 130.

Cole, ST, K Eiglmeier, J Parkhill, KD James, NR Thomson, PR Wheeler, N Honore, T Garnier, C Churcher, and D Harris. 2001. 'Massive gene decay in the leprosy bacillus', *Nature*, 409: 1007.

Contreras, Heidi, Nicholas Chim, Alfredo Credali, and Celia W Goulding. 2014. 'Heme uptake in bacterial pathogens', *Current opinion in chemical biology*, 19: 34-41.

Copeland, Robert A, David L Pompliano, and Thomas D Meek. 2006. 'Drug–target residence time and its implications for lead optimization', *Nature reviews Drug discovery*, 5: 730-39.

Corbett, A. J., S. B. Eckle, R. W. Birkinshaw, L. Liu, O. Patel, J. Mahony, Z. Chen, R. Reantragoon, B. Meehan, H. Cao, N. A. Williamson, R. A. Strugnell, D. Van Sinderen, J. Y. Mak, D. P. Fairlie, L. Kjer-Nielsen, J. Rossjohn, and J. McCluskey. 2014. 'T-cell activation by transitory neo-antigens derived from distinct microbial pathways', *Nature*, 509: 361-5.

Crossley, R. A., D. J. Gaskin, K. Holmes, F. Mulholland, J. M. Wells, D. J. Kelly, A. H. van Vliet, and N. J. Walton. 2007. 'Riboflavin biosynthesis is associated with assimilatory ferric reduction and iron acquisition by Campylobacter jejuni', *Appl Environ Microbiol*, 73: 7819-25.

da Silva Neto, J. F., R. F. Lourenco, and M. V. Marques. 2013. 'Global transcriptional response of Caulobacter crescentus to iron availability', *BMC Genomics*, 14: 549.

Dalla Vecchia, E., E. I. Suvorova, J. Maillard, and R. Bernier-Latmani. 2014. 'Fe(III) reduction during pyruvate fermentation by Desulfotomaculum reducens strain MI-1', *Geobiology*, 12: 48-61.

Darrah, P. A., J. J. Zeppa, P. Maiello, J. A. Hackney, M. H. Wadsworth, 2nd, T. K. Hughes, S. Pokkali, P. A. Swanson, 2nd, N. L. Grant, M. A. Rodgers, M. Kamath, C. M. Causgrove, D. J. Laddy, A. Bonavia, D. Casimiro, P. L. Lin, E. Klein, A. G. White, C. A. Scanga, A. K. Shalek, M. Roederer, J. L. Flynn, and R. A. Seder. 2020. 'Prevention of tuberculosis in macaques after intravenous BCG immunization', *Nature*, 577: 95-102.

De Colibus, L., and A. Mattevi. 2006. 'New frontiers in structural flavoenzymology', *Curr Opin Struct Biol*, 16: 722-8.

de Wet, Timothy J., Irene Gobe, Musa M. Mhlanga, and Digby F. Warner. 2018. 'CRISPRi-Seq for the Identification and Characterisation of Essential Mycobacterial Genes and Transcriptional Units', *bioRxiv*: 358275.

Degiacomi, G., A. Benjak, J. Madacki, F. Boldrin, R. Provvedi, G. Palu, J. Kordulakova, S. T. Cole, and R. Manganelli. 2017. 'Essentiality of mmpL3 and impact of its silencing on Mycobacterium tuberculosis gene expression', *Sci Rep*, 7: 43495.

DeJesus, M. A., E. R. Gerrick, W. Xu, S. W. Park, J. E. Long, C. C. Boutte, E. J. Rubin, D. Schnappinger, S. Ehrt, S. M. Fortune, C. M. Sassetti, and T. R. Ioerger. 2017. 'Comprehensive Essentiality Analysis of the Mycobacterium tuberculosis Genome via Saturating Transposon Mutagenesis', *MBio*, 8.

Deka, Ranjit K, Chad A Brautigam, Brent A Biddy, Wei Z Liu, and Michael V Norgard. 2013. 'Evidence for an ABC-type riboflavin transporter system in pathogenic spirochetes', *MBio*, 4: e00615-12.

Deltcheva, Elitza, Krzysztof Chylinski, Cynthia M. Sharma, Karine Gonzales, Yanjie Chao, Zaid A. Pirzada, Maria R. Eckert, Jörg Vogel, and Emmanuelle Charpentier. 2011. 'CRISPR RNA maturation by trans-encoded small RNA and host factor RNase III', *Nature*, 471: 602-07.

Deveau, H., R. Barrangou, J. E. Garneau, J. Labonte, C. Fremaux, P. Boyaval, D. A. Romero, P. Horvath, and S. Moineau. 2008. 'Phage response to CRISPR-encoded resistance in Streptococcus thermophilus', *J Bacteriol*, 190: 1390-400.

Doudna, J. A., and E. Charpentier. 2014. 'Genome editing. The new frontier of genome engineering with CRISPR-Cas9', *Science*, 346: 1258096.

Dubnau, Eugenie, John Chan, Catherine Raynaud, Vellore P Mohan, Marie-Antoinette Lanéelle, Keming Yu, Annaik Quémard, Issar Smith, and Mamadou Daffé. 2000. 'Oxygenated mycolic acids are necessary for virulence of Mycobacterium tuberculosis in mice', *Molecular microbiology*, 36: 630-37.

Dusseaux, M., E. Martin, N. Serriari, I. Peguillet, V. Premel, D. Louis, M. Milder, L. Le Bourhis, C. Soudais, E. Treiner, and O. Lantz. 2011. 'Human MAIT cells are xenobiotic-resistant, tissue-targeted, CD161hi IL-17-secreting T cells', *Blood*, 117: 1250-9.

Dye, C, S Scheele, and P Dolin. 1999. 'Consensus statement. Global burden of tuberculosis. WHO Global Surveillance and Monitoring Project', *JAMA*, 282: 677-86.

Edwards, A. M. 2014. 'Structure and general properties of flavins', *Methods Mol Biol*, 1146: 3-13.

Efimov, Igor, Vladislav Kuusk, Xiaoping Zhang, and William S McIntire. 1998. 'Proposed steady-state kinetic mechanism for Corynebacterium ammoniagenes FAD synthetase produced by Escherichia coli', *Biochemistry*, 37: 9716-23.

Eirich, L. D., G. D. Vogels, and R. S. Wolfe. 1978. 'Proposed structure for coenzyme F420 from Methanobacterium', *Biochemistry*, 17: 4583-93.

Evans, J. C., and V. Mizrahi. 2015. 'The application of tetracyclineregulated gene expression systems in the validation of novel drug targets in Mycobacterium tuberculosis', *Front Microbiol*, 6: 812.

Fenner, L., S. E. Reid, M. P. Fox, D. Garone, M. Wellington, H. Prozesky, M. Zwahlen, M. Schomaker, G. Wandeler, N. Kancheya, A. Boulle, R. Wood, G. Henostroza, M. Egger, and D. E. A. Southern Africa Ie. 2013. 'Tuberculosis and the risk of opportunistic infections and cancers in HIV-infected patients starting ART in Southern Africa', *Trop Med Int Health*, 18: 194-8.

Finberg, Robert W, Robert C Moellering, Francis P Tally, William A Craig, George A Pankey, E Patchen Dellinger, Michael A West, Manjari Joshi, Peter K Linden, and Ken V Rolston. 2004. 'The importance of bactericidal drugs: future directions in infectious disease', *Clinical infectious diseases*, 39: 1314-20.

Fine, P. E. 1995. 'Variation in protection by BCG: implications of and for heterologous immunity', *Lancet*, 346: 1339-45.

Franzblau, S. G., R. S. Witzig, J. C. McLaughlin, P. Torres, G. Madico, A. Hernandez, M. T. Degnan, M. B. Cook, V. K. Quenzer, R. M. Ferguson, and R. H. Gilman. 1998. 'Rapid, low-technology MIC determination with clinical Mycobacterium tuberculosis isolates by using the microplate Alamar Blue assay', *J Clin Microbiol*, 36: 362-6.

Fuller, S. J., D. G. McMillan, M. B. Renz, M. Schmidt, I. T. Burke, and D. I. Stewart. 2014. 'Extracellular electron transport-mediated Fe(III) reduction by a community of alkaliphilic bacteria that use flavins as electron shuttles', *Appl Environ Microbiol*, 80: 128-37.

Garst, A. D., A. L. Edwards, and R. T. Batey. 2011. 'Riboswitches: structures and mechanisms', *Cold Spring Harb Perspect Biol*, 3.

Gelfand, Mikhail S, Andrey A Mironov, Jurges Jomantas, Yuri I Kozlov, and Danila A Perumov. 1999. 'A conserved RNA structure element involved in the regulation of bacterial riboflavin synthesis genes', *Trends in Genetics*, 15: 439-42.

Getahun, Haileyesus, Alberto Matteelli, Richard E Chaisson, and Mario Raviglione. 2015. 'Latent Mycobacterium tuberculosis infection', *New England Journal of Medicine*, 372: 2127-35.

Gibbs, A., E. Leeansyah, A. Introini, D. Paquin-Proulx, K. Hasselrot, E. Andersson, K. Broliden, J. K. Sandberg, and A. Tjernlund. 2017. 'MAIT cells reside in the female genital mucosa and are biased towards IL-17 and IL-22 production in response to bacterial stimulation', *Mucosal Immunol*, 10: 35-45.

Gilbert, Luke A, Max A Horlbeck, Britt Adamson, Jacqueline E Villalta, Yuwen Chen, Evan H Whitehead, Carla Guimaraes, Barbara Panning, Hidde L Ploegh, and Michael C Bassik. 2014. 'Genome-scale CRISPR-mediated control of gene repression and activation', *Cell*, 159: 647-61.

Gler, M. T., V. Skripconoka, E. Sanchez-Garavito, H. Xiao, J. L. Cabrera-Rivero, D. E. Vargas-Vasquez, M. Gao, M. Awad, S. K. Park, T. S. Shim, G. Y. Suh, M. Danilovits, H. Ogata, A. Kurve, J. Chang, K. Suzuki, T. Tupasi, W. J. Koh, B. Seaworth, L. J. Geiter, and C. D. Wells. 2012. 'Delamanid for multidrug-resistant pulmonary tuberculosis', *N Engl J Med*, 366: 2151-60.

Gold, M. C., S. Cerri, S. Smyk-Pearson, M. E. Cansler, T. M. Vogt, J. Delepine, E. Winata, G. M. Swarbrick, W. J. Chua, Y. Y. Yu, O. Lantz, M. S. Cook, M. D. Null, D. B. Jacoby, M. J. Harriff, D. A. Lewinsohn, T. H. Hansen, and D. M. Lewinsohn. 2010. 'Human mucosal associated invariant T cells detect bacterially infected cells', *PLoS Biol*, 8: e1000407.

Goodman, Andrew L, Nathan P McNulty, Yue Zhao, Douglas Leip, Robi D Mitra, Catherine A Lozupone, Rob Knight, and Jeffrey I Gordon. 2009. 'Identifying genetic determinants needed to establish a human gut symbiont in its habitat', *Cell host & microbe*, 6: 279-89.

Grange, J. M. 1982. 'Koch's Tubercle Bacillus - a centenary reappraisal', *Zentralbl Bakteriol Mikrobiol Hyg A*, 251: 297-307.

Greene, J. M., P. Dash, S. Roy, C. McMurtrey, W. Awad, J. S. Reed, K. B. Hammond, S. Abdulhaqq, H. L. Wu, B. J. Burwitz, B. F. Roth, D. W. Morrow, J. C. Ford, G. Xu, J. Y. Bae, H. Crank, A. W. Legasse, T. H. Dang, H. Y. Greenaway, M. Kurniawan, M. C. Gold, M. J. Harriff, D. A. Lewinsohn, B. S. Park, M. K. Axthelm, J. J. Stanton, S. G. Hansen, L. J. Picker, V. Venturi, W. Hildebrand, P. G. Thomas, D. M. Lewinsohn, E. J. Adams, and J. B. Sacha. 2017. 'MR1-restricted mucosal-associated invariant T (MAIT) cells respond to mycobacterial vaccination and infection in nonhuman primates', *Mucosal Immunol*, 10: 802-13.

Griffin, J. E., J. D. Gawronski, M. A. Dejesus, T. R. Ioerger, B. J. Akerley, and C. M. Sassetti. 2011a. 'High-resolution phenotypic profiling defines genes essential for mycobacterial growth and cholesterol catabolism', *PLoS Pathog*, 7: e1002251.

Griffin, Jennifer E, Jeffrey D Gawronski, Michael A DeJesus, Thomas R Ioerger, Brian J Akerley, and Christopher M Sassetti. 2011b. 'High-resolution phenotypic profiling defines genes essential for mycobacterial growth and cholesterol catabolism', *PLoS pathogens*, 7.

Grill, S., S. Busenbender, M. Pfeiffer, U. Kohler, and M. Mack. 2008. 'The bifunctional flavokinase/flavin adenine dinucleotide synthetase from Streptomyces davawensis produces inactive flavin cofactors and is not involved in resistance to the antibiotic roseoflavin', *J Bacteriol*, 190: 1546-53.

Grill, S., H. Yamaguchi, H. Wagner, L. Zwahlen, U. Kusch, and M. Mack. 2007. 'Identification and characterization of two Streptomyces davawensis riboflavin biosynthesis gene clusters', *Arch Microbiol*, 188: 377-87.

Gurumurthy, Meera, Martin Rao, Tathagata Mukherjee, Srinivasa PS Rao, Helena I Boshoff, Thomas Dick, Clifton E Barry, and Ujjini H Manjunatha. 2013. 'A novel F420-dependent anti-oxidant mechanism protects Mycobacterium tuberculosis against oxidative stress and bactericidal agents', *Molecular microbiology*, 87: 744-55.

Gutiérrez-Preciado, Ana, Alfredo Gabriel Torres, Enrique Merino, Hernán Ruy Bonomi, Fernando Alberto Goldbaum, and Víctor Antonio García-Angulo. 2015. 'Extensive identification of bacterial riboflavin transporters and their distribution across bacterial species', *PloS one*, 10.

Haase, I., T. Grawert, B. Illarionov, A. Bacher, and M. Fischer. 2014. 'Recent advances in riboflavin biosynthesis', *Methods Mol Biol*, 1146: 15-40.

Harriff, M. J., E. Karamooz, A. Burr, W. F. Grant, E. T. Canfield, M. L. Sorensen, L. F. Moita, and D. M. Lewinsohn. 2016. 'Endosomal MR1 Trafficking Plays a Key Role in Presentation of Mycobacterium tuberculosis Ligands to MAIT Cells', *PLoS Pathog*, 12: e1005524.

Harriff, Melanie J, Curtis McMurtrey, Cara A Froyd, Haihong Jin, Meghan Cansler, Megan Null, Aneta Worley, Erin W Meermeier, Gwendolyn Swarbrick, and Aaron Nilsen. 2018. 'MR1 displays the microbial metabolome driving selective MR1-restricted T cell receptor usage', *Science immunology*, 3: eaao2556.

Hartkoorn, Ruben C, Swapna Uplekar, and Stewart T Cole. 2014. 'Cross-resistance between clofazimine and bedaquiline through upregulation of MmpL5 in Mycobacterium tuberculosis', *Antimicrobial agents and chemotherapy*, 58: 2979-81.

Hasan, Mohammad Rubayet, Mahbuba Rahman, Sandford Jaques, Endang Purwantini, and Lacy Daniels. 2010. 'Glucose 6-phosphate accumulation in mycobacteria implications for a novel F420-dependent anti-oxidant defense system', *Journal of Biological Chemistry*, 285: 19135-44.

Hemberger, S., D. B. Pedrolli, J. Stolz, C. Vogl, M. Lehmann, and M. Mack. 2011. 'RibM from Streptomyces davawensis is a riboflavin/roseoflavin transporter and may be useful for the optimization of riboflavin production strains', *BMC Biotechnol*, 11: 119.

Hemmerich, P., G. Nagelschneider, and C. Veeger. 1970. 'Chemistry and molecular biology of flavins and flavoproteins', *FEBS Lett*, 8: 69-83.

Herguedas, Beatriz, Marta Martinez-Julvez, Susana Frago, Milagros Medina, and Juan A Hermoso. 2009. 'Crystallization and preliminary X-ray diffraction studies of FAD synthetase from Corynebacterium ammoniagenes', *Acta Crystallographica Section F: Structural Biology and Crystallization Communications*, 65: 1285-88.

Hesseling, A. C., B. J. Marais, R. P. Gie, H. S. Schaaf, P. E. Fine, P. Godfrey-Faussett, and N. Beyers. 2007. 'The risk of disseminated Bacille Calmette-Guerin (BCG) disease in HIV-infected children', *Vaccine*, 25: 14-8.

Higashitsuji, Y., A. Angerer, S. Berghaus, B. Hobl, and M. Mack. 2007. 'RibR, a possible regulator of the Bacillus subtilis riboflavin biosynthetic operon, in vivo interacts with the 5'-untranslated leader of rib mRNA', *FEMS Microbiol Lett*, 274: 48-54.

Hinchey, J.; Lee, S.; Jeon, BY.; Basaraba, RJ.; Venkataswamy, MM.; Chen, B.; Chan, J.; Braunstein, M.; Orme, IM.; Derrick, SC.; Morris, SL.; Jacobs, WR Jr.; Porcelli, SA. 2007. 'Enhanced priming of adaptive immunity by a proapoptotic mutant of Mycobacterium tuberculosis'.

Hirano, H., T. Yoshida, H. Fuse, T. Endo, H. Habe, H. Nojiri, and T. Omori. 2003. 'Marinobacterium sp. strain DMS-S1 uses dimethyl sulphide as a sulphur source after light-dependent transformation by excreted flavins', *Environ Microbiol*, 5: 503-9.

Holmes, C. B., E. Losina, R. P. Walensky, Y. Yazdanpanah, and K. A. Freedberg. 2003. 'Review of human immunodeficiency virus type 1-related opportunistic infections in sub-Saharan Africa', *Clin Infect Dis*, 36: 652-62.

Horvath, P., D. A. Romero, A. C. Coute-Monvoisin, M. Richards, H. Deveau, S. Moineau, P. Boyaval, C. Fremaux, and R. Barrangou. 2008. 'Diversity, activity, and evolution of CRISPR loci in Streptococcus thermophilus', *J Bacteriol*, 190: 1401-12.

Janeway, C. A. Jr., Travers, P., Waplort, M. et al. 2001. 'Principles of innate and adaptive immunity', *Immunobiology: The immune system in Health and Disease.*, 5th edition.

Jankowitsch, F., C. Kuhm, R. Kellner, J. Kalinowski, S. Pelzer, P. Macheroux, and M. Mack. 2011. 'A novel N,N-8-amino-8-demethyl-D-riboflavin Dimethyltransferase (RosA) catalyzing the two terminal steps of roseoflavin biosynthesis in Streptomyces davawensis', *J Biol Chem*, 286: 38275-85.

Jankowitsch, F., J. Schwarz, C. Ruckert, B. Gust, R. Szczepanowski, J. Blom, S. Pelzer, J. Kalinowski, and M. Mack. 2012. 'Genome sequence of the bacterium Streptomyces davawensis JCM 4913 and heterologous production of the unique antibiotic roseoflavin', *J Bacteriol*, 194: 6818-27.

Janssen, B.D., Chen, Yi-Pei.,Molgora, B.M., Wang, S.E., Simoes-Barbosa, A., Johnson, P.J. 2018. 'CRISPR/Cas9-mediated gene modifcation and gene knock out in the human-infective parasite Trichomonas vaginalis', *Sci. Rep*

Jesteadt, E., I. Zhang, H. Yu, A. Meierovics, W. J. Chua Yankelevich, and S. Cowley. 2018. 'Interleukin-18 Is Critical for Mucosa-Associated Invariant T Cell Gamma Interferon Responses to Francisella Species In Vitro but Not In Vivo', *Infect Immun*, 86.

Johnson, M. D., C. MacDougall, L. Ostrosky-Zeichner, J. R. Perfect, and J. H. Rex. 2004. 'Combination antifungal therapy', *Antimicrob Agents Chemother*, 48: 693-715.

Keller, A. N., A. J. Corbett, J. M. Wubben, J. McCluskey, and J. Rossjohn. 2017. 'MAIT cells and MR1-antigen recognition', *Curr Opin Immunol*, 46: 66-74.

Keller, A. N., S. B. Eckle, W. Xu, L. Liu, V. A. Hughes, J. Y. Mak, B. S. Meehan, T. Pediongco, R. W. Birkinshaw, Z. Chen, H. Wang, C. D'Souza, L. Kjer-Nielsen, N. A. Gherardin, D. I. Godfrey, L. Kostenko, A. J. Corbett, A. W. Purcell, D. P. Fairlie, J. McCluskey, and J. Rossjohn. 2017. 'Drugs and drug-like molecules can modulate the function of mucosal-associated invariant T cells', *Nat Immunol*, 18: 402-11.

Kim, D., S. Bae, J. Park, E. Kim, S. Kim, H. R. Yu, J. Hwang, J. I. Kim, and J. S. Kim. 2015. 'Digenome-seq: genome-wide profiling of CRISPR-Cas9 off-target effects in human cells', *Nat Methods*, 12: 237-43, 1 p following 43.

Kinjo, Y., P. Illarionov, J. L. Vela, B. Pei, E. Girardi, X. Li, Y. Li, M. Imamura, Y. Kaneko, A. Okawara, Y. Miyazaki, A. Gomez-Velasco, P. Rogers, S. Dahesh, S. Uchiyama, A. Khurana, K. Kawahara, H. Yesilkaya, P. W. Andrew, C. H. Wong, K. Kawakami, V. Nizet, G. S. Besra, M. Tsuji, D. M. Zajonc, and M. Kronenberg. 2011. 'Invariant natural killer T cells recognize glycolipids from pathogenic Gram-positive bacteria', *Nat Immunol*, 12: 966-74.

Kjer-Nielsen, L., O. Patel, A. J. Corbett, J. Le Nours, B. Meehan, L. Liu, M. Bhati, Z. Chen, L. Kostenko, R. Reantragoon, N. A. Williamson, A. W. Purcell, N. L. Dudek, M. J. McConville, R. A. O'Hair, G. N. Khairallah, D. I. Godfrey, D. P. Fairlie, J. Rossjohn, and J. McCluskey. 2012. 'MR1 presents microbial vitamin B metabolites to MAIT cells', *Nature*, 491: 717-23.

Kotloski, N. J., and J. A. Gralnick. 2013. 'Flavin electron shuttles dominate extracellular electron transfer by Shewanella oneidensis', *MBio*, 4.

Kreneva, R. A., M. S. Gel'fand, A. A. Mironov, A. Iomantas Iu, I. Kozlov Iu, A. S. Mironov, and D. A. Perumov. 2000. '[Study of the phenotypic occurrence of ura gene inactivation in Bacillus subtilis]', *Genetika*, 36: 1166-8.

Kumar, Ashwani, Jessy S Deshane, David K Crossman, Subhashini Bolisetty, Bo-Shiun Yan, Igor Kramnik, Anupam Agarwal, and Adrie JC Steyn. 2008. 'Heme oxygenase-1-derived carbon monoxide induces the Mycobacterium tuberculosis dormancy regulon', *Journal of Biological Chemistry*, 283: 18032-39.

Kurioka, A, JE Ussher, C Cosgrove, C Clough, JR Fergusson, K Smith, YH Kang, LJ Walker, TH Hansen, and CB Willberg. 2015. 'MAIT cells are licensed through granzyme exchange to kill bacterially sensitized targets', *Mucosal immunology*, 8: 429-40.

Langer, S., S. Nakanishi, T. Mathes, T. Knaus, A. Binter, P. Macheroux, T. Mase, T. Miyakawa, M. Tanokura, and M. Mack. 2013. 'The flavoenzyme azobenzene reductase AzoR from Escherichia coli binds roseoflavin mononucleotide (RoFMN) with high affinity and is less active in its RoFMN form', *Biochemistry*, 52: 4288-95.

Le Bourhis, L., E. Martin, I. Peguillet, A. Guihot, N. Froux, M. Core, E. Levy, M. Dusseaux, V. Meyssonnier, V. Premel, C. Ngo, B. Riteau, L. Duban, D. Robert, S. Huang, M. Rottman, C. Soudais, and O. Lantz. 2010. 'Antimicrobial activity of mucosal-associated invariant T cells', *Nat Immunol*, 11: 701-8.

Lee, E. R., K. F. Blount, and R. R. Breaker. 2009. 'Roseoflavin is a natural antibacterial compound that binds to FMN riboswitches and regulates gene expression', *RNA Biol*, 6: 187-94.

Lee, J. M., S. Zhang, S. Saha, S. Santa Anna, C. Jiang, and J. Perkins. 2001. 'RNA expression analysis using an antisense Bacillus subtilis genome array', *J Bacteriol*, 183: 7371-80.

Lepore, M., A. Kalinichenko, S. Calogero, P. Kumar, B. Paleja, M. Schmaler, V. Narang, F. Zolezzi, M. Poidinger, L. Mori, and G. De Libero. 2017. 'Functionally diverse human T cells recognize non-microbial antigens presented by MR1', *Elife*, 6.

Lepore, M., A. Kalinichenko, A. Colone, B. Paleja, A. Singhal, A. Tschumi, B. Lee, M. Poidinger, F. Zolezzi, L. Quagliata, P. Sander, E. Newell, A. Bertoletti, L. Terracciano, G. De Libero, and L. Mori. 2014. 'Parallel T-cell cloning and deep sequencing of human MAIT cells reveal stable oligoclonal TCRbeta repertoire', *Nat Commun*, 5: 3866.

Lillebaek, Troels, Asger Dirksen, Inga Baess, Benedicte Strunge, Vibeke Ø Thomsen, and Åse B Andersen. 2002. 'Molecular evidence of endogenous reactivation of Mycobacterium tuberculosis after 33 years of latent infection', *The Journal of infectious diseases*, 185: 401-04.

Lin, XL, and RH White. 1986. 'Occurrence of coenzyme F420 and its gamma-monoglutamyl derivative in nonmethanogenic archaebacteria', *Journal of bacteriology*, 168: 444-48.

Lopez-Sagaseta, J., C. L. Dulberger, J. E. Crooks, C. D. Parks, A. M. Luoma, A. McFedries, I. Van Rhijn, A. Saghatelian, and E. J. Adams. 2013. 'The molecular basis for Mucosal-Associated Invariant T cell recognition of MR1 proteins', *Proc Natl Acad Sci U S A*, 110: E1771-8.

Lopez-Sagaseta, J., C. L. Dulberger, A. McFedries, M. Cushman, A. Saghatelian, and E. J. Adams. 2013. 'MAIT recognition of a stimulatory bacterial antigen bound to MR1', *J Immunol*, 191: 5268-77.

Luciani, F., S. A. Sisson, H. Jiang, A. R. Francis, and M. M. Tanaka. 2009. 'The epidemiological fitness cost of drug resistance in Mycobacterium tuberculosis', *Proc Natl Acad Sci U S A*, 106: 14711-5.

Macheroux, Peter, Barbara Kappes, and Steven E Ealick. 2011. 'Flavogenomics–a genomic and structural view of flavin-dependent proteins', *The FEBS journal*, 278: 2625-34.

Mack, M., A. P. van Loon, and H. P. Hohmann. 1998a. 'Regulation of riboflavin biosynthesis in Bacillus subtilis is affected by the activity of the flavokinase/flavin adenine dinucleotide synthetase encoded by ribC', *J Bacteriol*, 180: 950-5.

Mack, Matthias, Adolphus PGM van Loon, and Hans-Peter Hohmann. 1998b. 'Regulation of riboflavin biosynthesis inbacillus subtilis is affected by the activity of the flavokinase/flavin adenine dinucleotide synthetase encoded byribc', *Journal of bacteriology*, 180: 950-55.

Makarov, V., J. Neres, R. C. Hartkoorn, O. B. Ryabova, E. Kazakova, M. Sarkan, S. Huszar, J. Piton, G. S. Kolly, A. Vocat, T. M. Conroy, K. Mikusova, and S. T. Cole. 2015. 'The 8-Pyrrole-Benzothiazinones Are Noncovalent Inhibitors of DprE1 from Mycobacterium tuberculosis', *Antimicrob Agents Chemother*, 59: 4446-52.

Makarova, K. S., D. H. Haft, R. Barrangou, S. J. Brouns, E. Charpentier, P. Horvath, S. Moineau, F. J. Mojica, Y. I. Wolf, A. F. Yakunin, J. van der Oost, and E. V. Koonin. 2011. 'Evolution and classification of the CRISPR-Cas systems', *Nat Rev Microbiol*, 9: 467-77.

Mangtani, P., I. Abubakar, C. Ariti, R. Beynon, L. Pimpin, P. E. Fine, L. C. Rodrigues, P. G. Smith, M. Lipman, P. F. Whiting, and J. A. Sterne. 2014. 'Protection by BCG vaccine against tuberculosis: a systematic review of randomized controlled trials', *Clin Infect Dis*, 58: 470-80.

Manjunatha, Ujjini, Helena IM Boshoff, and Clifton E Barry. 2009. 'The mechanism of action of PA-824: novel insights from transcriptional profiling', *Communicative & integrative biology*, 2: 215-18.

Manjunatha, Ujjini H, Helena Boshoff, Cynthia S Dowd, Liang Zhang, Thomas J Albert, Jason E Norton, Lacy Daniels, Thomas Dick, Siew Siew Pang, and Clifton E Barry. 2006. 'Identification of a nitroimidazo-oxazine-specific protein involved in PA-824 resistance in Mycobacterium tuberculosis', *Proceedings of the National Academy of Sciences of the United States of America*, 103: 431-36.

Mansjo, M., and J. Johansson. 2011. 'The riboflavin analog roseoflavin targets an FMN-riboswitch and blocks Listeria monocytogenes growth, but also stimulates virulence gene-expression and infection', *RNA Biol*, 8: 674-80.

Marsili, E., D. B. Baron, I. D. Shikhare, D. Coursolle, J. A. Gralnick, and D. R. Bond. 2008. 'Shewanella secretes flavins that mediate extracellular electron transfer', *Proc Natl Acad Sci U S A*, 105: 3968-73.

Martin, E., E. Treiner, L. Duban, L. Guerri, H. Laude, C. Toly, V. Premel, A. Devys, I. C. Moura, F. Tilloy, S. Cherif, G. Vera, S. Latour, C. Soudais, and O. Lantz. 2009. 'Stepwise development of MAIT cells in mouse and human', *PLoS Biol*, 7: e54.

Matsumoto, M., H. Hashizume, T. Tomishige, M. Kawasaki, H. Tsubouchi, H. Sasaki, Y. Shimokawa, and M. Komatsu. 2006. 'OPC-67683, a nitro-dihydro-imidazooxazole derivative with promising action against tuberculosis in vitro and in mice', *PLoS Med*, 3: e466.

McNeil, M. B., and G. M. Cook. 2019a. 'Utilization of CRISPR Interference To Validate MmpL3 as a Drug Target in Mycobacterium tuberculosis', *Antimicrob Agents Chemother*, 63.

McNeil, Matthew B, and Gregory M Cook. 2019b. 'Utilization of CRISPR interference to validate MmpL3 as a drug target in Mycobacterium tuberculosis', *Antimicrobial agents and chemotherapy*, 63: e00629-19.

Medzhitov, R., and C. A. Janeway, Jr. 2002. 'Decoding the patterns of self and nonself by the innate immune system', *Science*, 296: 298-300.

Meermeier, E. W., B. F. Laugel, A. K. Sewell, A. J. Corbett, J. Rossjohn, J. McCluskey, M. J. Harriff, T. Franks, M. C. Gold, and D. M. Lewinsohn. 2016. 'Human TRAV1-2-negative MR1-restricted T cells detect S. pyogenes and alternatives to MAIT riboflavin-based antigens', *Nat Commun*, 7: 12506.

Mehta-Kolte, M. G., and D. R. Bond. 2012. 'Geothrix fermentans secretes two different redox-active compounds to utilize electron acceptors across a wide range of redox potentials', *Appl Environ Microbiol*, 78: 6987-95.

Meierovics, A., W. J. Yankelevich, and S. C. Cowley. 2013. 'MAIT cells are critical for optimal mucosal immune responses during in vivo pulmonary bacterial infection', *Proc Natl Acad Sci U S A*, 110: E3119-28.

Mellin, JR, and Pascale Cossart. 2015. 'Unexpected versatility in bacterial riboswitches', *Trends in Genetics*, 31: 150-56.

Mironov, A. S., I. Gusarov, R. Rafikov, L. E. Lopez, K. Shatalin, R. A. Kreneva, D. A. Perumov, and E. Nudler. 2002a. 'Sensing small molecules by nascent RNA: a mechanism to control transcription in bacteria', *Cell*, 111: 747-56.

Mironov, Alexander S, Ivan Gusarov, Ruslan Rafikov, Lubov Errais Lopez, Konstantin Shatalin, Rimma A Kreneva, Daniel A Perumov, and Evgeny Nudler. 2002b. 'Sensing small molecules by nascent RNA: a mechanism to control transcription in bacteria', *Cell*, 111: 747-56.

Mitchison, DAVIESG, and G Davies. 2012. 'The chemotherapy of tuberculosis: past, present and future [State of the art]', *The International Journal of Tuberculosis and Lung Disease*, 16: 724-32.

Moullan, N., L. Mouchiroud, X. Wang, D. Ryu, E. G. Williams, A. Mottis, V. Jovaisaite, M. V. Frochaux, P. M. Quiros, B. Deplancke, R. H. Houtkooper, and J. Auwerx. 2015. 'Tetracyclines Disturb Mitochondrial Function across Eukaryotic Models: A Call for Caution in Biomedical Research', *Cell Rep*, 10: 1681-91.

Nambu, Shusuke, Toshitaka Matsui, Celia W Goulding, Satoshi Takahashi, and Masao Ikeda-Saito. 2013. 'A new way to degrade heme the Mycobacterium tuberculosis enzyme MhuD catalyzes heme degradation without generating CO', *Journal of Biological Chemistry*, 288: 10101-09.

Netea, Mihai G, Leo AB Joosten, Eicke Latz, Kingston HG Mills, Gioacchino Natoli, Hendrik G Stunnenberg, Luke AJ O'Neill, and Ramnik J Xavier. 2016. 'Trained immunity: a program of innate immune memory in health and disease', *Science*, 352: aaf1098.

Nielsen, Alec AK, and Christopher A Voigt. 2014. 'Multi-input CRISPR/Cas genetic circuits that interface host regulatory networks', *Molecular systems biology*, 10: 763.

Northrop-Clewes, C. A., and D. I. Thurnham. 2012. 'The discovery and characterization of riboflavin', *Ann Nutr Metab*, 61: 224-30.

O'Brien, D. E., L. T. Weinstock, and C. C. Cheng. 1967. '10-deazariboflavin', *Chem Ind*, 48: 2044-5.

O'Brien, Darrcll E, Louis T Weinslock, and CC Cheng. 1970. 'Synthesis of 10-deazariboflavin and related 2, 4-Dioxopyrimido [4, 5-b] quinolines', *Journal of Heterocyclic Chemistry*, 7: 99-105.

Odds, F. C. 2003. 'Synergy, antagonism, and what the chequerboard puts between them', *J Antimicrob Chemother*, 52: 1.

Omollo, Charles Onyango, Vinayak Singh, Elizabeth Kigondu, Antonina Wasuna, Pooja Agarwal, Atica Moosa, Thomas R Ioerger, Valerie Mizrahi, Kelly Chibale, and Digby Francis Warner. 2019. 'Developing synergistic drug combinations to restore antibiotic sensitivity in drug-resistant Mycobacterium tuberculosis', *bioRxiv*: 860288.

Otani, S., M. Takatsu, M. Nakano, S. Kasai, and R. Miura. 1974. 'Letter: Roseoflavin, a new antimicrobial pigment from Streptomyces', *J Antibiot (Tokyo)*, 27: 86-7.

Ott, E., J. Stolz, M. Lehmann, and M. Mack. 2009. 'The RFN riboswitch of Bacillus subtilis is a target for the antibiotic roseoflavin produced by Streptomyces davawensis', *RNA Biol*, 6: 276-80.

Pancer, Z., and M. D. Cooper. 2006. 'The evolution of adaptive immunity', *Annu Rev Immunol*, 24: 497-518.

Patel, O., L. Kjer-Nielsen, J. Le Nours, S. B. Eckle, R. Birkinshaw, T. Beddoe, A. J. Corbett, L. Liu, J. J. Miles, B. Meehan, R. Reantragoon, M. L. Sandoval-Romero, L. C. Sullivan, A. G. Brooks, Z. Chen, D. P. Fairlie, J. McCluskey, and J. Rossjohn. 2013. 'Recognition of vitamin B metabolites by mucosal-associated invariant T cells', *Nat Commun*, 4: 2142.

Pedrolli, D. B., C. Kuhm, D. C. Sevin, M. P. Vockenhuber, U. Sauer, B. Suess, and M. Mack. 2015. 'A dual control mechanism synchronizes riboflavin and sulphur metabolism in Bacillus subtilis', *Proc Natl Acad Sci U S A*, 112: 14054-9.

Pedrolli, D. B., A. Matern, J. Wang, M. Ester, K. Siedler, R. Breaker, and M. Mack. 2012. 'A highly specialized flavin mononucleotide riboswitch responds differently to similar ligands and confers roseoflavin resistance to Streptomyces davawensis', *Nucleic Acids Res*, 40: 8662-73.

Pedrolli, D. B., S. Nakanishi, M. Barile, M. Mansurova, E. C. Carmona, A. Lux, W. Gartner, and M. Mack. 2011. 'The antibiotics roseoflavin and 8-demethyl-8-amino-riboflavin from Streptomyces davawensis are metabolized by human flavokinase and human FAD synthetase', *Biochem Pharmacol*, 82: 1853-9.

Pedrolli, D., S. Langer, B. Hobl, J. Schwarz, M. Hashimoto, and M. Mack. 2015a. 'The ribB FMN riboswitch from Escherichia coli operates at the transcriptional and translational level and regulates riboflavin biosynthesis', *FEBS J*, 282: 3230-42.

Pedrolli, Danielle, Simone Langer, Birgit Hobl, Julia Schwarz, Masayuki Hashimoto, and Matthias Mack. 2015b. 'The ribB FMN riboswitch from Escherichia coli operates at the transcriptional and translational level and regulates riboflavin biosynthesis', *The FEBS journal*, 282: 3230-42.

Peters, Jason M, Alexandre Colavin, Handuo Shi, Tomasz L Czarny, Matthew H Larson, Spencer Wong, John S Hawkins, Candy HS Lu, Byoung-Mo Koo, and Elizabeth Marta. 2016. 'A comprehensive, CRISPR-based functional analysis of essential genes in bacteria', *Cell*, 165: 1493-506.

Purwantini, Endang, Thomas P Gillis, and Lacy Daniels. 1997. 'Presence of F420-dependent glucose-6-phosphate dehydrogenase in Mycobacterium and Nocardia species, but absence from Streptomyces and Corynebacterium species and methanogenic Archaea', *FEMS microbiology letters*, 146: 129-34.

Purwantini, Endang, and Biswarup Mukhopadhyay. 2009. 'Conversion of NO2 to NO by reduced coenzyme F420 protects mycobacteria from nitrosative damage', *Proceedings of the National Academy of Sciences*, 106: 6333-38.

———. 2013. 'Rv0132c of Mycobacterium tuberculosis encodes a coenzyme F420-dependent hydroxymycolic acid dehydrogenase', *PloS one*, 8: e81985.

Qi, L. S., M. H. Larson, L. A. Gilbert, J. A. Doudna, J. S. Weissman, A. P. Arkin, and W. A. Lim. 2013a. 'Repurposing CRISPR as an RNA-guided platform for sequence-specific control of gene expression', *Cell*, 152: 1173-83.

Qi, Lei S, Matthew H Larson, Luke A Gilbert, Jennifer A Doudna, Jonathan S Weissman, Adam P Arkin, and Wendell A Lim. 2013b. 'Repurposing CRISPR as an RNA-guided platform for sequence-specific control of gene expression', *Cell*, 152: 1173-83.

Reantragoon, R., A. J. Corbett, I. G. Sakala, N. A. Gherardin, J. B. Furness, Z. Chen, S. B. Eckle, A. P. Uldrich, R. W. Birkinshaw, O. Patel, L. Kostenko, B. Meehan, K. Kedzierska, L. Liu, D. P. Fairlie, T. H. Hansen, D. I. Godfrey, J. Rossjohn, J. McCluskey, and L. Kjer-Nielsen. 2013. 'Antigen-loaded MR1 tetramers define T cell receptor heterogeneity in mucosal-associated invariant T cells', *J Exp Med*, 210: 2305-20.

Rock, J. M., F. F. Hopkins, A. Chavez, M. Diallo, M. R. Chase, E. R. Gerrick, J. R. Pritchard, G. M. Church, E. J. Rubin, C. M. Sassetti, D. Schnappinger, and S. M. Fortune. 2017. 'Programmable transcriptional repression in mycobacteria using an orthogonal CRISPR interference platform', *Nat Microbiol*, 2: 16274.

Sakula, A. 1983. 'Robert koch: centenary of the discovery of the tubercle bacillus, 1882', *Can Vet J*, 24: 127-31.

Sambandan, Dhinakaran, Dee N Dao, Brian C Weinrick, Catherine Vilchèze, Sudagar S Gurcha, Anil Ojha, Laurent Kremer, Gurdyal S Besra, Graham F Hatfull, and William R Jacobs. 2013. 'Keto-mycolic acid-dependent pellicle formation confers tolerance to drug-sensitive Mycobacterium tuberculosis', *MBio*, 4: e00222-13.

Sassetti, C. M., D. H. Boyd, and E. J. Rubin. 2003a. 'Genes required for mycobacterial growth defined by high density mutagenesis', *Mol Microbiol*, 48: 77-84.

Sassetti, Christopher M, Dana H Boyd, and Eric J Rubin. 2003b. 'Genes required for mycobacterial growth defined by high density mutagenesis', *Molecular microbiology*, 48: 77-84.

Saviola, Beatrice, and William Bishai. 2006. 'The Genus Mycobacterium--Medical.' in, *The Prokaryotes* (Springer).

Schwarz, J., V. Konjik, F. Jankowitsch, R. Sandhoff, and M. Mack. 2016. 'Identification of the Key Enzyme of Roseoflavin Biosynthesis', *Angew Chem Int Ed Engl*, 55: 6103-6.

Sebastian, M., E. Anoz-Carbonell, B. Gracia, P. Cossio, J. A. Ainsa, I. Lans, and M. Medina. 2018. 'Discovery of antimicrobial compounds targeting bacterial type FAD synthetases', *J Enzyme Inhib Med Chem*, 33: 241-54.

Sebastián, María, Ernesto Anoz-Carbonell, Begoña Gracia, Pilar Cossio, José Antonio Aínsa, Isaías Lans, and Milagros Medina. 2018. 'Discovery of antimicrobial compounds targeting bacterial type FAD synthetases', *Journal of enzyme inhibition and medicinal chemistry*, 33: 241-54.

Sepúlveda Cisternas, Ignacio, Juan C Salazar, and Víctor A García-Angulo. 2018. 'Overview on the bacterial iron-riboflavin metabolic axis', *Frontiers in microbiology*, 9: 1478.

Serganov, Alexander, Lili Huang, and Dinshaw J Patel. 2009. 'Coenzyme recognition and gene regulation by a flavin mononucleotide riboswitch', *Nature*, 458: 233-37.

Serrano, Ana, Susana Frago, Adrián Velázquez-Campoy, and Milagros Medina. 2012. 'Role of key residues at the flavin mononucleotide (FMN): adenylyltransferase catalytic site of the bifunctional riboflavin kinase/flavin adenine dinucleotide (FAD) Synthetase from Corynebacterium ammoniagenes', *International journal of molecular sciences*, 13: 14492-517.

Shiloh, M. U., and P. A. Champion. 2010. 'To catch a killer. What can mycobacterial models teach us about Mycobacterium tuberculosis pathogenesis?', *Curr Opin Microbiol*, 13: 86-92.

Singh, A. K., X. Carette, L. P. Potluri, J. D. Sharp, R. Xu, S. Prisic, and R. N. Husson. 2016. 'Investigating essential gene function in Mycobacterium tuberculosis using an efficient CRISPR interference system', *Nucleic Acids Res*, 44: e143.

Singh, Vinayak, Stefano Donini, Angela Pacitto, Claudia Sala, Ruben C Hartkoorn, Neeraj Dhar, Gyorgy Keri, David B Ascher, Guillaume Mondésert, and Anthony Vocat. 2017. 'The inosine monophosphate dehydrogenase, GuaB2, is a vulnerable new bactericidal drug target for tuberculosis', *ACS infectious diseases*, 3: 5-17.

Solovieva, I. M., R. A. Kreneva, D. J. Leak, and D. A. Perumov. 1999. 'The ribR gene encodes a monofunctional riboflavin kinase which is involved in regulation of the Bacillus subtilis riboflavin operon', *Microbiology*, 145 (Pt 1): 67-73.

Somoskovi, A., V. Bruderer, R. Homke, G. V. Bloemberg, and E. C. Bottger. 2015. 'A mutation associated with clofazimine and bedaquiline cross-resistance in MDR-TB following bedaquiline treatment', *Eur Respir J*, 45: 554-7.

Sontheimer, E. J., and R. Barrangou. 2015. 'The Bacterial Origins of the CRISPR Genome-Editing Revolution', *Hum Gene Ther*, 26: 413-24.

Sundstrom, P., F. Ahlmanner, P. Akeus, M. Sundquist, S. Alsen, U. Yrlid, L. Borjesson, A. Sjoling, B. Gustavsson, S. B. Wong, and M. Quiding-Jarbrink. 2015. 'Human Mucosa-Associated Invariant T Cells Accumulate in Colon Adenocarcinomas but Produce Reduced Amounts of IFN-gamma', *J Immunol*, 195: 3472-81.

Tagua, V. G., M. Pausch, M. Eckel, G. Gutierrez, A. Miralles-Duran, C. Sanz, A. P. Eslava, R. Pokorny, L. M. Corrochano, and A. Batschauer. 2015. 'Fungal cryptochrome with DNA repair activity reveals an early stage in cryptochrome evolution', *Proc Natl Acad Sci U S A*, 112: 15130-5.

Takahashi, J. S. 2015. 'Molecular components of the circadian clock in mammals', *Diabetes Obes Metab*, 17 Suppl 1: 6-11.

Tang, X. Z., J. Jo, A. T. Tan, E. Sandalova, A. Chia, K. C. Tan, K. H. Lee, A. J. Gehring, G. De Libero, and A. Bertoletti. 2013. 'IL-7 licenses activation of human liver intrasinusoidal mucosal-associated invariant T cells', *J Immunol*, 190: 3142-52.

Taylor, Matthew C, Colin J Jackson, David B Tattersall, Nigel French, Thomas S Peat, Janet Newman, Lyndall J Briggs, Gauri V Lapalikar, Peter M Campbell, and Colin Scott. 2010. 'Identification and characterization of two families of F420H2-dependent reductases from Mycobacteria that catalyse aflatoxin degradation', *Molecular microbiology*, 78: 561-75.

Terns, R. M., and M. P. Terns. 2014. 'CRISPR-based technologies: prokaryotic defense weapons repurposed', *Trends Genet*, 30: 111-8.

Tongsook, C., M. K. Uhl, F. Jankowitsch, M. Mack, K. Gruber, and P. Macheroux. 2016. 'Structural and kinetic studies on RosA, the enzyme catalysing the methylation of 8-demethyl-8-amino-d-riboflavin to the antibiotic roseoflavin', *FEBS J*, 283: 1531-49.

Treiner, E., L. Duban, S. Bahram, M. Radosavljevic, V. Wanner, F. Tilloy, P. Affaticati, S. Gilfillan, and O. Lantz. 2003. 'Selection of evolutionarily conserved mucosal-associated invariant T cells by MR1', *Nature*, 422: 164-9.

Ussher, J. E., M. Bilton, E. Attwod, J. Shadwell, R. Richardson, C. de Lara, E. Mettke, A. Kurioka, T. H. Hansen, P. Klenerman, and C. B. Willberg. 2014. 'CD161++ CD8+ T cells, including the MAIT cell subset, are specifically activated by IL-12+IL-18 in a TCR-independent manner', *Eur J Immunol*, 44: 195-203.

Van Opijnen, Tim, Kip L Bodi, and Andrew Camilli. 2009. 'Tn-seq: high-throughput parallel sequencing for fitness and genetic interaction studies in microorganisms', *Nature methods*, 6: 767.

Vandal, Omar H., Lynda M. Pierini, Dirk Schnappinger, Carl F. Nathan, and Sabine Ehrt. 2008. 'A membrane protein preserves intrabacterial pH in intraphagosomal Mycobacterium tuberculosis', *Nature Medicine*, 14: 849-54.

Vigouroux, Antoine, Enno Oldewurtel, Lun Cui, David Bikard, and Sven van Teeffelen. 2018. 'Tuning dCas9's ability to block transcription enables robust, noiseless knockdown of bacterial genes', *Molecular systems biology*, 14.

Vitreschak, A. G., D. A. Rodionov, A. A. Mironov, and M. S. Gelfand. 2002a. 'Regulation of riboflavin biosynthesis and transport genes in bacteria by transcriptional and translational attenuation', *Nucleic Acids Res*, 30: 3141-51.

Vitreschak, Alexey G, Dmitry A Rodionov, Andrey A Mironov, and Mikhail S Gelfand. 2002b. 'Regulation of riboflavin biosynthesis and transport genes in bacteria by transcriptional and translational attenuation', *Nucleic acids research*, 30: 3141-51.

Vogl, C., S. Grill, O. Schilling, J. Stulke, M. Mack, and J. Stolz. 2007. 'Characterization of riboflavin (vitamin B2) transport proteins from Bacillus subtilis and Corynebacterium glutamicum', *J Bacteriol*, 189: 7367-75.

von Canstein, H., J. Ogawa, S. Shimizu, and J. R. Lloyd. 2008. 'Secretion of flavins by Shewanella species and their role in extracellular electron transfer', *Appl Environ Microbiol*, 74: 615-23.

Walsh, C., J. Fisher, R. Spencer, D. W. Graham, W. T. Ashton, J. E. Brown, R. D. Brown, and E. F. Rogers. 1978. 'Chemical and enzymatic properties of riboflavin analogues', *Biochemistry*, 17: 1942-51.

Walsh, Christopher. 1980. 'Flavin coenzymes: at the crossroads of biological redox chemistry', *Accounts of Chemical Research*, 13: 148-55.

Wang, Hao, Paul A Mann, Li Xiao, Charles Gill, Andrew M Galgoci, John A Howe, Artjohn Villafania, Christopher M Barbieri, Juliana C Malinverni, and Xinwei Sher. 2017. 'Dual-targeting small-molecule inhibitors of the Staphylococcus aureus FMN riboswitch disrupt riboflavin homeostasis in an infectious setting', *Cell chemical biology*, 24: 576-88. e6.

Wang, Tim, Kıvanç Birsoy, Nicholas W Hughes, Kevin M Krupczak, Yorick Post, Jenny J Wei, Eric S Lander, and David M Sabatini. 2015. 'Identification and characterization of essential genes in the human genome', *Science*, 350: 1096-101.

Wang, Weiru, Rosalind Kim, Jaru Jancarik, Hisao Yokota, and Sung-Hou Kim. 2003. 'Crystal structure of a flavin-binding protein from Thermotoga maritima', *Proteins: Structure, Function, and Bioinformatics*, 52: 633-35.

Wang, Weiru, Rosalind Kim, Hisao Yokota, and Sung-Hou Kim. 2005. 'Crystal structure of flavin binding to FAD synthetase of Thermotoga maritima', *Proteins: Structure, Function, and Bioinformatics*, 58: 246-48.

Watanakunakorn, C. 1984. 'Mode of action and in-vitro activity of vancomycin', *J Antimicrob Chemother*, 14 Suppl D: 7-18.

Wei, Jun-Rong, Vidhya Krishnamoorthy, Kenan Murphy, Jee-Hyun Kim, Dirk Schnappinger, Tom Alber, Christopher M Sassetti, Kyu Y Rhee, and Eric J Rubin. 2011. 'Depletion of antibiotic targets has widely varying effects on growth', *Proceedings of the National Academy of Sciences*, 108: 4176-81.

WHO. 2006. 'Recommendations for prevention and control, weekly epidemiological record'.

———. 2008. 'Global Tuberculosis Control 2008': 1-293.

———. 2010. 'Treatment of Tuberculosis Guidelines'.

———. 2014a. 'Companion handbook to the WHO guidelines for the programmatic management of drug-resistant tuberculosis'.

———. 2014b. 'Global Tuberculosis Report'.

———. 2016a. 'Global tuberculosis report 2016': 1-201.

———. 2016b. 'Treatment guidelines for drug resistant tuberculosis'.

———. 2019. 'Global Tuberculosis Report 2019': p189-249.

Winkler, W. C., and R. R. Breaker. 2005. 'Regulation of bacterial gene expression by riboswitches', *Annu Rev Microbiol*, 59: 487-517.

Winkler, W. C., S. Cohen-Chalamish, and R. R. Breaker. 2002a. 'An mRNA structure that controls gene expression by binding FMN', *Proc Natl Acad Sci U S A*, 99: 15908-13.

Winkler, Wade C, Smadar Cohen-Chalamish, and Ronald R Breaker. 2002b. 'An mRNA structure that controls gene expression by binding FMN', *Proceedings of the National Academy of Sciences*, 99: 15908-13.

Winzeler, Elizabeth A, Daniel D Shoemaker, Anna Astromoff, Hong Liang, Keith Anderson, Bruno Andre, Rhonda Bangham, Rocio Benito, Jef D Boeke, and Howard Bussey. 1999. 'Functional characterization of the S. cerevisiae genome by gene deletion and parallel analysis', *Science*, 285: 901-06.

Wright, A. V., J. K. Nunez, and J. A. Doudna. 2016. 'Biology and Applications of CRISPR Systems: Harnessing Nature's Toolbox for Genome Engineering', *Cell*, 164: 29-44.

Xavier, Alphienes Stanley, and Mageshwaran Lakshmanan. 2014. 'Delamanid: A new armor in combating drug-resistant tuberculosis', *Journal of pharmacology & pharmacotherapeutics*, 5: 222.

Xu, H., C. L. Gustafson, P. J. Sammons, S. K. Khan, N. C. Parsley, C. Ramanathan, H. W. Lee, A. C. Liu, and C. L. Partch. 2015. 'Cryptochrome 1 regulates the circadian clock through dynamic interactions with the BMAL1 C terminus', *Nat Struct Mol Biol*, 22: 476-84.

Xu, Z., V. A. Meshcheryakov, G. Poce, and S. S. Chng. 2017a. 'MmpL3 is the flippase for mycolic acids in mycobacteria', *Proc Natl Acad Sci U S A*, 114: 7993-98.

Xu, Zhujun, Vladimir A Meshcheryakov, Giovanna Poce, and Shu-Sin Chng. 2017b. 'MmpL3 is the flippase for mycolic acids in mycobacteria', *Proceedings of the National Academy of Sciences*, 114: 7993-98.

Yang, T., M. Guo, H. Yang, S. Guo, and C. Dong. 2016. 'The blue-light receptor CmWC-1 mediates fruit body development and secondary metabolism in Cordyceps militaris', *Appl Microbiol Biotechnol*, 100: 743-55.

Yuan, Ying, YaQi Zhu, Deborah D Crane, and Clifton E Barry III. 1998. 'The effect of oxygenated mycolic acid composition on cell wall function and macrophage growth in Mycobacterium tuberculosis', *Molecular microbiology*, 29: 1449-58.

Zink, A. R., E. Molnar, N. Motamedi, G. Palfy, A. Marcsik, and A. G. Nerlich. 2007. 'Molecular history of tuberculosis from ancient mummies and skeletons', *International Journal of Osteoarchaeology*, 17: 380-91.

Supplementary figures

Table 1: List of genes predicted to participate in RF biosynthesis. The genes in green represent *rib* genes from *Mtb* whereas the genes in blue represent homologous *rib* genes from *Msm (adapted from Mycobrowser database, https://mycobrowser.epfl.ch/).*

Mtb gene name	*Msm* gene name	Locus	Product
ribA2	*ribAB*	MSMEG_3072	GTP cyclohydrolase II + 3,4-dihydroxy-2-butanone 4-phosphate (DHBP) synthase
ribG	*ribD*	MSMEG_3067	Diaminohydroxyphospho ribosylaminopyrimidine deaminase (riboflavin-specific deaminase) + 5-amino-6-(5-phosphoribosylamino) uracil reductase (HTP reductase)
ribH	*ribH*	MSMEG_3073	6,7- dimethyl-8-ribityllumazine synthase
ribC	*ribE*	MSMEG_3071	Riboflavin synthase, alpha subunit
ribF	*ribF*	MSMEG_2653	Riboflavin kinase (flavokinase) + FMN adenylyltransferase (FAD pyrophosphorylase) (FAD synthetase)(FAD diphosphorylase) (flavin adenine dinucleotide synthetase)
Rv0306	bluB	MSMEG_6053	cob(II)yrinic acid a,c-diamide reductase
Unknown	MSMEG_2800	MSMEG_2800	NADPH-dependent fmn reductase

- *Mycobacterium smegmatis*

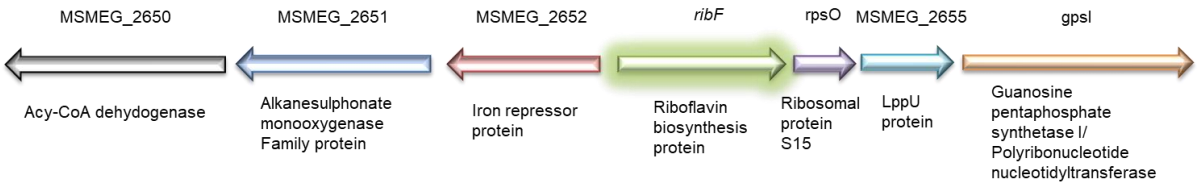

- *Mycobacterium tuberculosis*

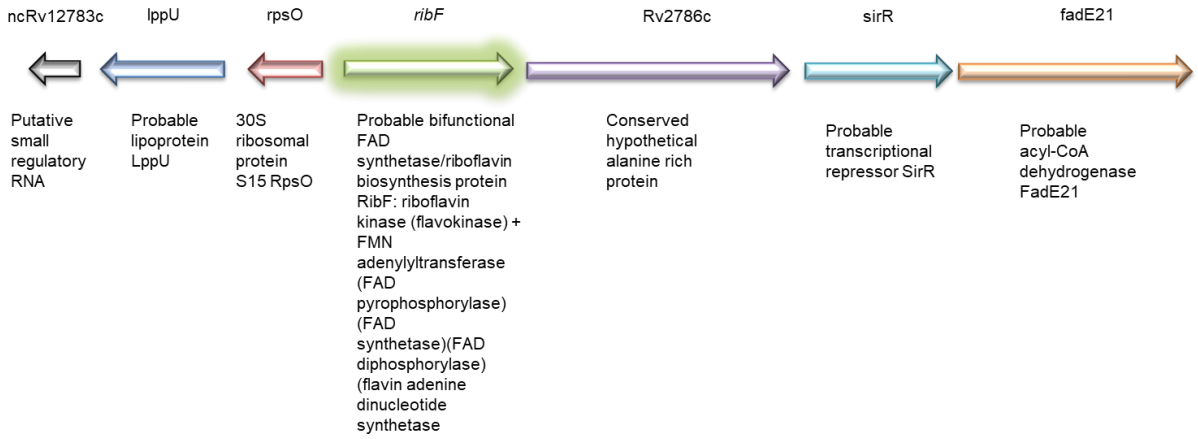

- *Mycobacterium leprae*

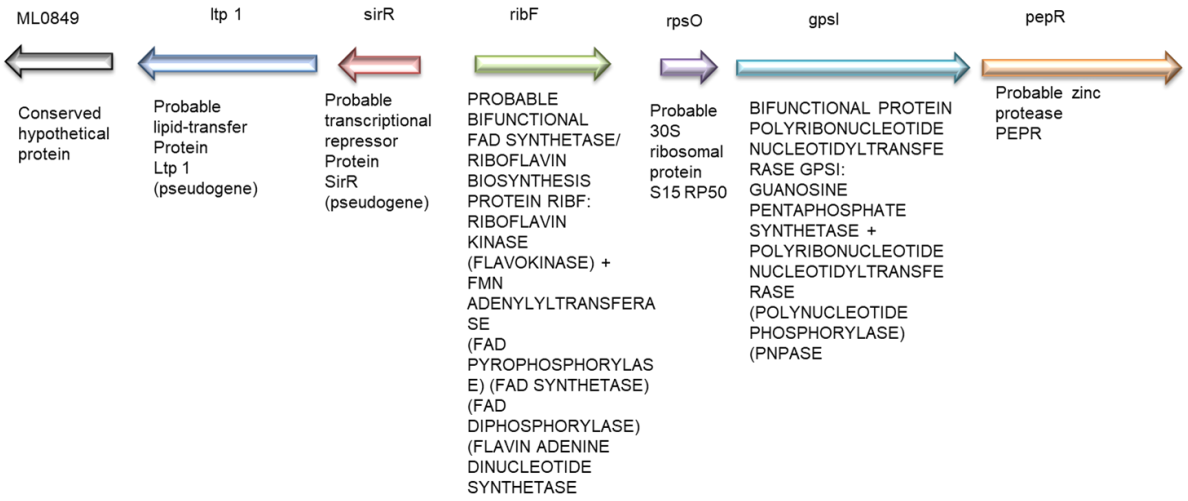

- *Escherichia coli*

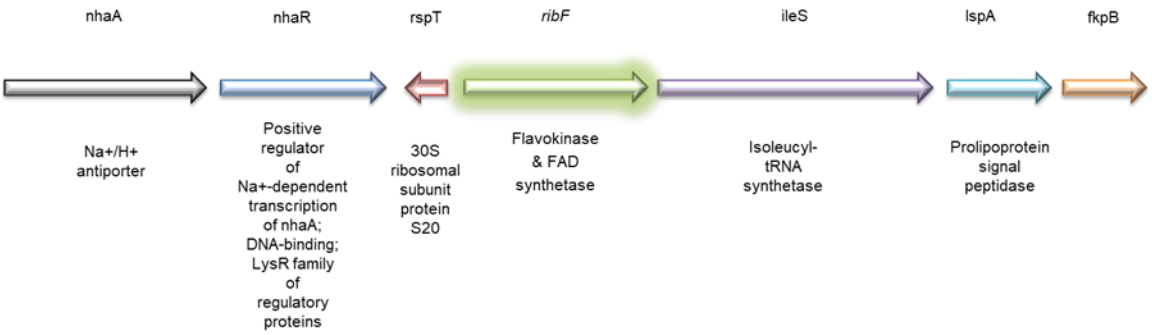

- *Bacillus subtilis* (*ribC*)

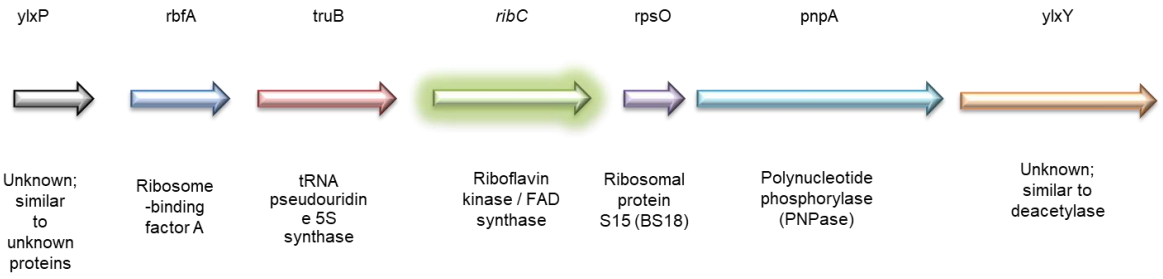

- Bacillus subtilis (*ribR*)

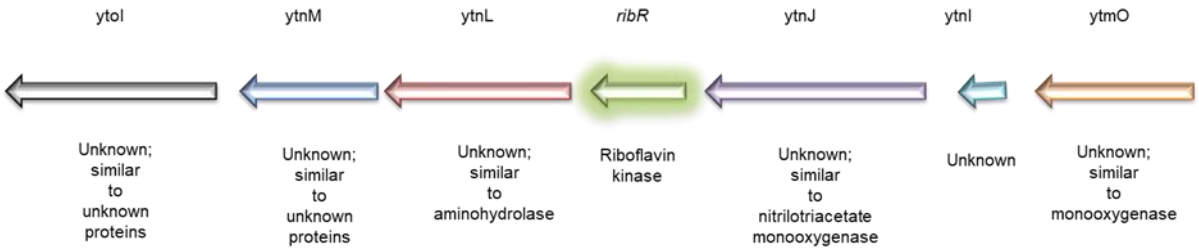

Figure S1: Genomic contexts of *ribF* in *Msm*, *Mtb*, *M. leprae*, *E. coli* and; *ribC* and *ribR* representative of *ribF* in *B. subtilis (adapted from Mycobrowser and GenoList databases).*

Genomic context of *ribD* (MSMEG_5219)

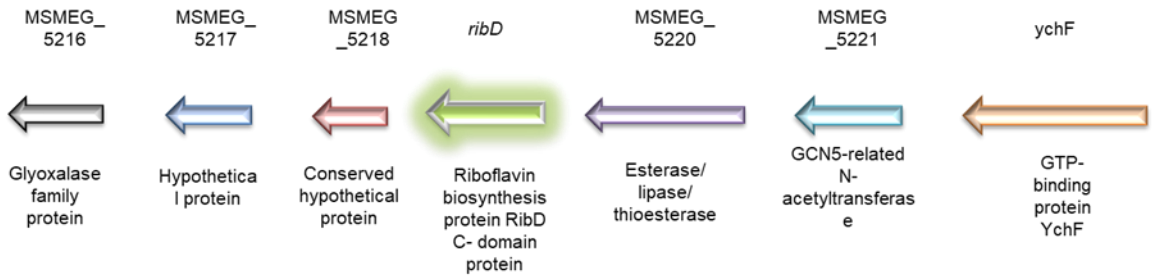

Genomic context of *ribD* (MSMEG_2787)

Genomic context of *ribD* (MSMEG_3067)

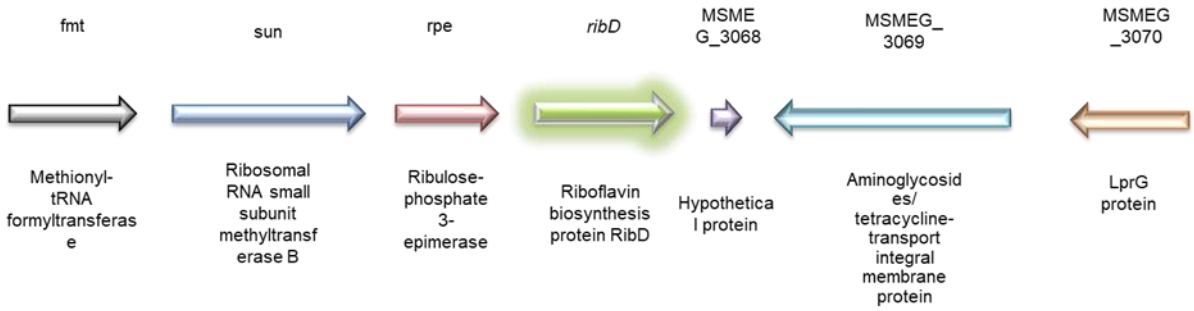

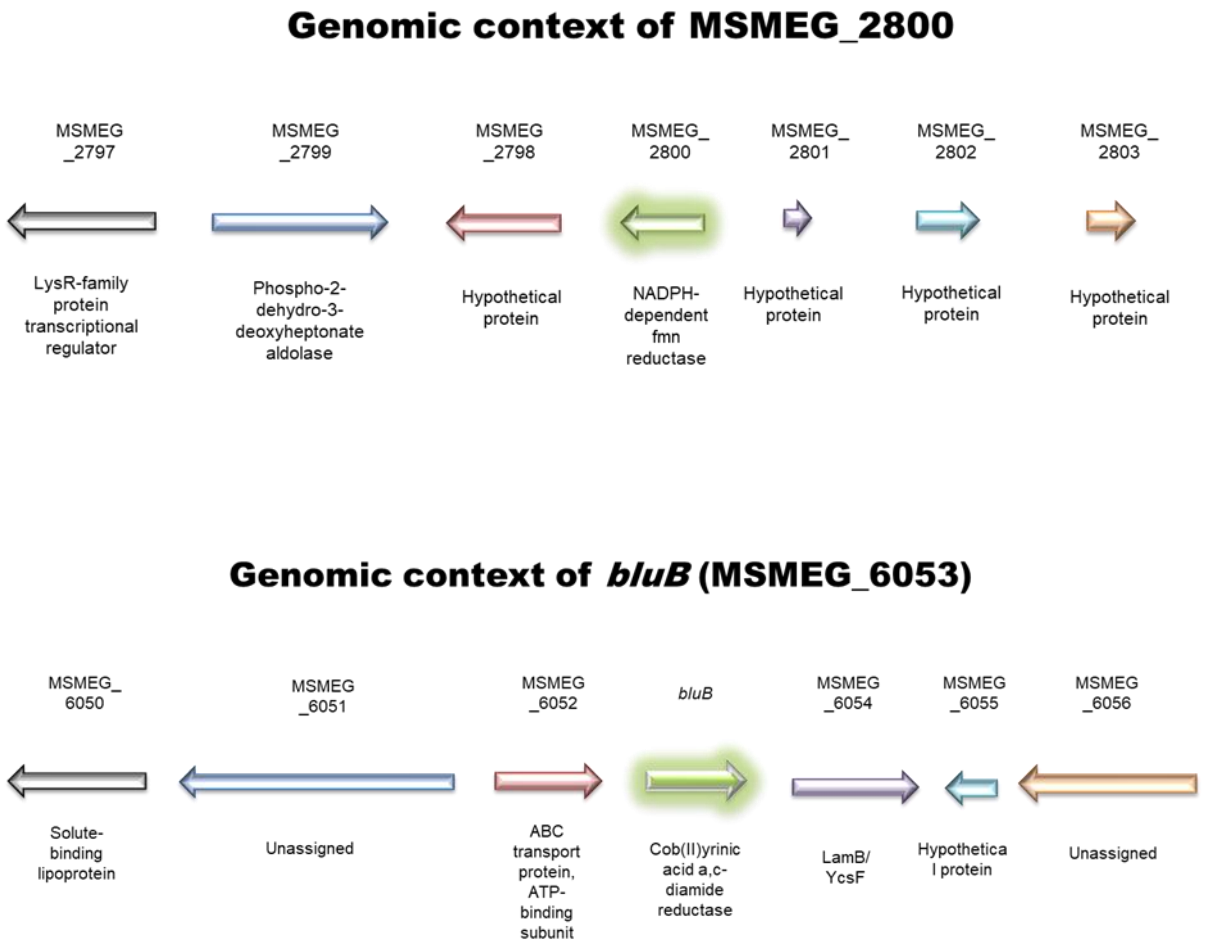

Figure S2: Genomic contexts of all remaining (MSMEG_3067, 2800 and 6053) and duplicate (MSMEG_5219, 2787) genes that participate the RF biosynthetic pathway and gene products they encode in *Mycobacterium smegmatis* (a*dapted from the Mycobrowser database).*

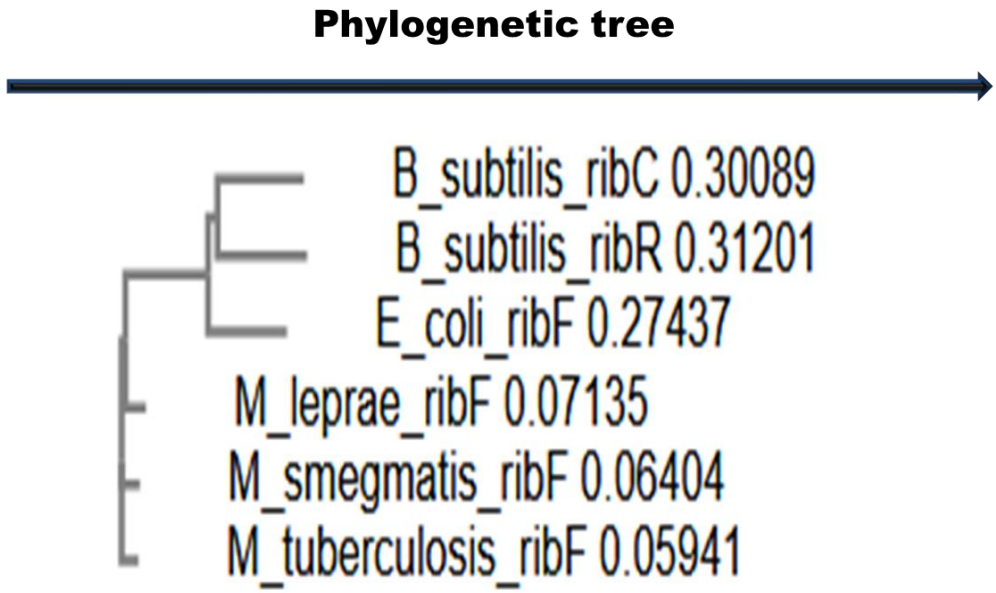

Figure S3: Illustration of nucleotide sequence homology between *ribF* in *Msm*, *Mtb*, *M. leprae*, *E. coli* and *B. subtilis* (adapted from the Clustal omega database; https://www.ebi.ac.uk/Tools/msa/clustalo/).

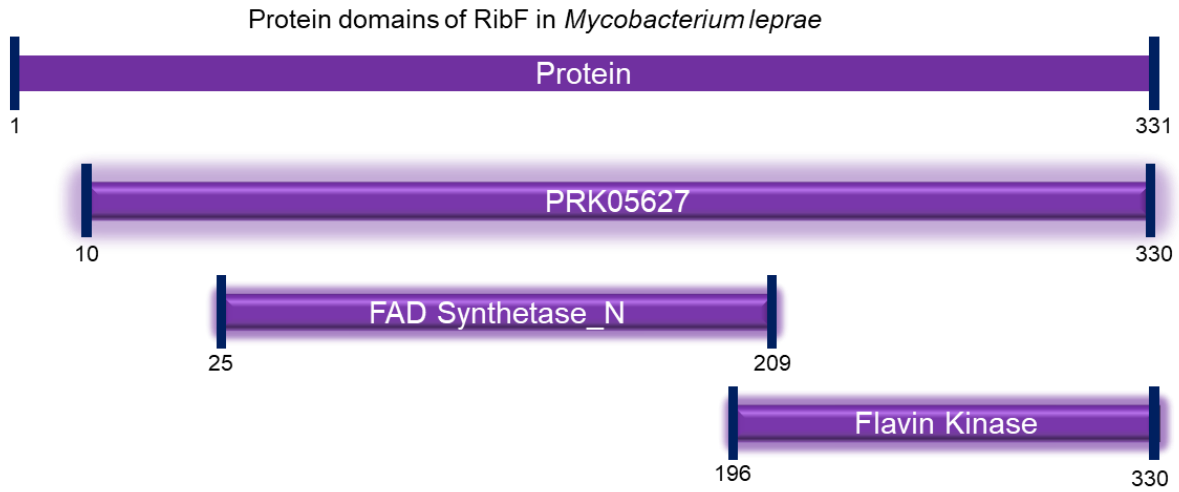

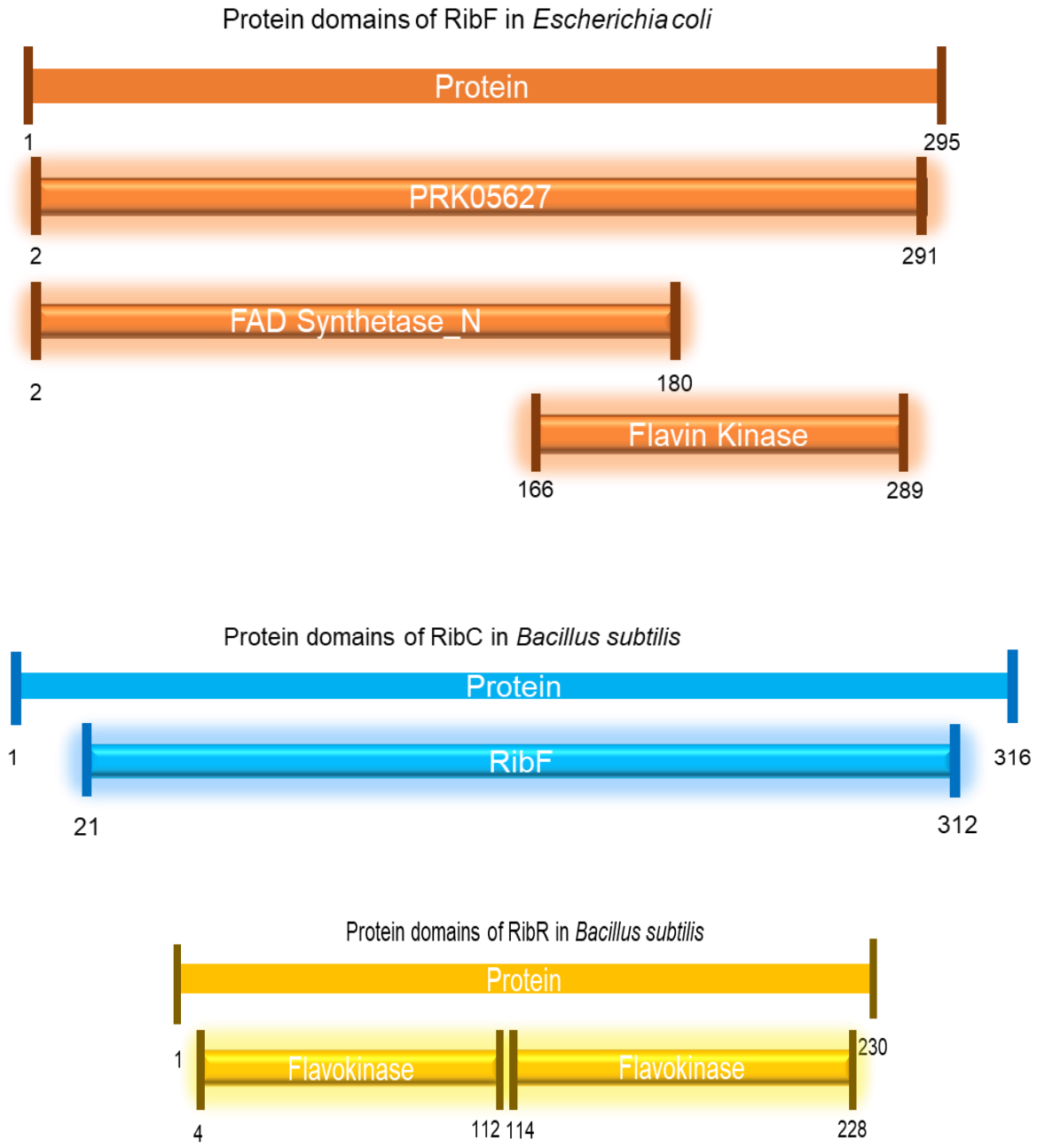

Figure S4: Conserved protein domains of RibF in various microorganisms (a*dapted from protein blast database).*

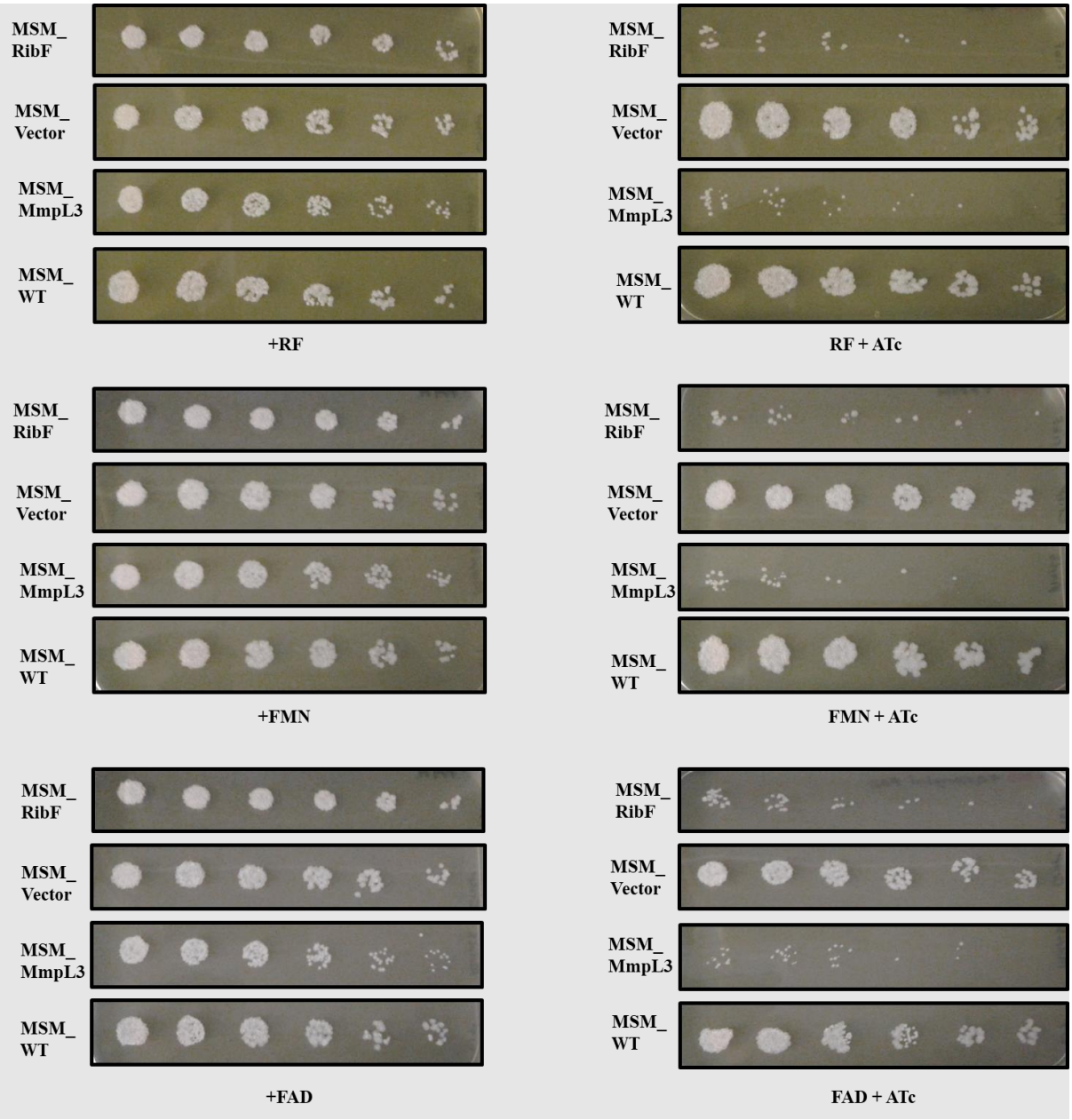

Figure S5: MSM_RibF lethality cannot be rescued by riboflavin, FMN and FAD. Spotting assays of exponential phase cultures in 2-fold dilutions on standard 7H10 medium without ATc plus substrate (-ATc/+substrate) (Left) and with ATc plus substrate (+ATc/+substrate) (Right). Strain names are indicated on the left of the images. Results represent one of the three biological replicates. The first spot in each case contains approximately 5000 mycobacterial cells

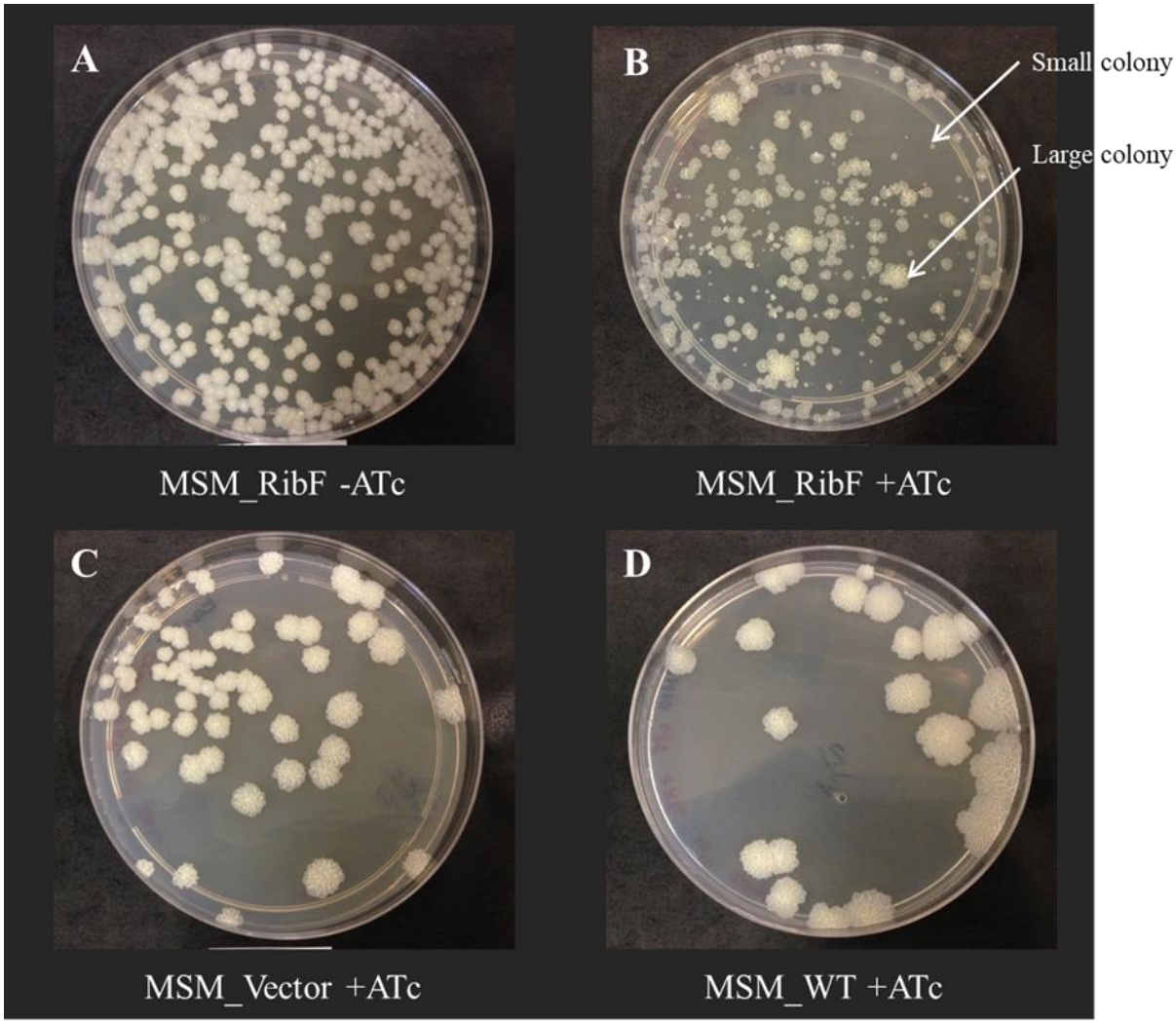

Figure S6: Images of colony morphologies observed post-5-day incubation. Bacterial cultures were plated on 7H10/OADC supplemented agar prior to non-ATc (-ATc) and ATc (+ATc) induction for a period of 24 hours in liquid media. Strain names and conditions exposed to, are indicated below each image.

MSM_RibF

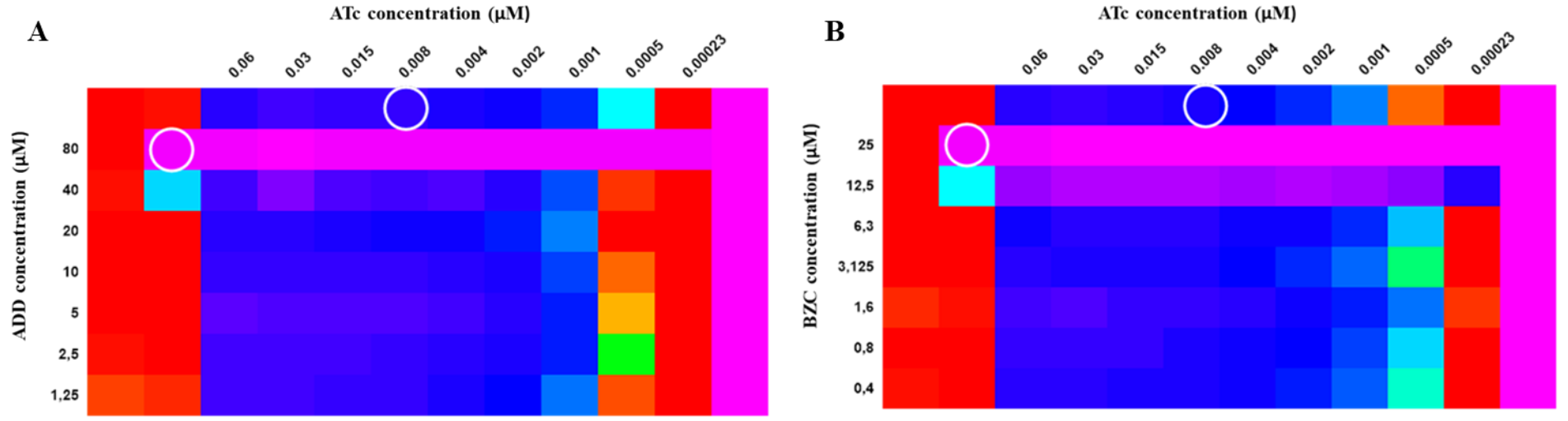

MSM_WT

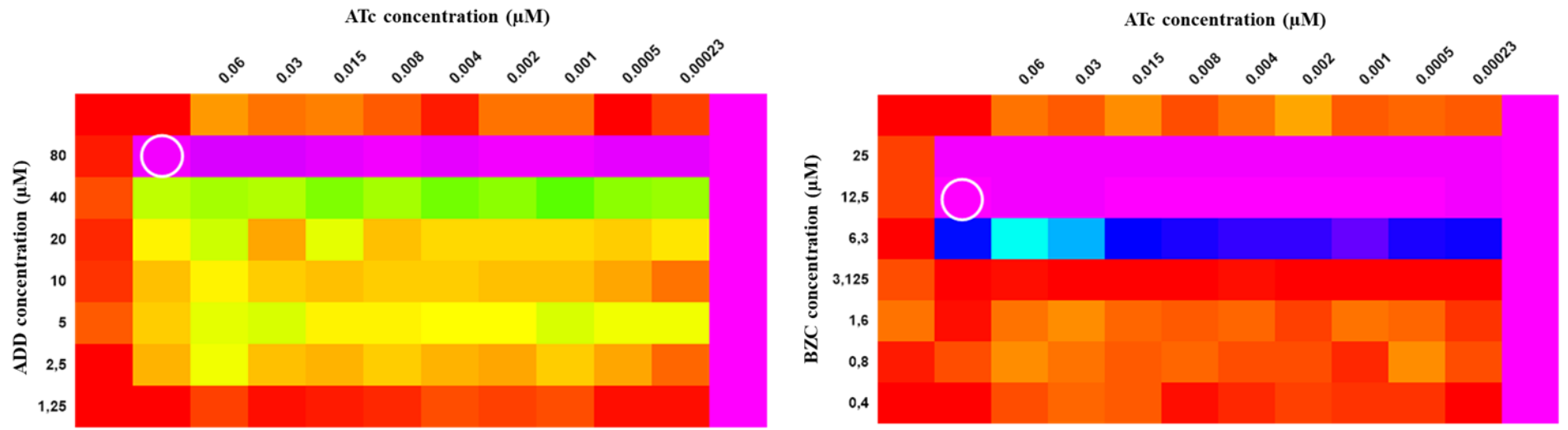

MSM_MmpL3

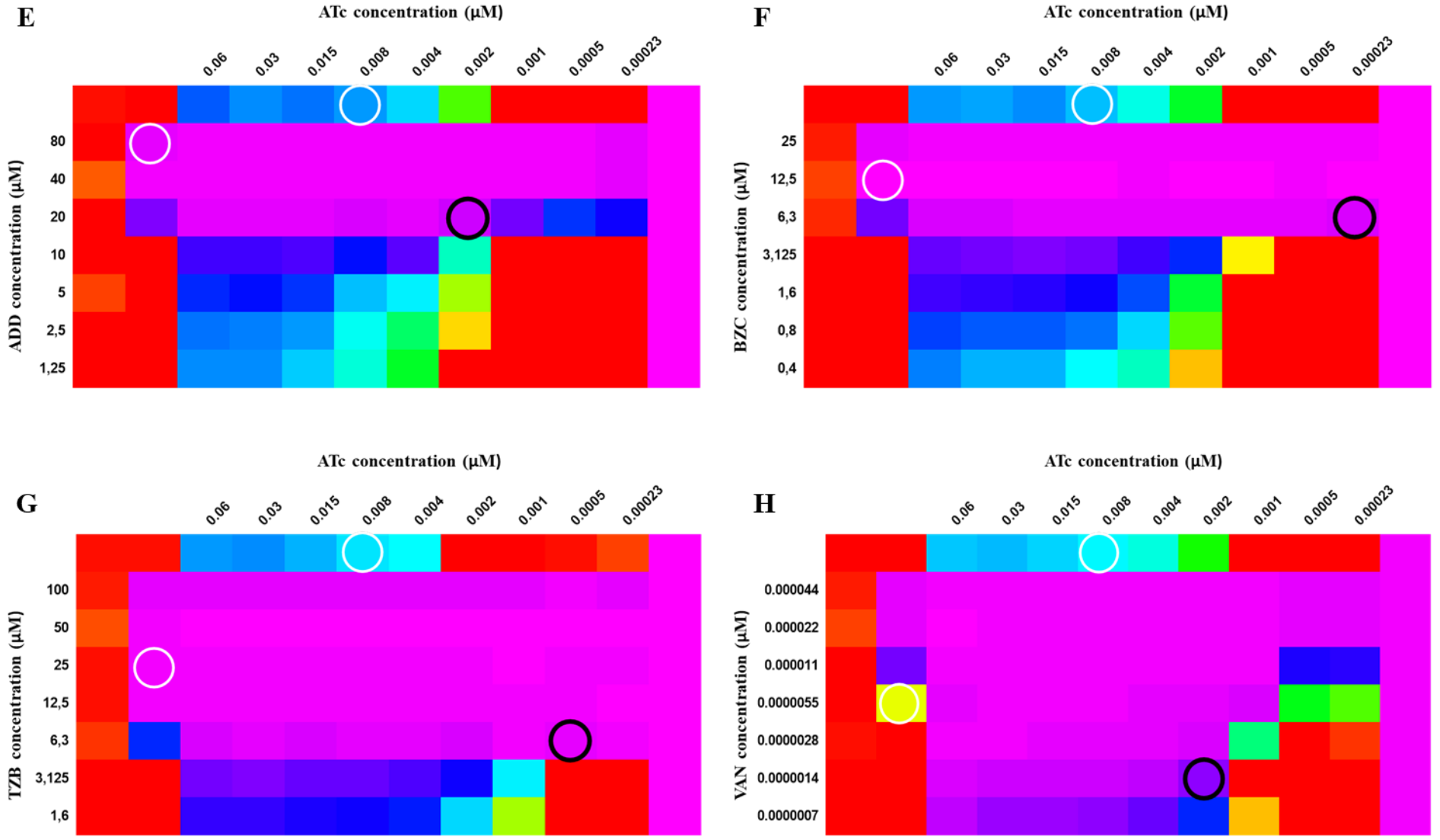
E
ATc concentration (µM)
0.06
0.03
0.015
0.008
0.004
0.002
0.001
0.0005
0.00023
ADD concentration (µM)
80
40
20
10
5
2,5
1,25
F
ATc concentration (µM)
BZC concentration (µM)
25
12,5
6,3
3,125
1,6
0,8
0,4
G
TZB concentration (µM)
100
50
25
12,5
6,3
3,125
1,6
H
VAN concentration (µM)
0.000044
0.000022
0.000011
0.0000055
0.0000028
0.0000014
0.0000007

MSM_Vector

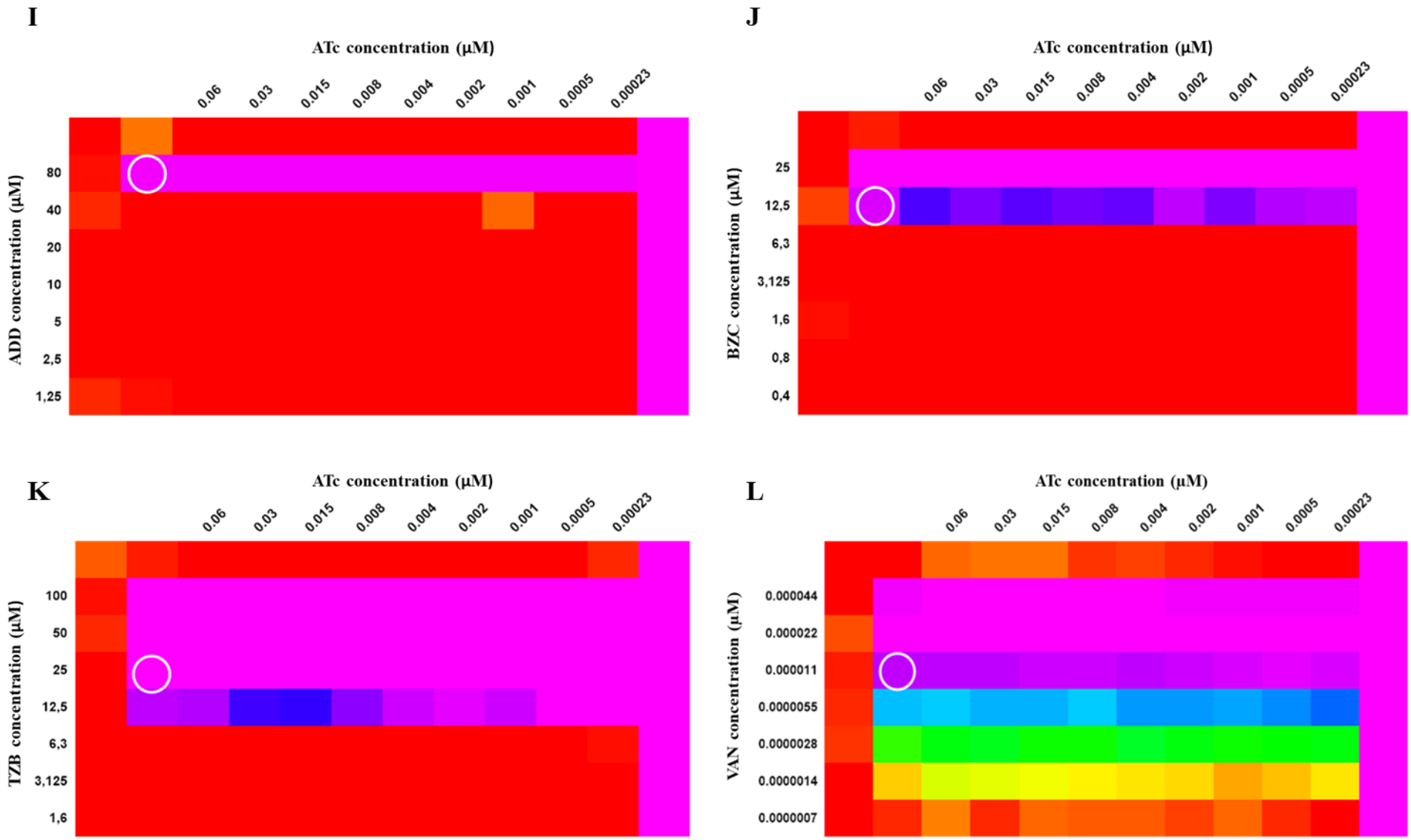
I
ATc concentration (µM)
0.06
0.03
0.015
0.008
0.004
0.002
0.001
0.0005
0.00023
ADD concentration (µM)
80
40
20
10
5
2,5
1,25
J
ATc concentration (µM)
0.06
0.03
0.015
0.008
0.004
0.002
0.001
0.0005
0.00023
BZC concentration (µM)
25
12,5
6,3
3,125
1,6
0,8
0,4
K
ATc concentration (µM)
0.06
0.03
0.015
0.008
0.004
0.002
0.001
0.0005
0.00023
TZB concentration (µM)
100
50
25
12,5
6,3
3,125
1,6
L
ATc concentration (µM)
0.06
0.03
0.015
0.008
0.004
0.002
0.001
0.0005
0.00023
VAN concentration (µM)
0.000044
0.000022
0.000011
0.0000055
0.0000028
0.0000014
0.0000007

Figure S7: CRISPRi *mmpL3* knockdown strain demonstrates increased susceptibility to vancomycin and FAD synthetase inhibitors; ADD and TZC. Standard checkerboard assays representing combinatorial data compiled in a 9 ATc x 7 drug matrix. Cells were treated with ADD, BZC, TZB and VAN against *ribF* (**A** and **B**), *mmpL3* (**E**, **F**, **G** and **H**) deficient, WT (**C** and **D**) and Vector (**I**, **J**, **K** and **L**) control strains for 24 hours. The MICs for both ATc and tested drugs are represented in white ovals, with the well used to calculate the FICI indicated by a black circle.

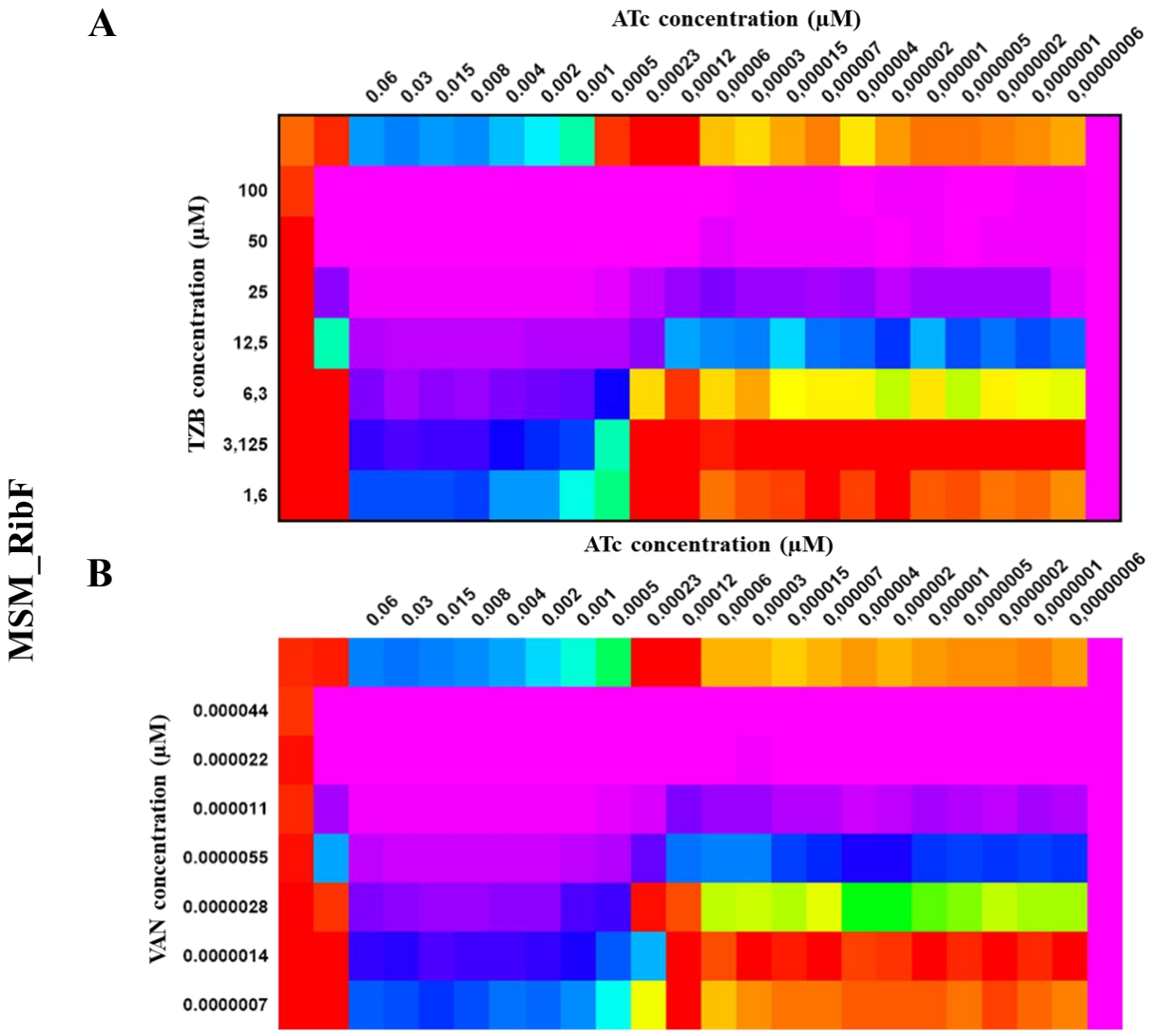

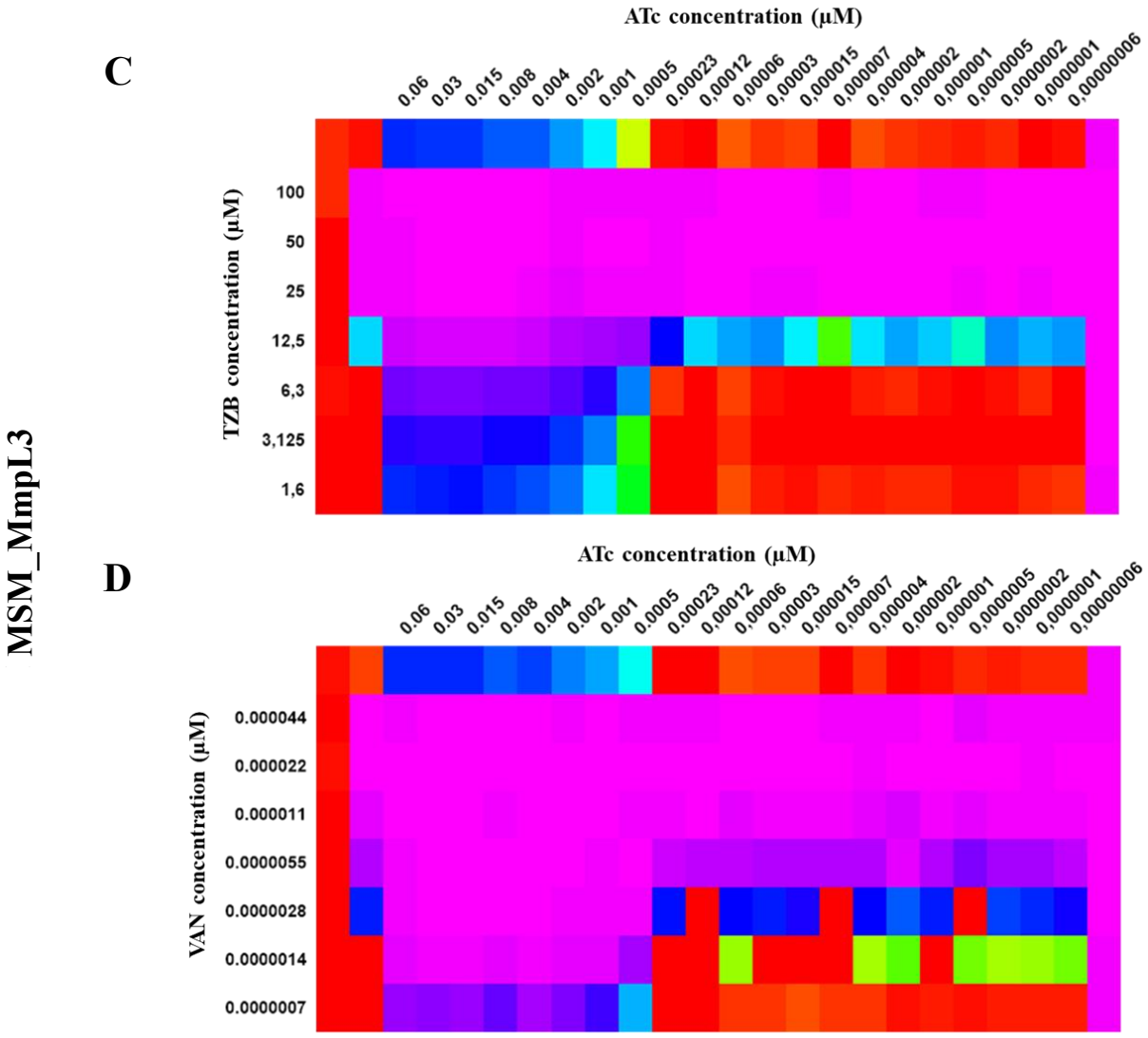

Figure S8: Standard checkerboard assays representing combinatorial data compiled in a 18 ATc x 7 drug matrix (2 x 96 well-microtiter plates). Cells were treated with TZB and VAN against *ribF* (**A** and **B**) and *mmpL3* (**C** and **D**) deficient strains for 24 hours.

1) Flavin mononucleotide:
$C_{17}H_{21}N_4O_9P$

Sample ID	Std. Conc.	Conc. (ug/ml)	Accuracy[%]	Area
27June2019_Ph	1	0.921	92.1	96,414
27June2019_Ph	0.1	0.109	108.7	14,619
27June2019_Ph	0.01	0.010	99.2	4,681

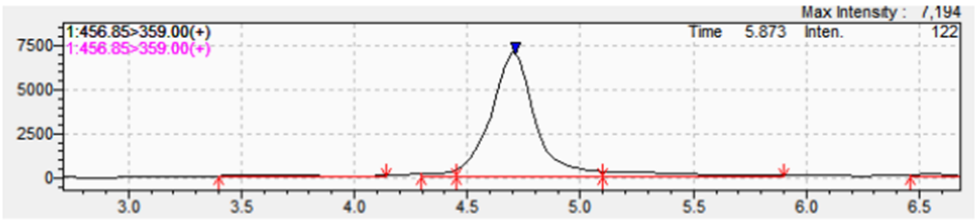

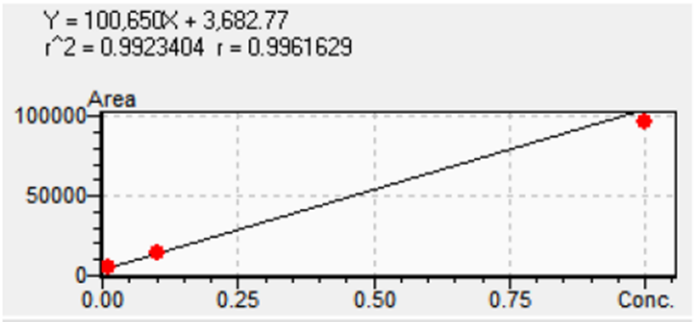

2) Folic acid
$C_{19}H_{19}N_7O_6$

Sample ID	Std. Conc.	Conc. (ug/ml)	Accuracy[%]	Area
27June2019_Ph	1	0.817	81.7	203,155
27June2019_Ph	0.1	0.120	120.1	30,484
27June2019_Ph	0.01	0.010	98.2	3,151

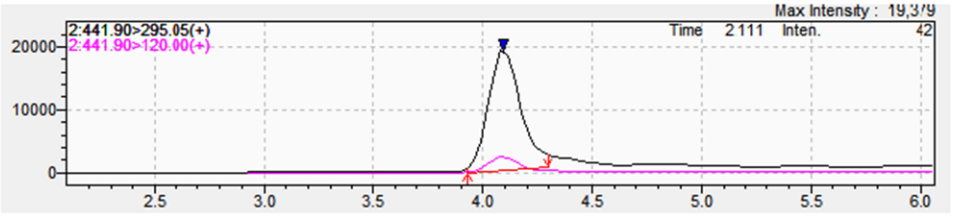

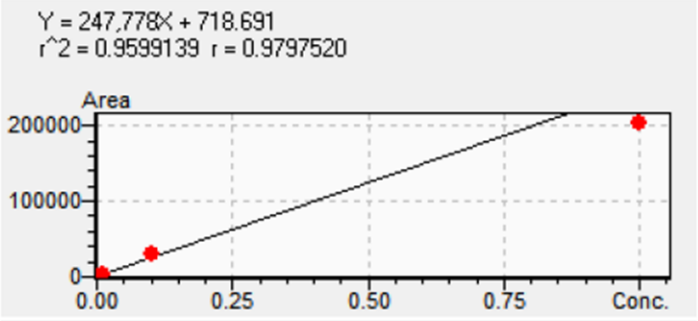

3) Flavin Adenine Dinucleotide
$C_{27}H_{33}N_9O_{15}P_2$

Sample ID	Std. Conc.	Conc. (ug/ml)	Accuracy[%]	Area
27June2019_Ph	1	1.027	102.7	339,139
27June2019_Ph	0.1	0.097	97.1	42,051
27June2019_Ph	0.01	0.010	100.3	14,234

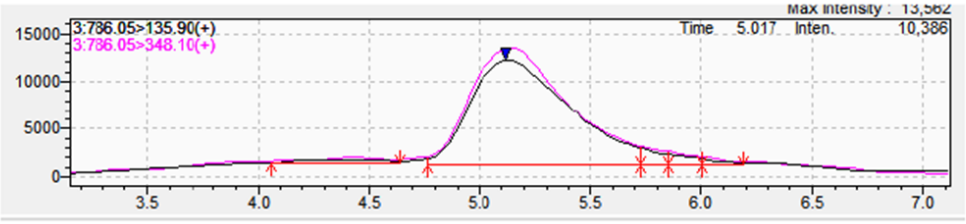

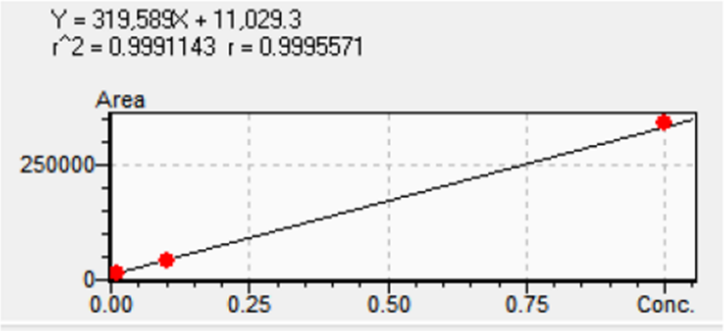

4) Riboflavin
$C_{17}H_{20}N_4O_6$

Sample ID	Std. Conc.	Conc. (ug/ml)	Accuracy[%]	Area
27June2019_Ph	1	0.892	89.2	969,727
27June2019_Ph	0.1	0.112	111.8	122,299
27June2019_Ph	0.01	0.010	98.9	11,625

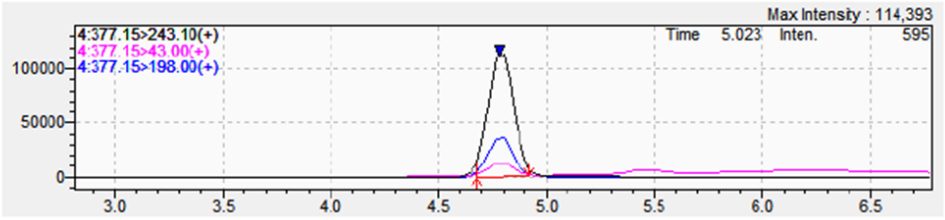

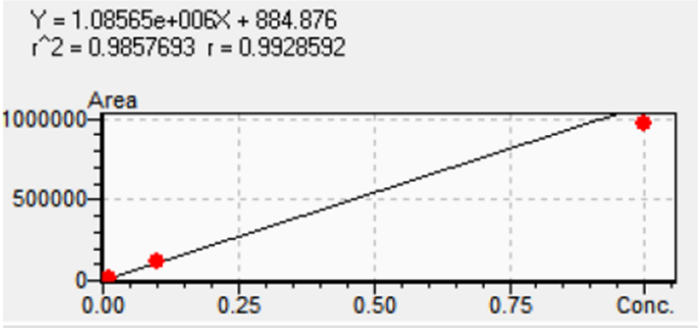

5) 6,7-Dimethyl-8-(D-ribityl) lumazine
$C_{13}H_{18}N_4O_6$

Sample ID	Std. Conc.	Conc. (ug/ml)	Accuracy[%]	Area
27June2019_Ph	1	0.917	91.7	290,175
27June2019_Ph	0.1	0.109	109.1	34,748
27June2019_Ph	0.01	0.010	99.2	3,413

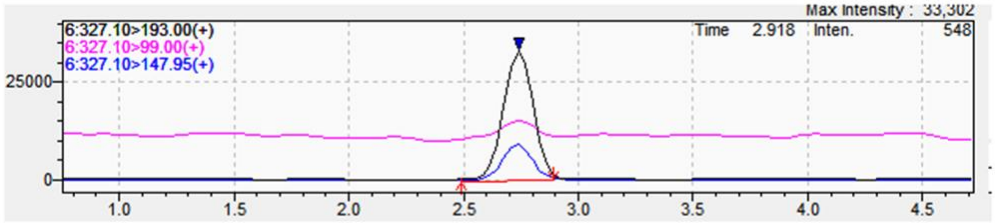

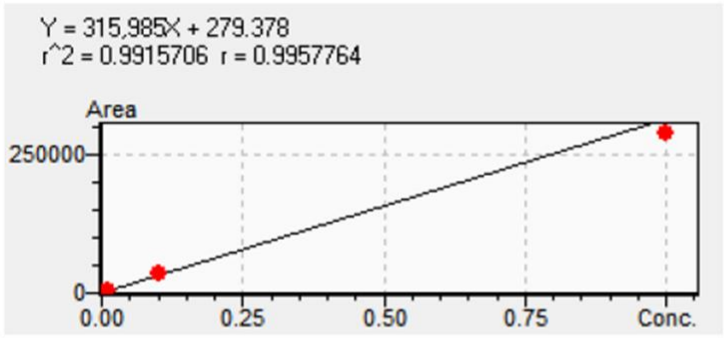

6) Vitamin B12
Formula: C62H88CoN13O14PR

Sample ID	Std. Conc.	Conc. (ug/ml)	Accuracy[%]	Area
27June2019_Ph	1	0.730	73.0	63,798
27June2019_Ph	0.1	0.130	129.8	11,117
27June2019_Ph	0.01	0.010	97.3	575

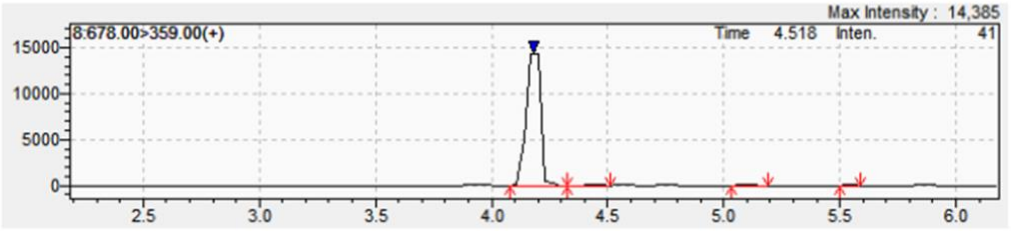

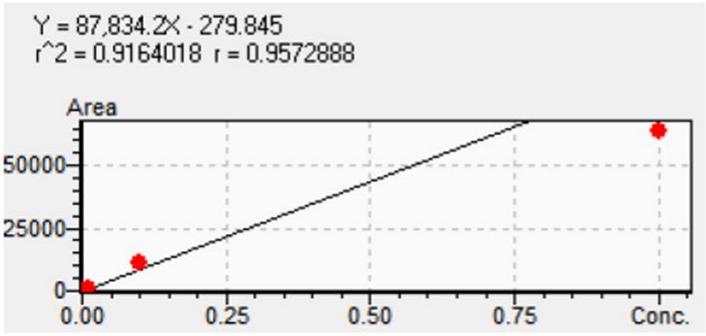

Figure S9: LC-MS analytical standard traces of each of the compounds. Results reflect the concentration, chromatogram and calibration line and fit.

Appendix

Table 1: Different media used in this study and their compositions

Media name	Composition
Luria-Bertani Broth	10 g tryptone 10 g NaCl 5 g yeast extract
Luria-Bertani Agar	10 g tryptone 10 g NaCl 5 g yeast extract 15 g bacteriological agar
2 x TY	4 g NaCl 10 g yeast extract 16 g tryptone
7H9-OADC	4.7 g Middelbrook 7H9 broth powder (Difco™ USA) 2 ml glycerol (Merck, Germany) 2 ml 25% Tween 80 100 ml OADC Middelbrook OADC Enchrichment (BD Microbiology Systems, USA)
7H10-OADC	19 g Middelbrook 7H9 broth powder (Difco™ USA) 5 ml glycerol (Merck, Germany) 100 ml OADC Middelbrook OADC Enchrichment (BD Microbiology Systems, USA)

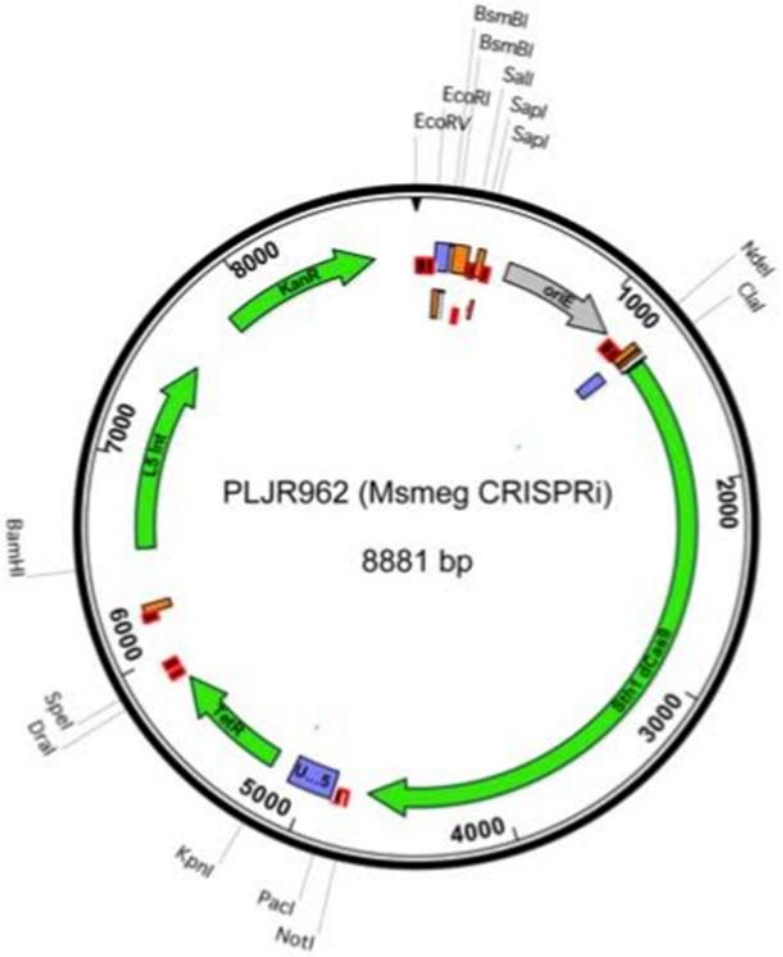

Figure 1: Schematic diagram of the CRISPRi backbone (PLJ962) used for *Msm*

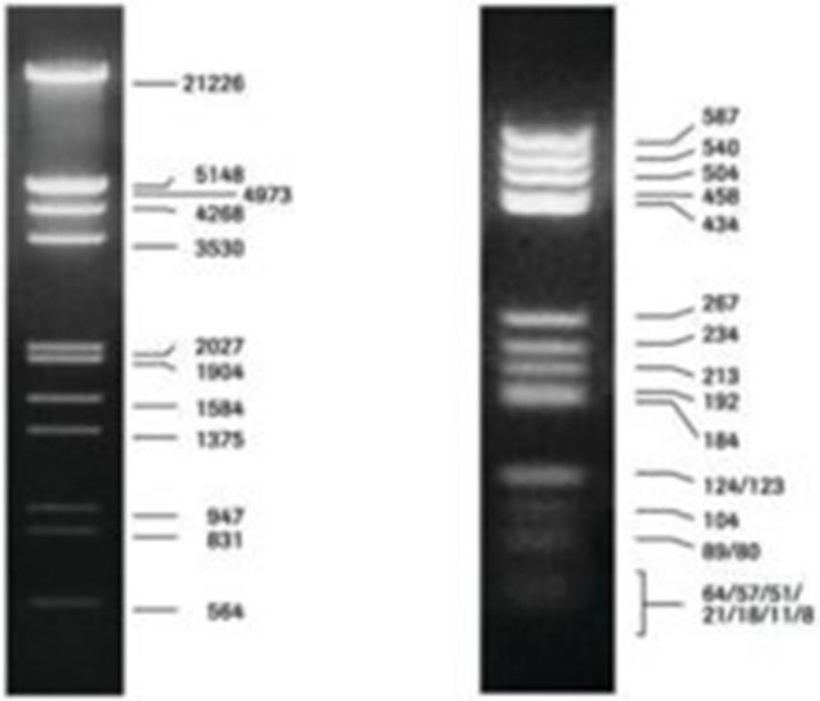

Figure 2: Gel electrophoresis images of DNA Molecular weight marker III (left) and V (right).